Electronic Theses and Dissertations                    Theses, Dissertations, and Major Papers

1-7-2019

# Using Parametric CAD and FDM to Produce High Fidelity Anatomical Structures for Thoracentesis Training

Andre Khayat
*University of Windsor*

Follow this and additional works at: https://scholar.uwindsor.ca/etd

Using Parametric CAD and FDM to Produce High Fidelity Anatomical Structures
for Thoracentesis Training

By

**Andre Khayat**

A Thesis
Submitted to the Faculty of Graduate Studies
Through the Department of Mechanical, Automotive, and Materials Engineering
in Partial Fulfillment of the Requirements for
the Degree of Master of Applied Science
at the University of Windsor

Windsor, Ontario, Canada

2018

Using Parametric CAD and FDM to Produce High Fidelity Anatomical Structures
for Thoracentesis Training


by

Andre Khayat



APPROVED BY:


_____ .


A. J. Cort

Faculty of Human Kinetics


_____ .


B. J. Defoe

Department of Mechanical, Automotive and Materials Engineering


_____ .


C. B.-A. Schuelke-Leech, Co-Advisor

Department of Mechanical, Automotive and Materials Engineering


_____ .


D. R.-J. Urbanic, Co-Advisor

Department of Mechanical, Automotive and Materials Engineering



December 18th 2018

# DECLARATION OF CO-AUTHORSHIP / PREVIOUS PUBLICATION

I.  Co-Authorship

I hereby declare that this thesis incorporates material that is result of joint research, as follows:

Chapters 1-5 of this thesis represent expansions on related research co-authored by Dr. R. J. Urbanic, Dr. B.-A. Schuelke-Leech, and Ms. A. Farias. The research presented in these chapters was performed under the supervision of Dr. Urbanic and Dr. Schuelke-Leech, and Ms. Farias assisted in the medical experiments, and also served as a medical expert for reference throughout. Chapters 1.4 and 2.4 contain expansions of previous research co-authored by H. Kalami, who helped develop the framework which formed the general approach to in this thesis. Chapters 3.2, 3.4, 4.2 and 4.6 contain information from research co-authored by B. Kalajdzic, Dr. R. J. Urbanic and Ms. A. Farias. The research was performed under supervision of Dr. Urbanic and Dr. Schuelke-Leech, and B. Kalajdzic and Ms. Farias assisted in data collection procedures. In all cases, application and adaptation of previous research content to this thesis was done by the author, under the supervision of Dr. Urbanic and Dr. Schuelke-Leech.

I am aware of the University of Windsor Senate Policy on Authorship and I certify that I have properly acknowledged the contribution of other researchers to my thesis, and have obtained written permission from each of the co-author(s) to include the above material(s) in my thesis.

I certify that, with the above qualification, this thesis, and the research to which it refers, is the product of my own work.

II.  Previous Publication

This thesis includes 4 original papers that have been previously published/submitted for publication in peer reviewed journals, as follows:

| Thesis Chapter | Publication title/full citation | Publication status* |
|---|---|---|
| *Chapters 1-5* | A. Khayat, R.J. Urbanic, B.A. Schuelke-Leech and A. Farias, "Development of a Reconfigurable Thoracentesis Training Mannequin," *Computer-Aided Design and Applications*, Forthcoming | *In Press* |
| *Chapters 1-5* | A. Khayat, R.J. Urbanic, B.A. Schuelke-Leech and A. Farias, "Development of a Reconfigurable Thoracentesis Training Mannequin," in *Computer-Aided Design & Applications 2018 Conference.* Taylor & Francis, 2018. | *In Press* |
| *Chapter 1.4, 2.4* | H. Kalami, A. Khayat and R.J. Urbanic, "Investigating 'Exo-Skeleton' Design and Fabrication Challenges for the Hand Region Using Material Extrusion Processes," *IFAC-PapersOnLine*, vol. 49, pp. 30-35, Feb. 2017. [Online]. https://doi.org/10.1016/j.ifacol.2016.12.157 | *Published* |
| *Chapter 3.2, 3.4, 4.2, 4.6* | *B. Kalajdzic, R.J. Urbanic, A. Khayat and A. Farias, "UTILIZING ADVANCED MANUFACTURING TECHNOLOGIES TO DEVELOP A RECONFIGURABLE LUMBAR PUNCTURE TRAINING MODEL" in Proceedings of the ASME 2018 International Mechanical Engineering Congress and Exposition IMECE,* 2018. | *In Press* |

I certify that I have obtained a written permission from the copyright owner(s) to include the above published material(s) in my thesis. I certify that the above material describes work completed during my registration as a graduate student at the University of Windsor.

I declare that, to the best of my knowledge, my thesis does not infringe upon anyone's copyright nor violate any proprietary rights and

that any ideas, techniques, quotations, or any other material from the work of other people included in my thesis, published or otherwise, are fully acknowledged in accordance with the standard referencing practices. Furthermore, to the extent that I have included copyrighted material that surpasses the bounds of fair dealing within the meaning of the Canada Copyright Act, I certify that I have obtained a written permission from the copyright owner(s) to include such material(s) in my thesis.

I declare that this is a true copy of my thesis, including any final revisions, as approved by my thesis committee and the Graduate Studies office, and that this thesis has not been submitted for a higher degree to any other University or Institution.

ABSTRACT

Currently available thoracentesis medical training simulators lack tactile realism and do not represent the physiological variations in patient characteristics, impeding optimal experiential learning. By systematically implementing advanced computer-aided design (CAD) techniques and additive manufacturing (AM) tools, with a flexible design methodology, thoracic wall representations for a 2-year-old male, an 18-year-old female, and a 30-year-old male, with complete skeletal structures necessary for palpation sequencing were modelled. Models for the 2-year-old male and 18-year-old female were fabricated, complete with realistic tissues that accurately represent the various discrete tissue layers of the human thoracic cross section. Clavicular growth rates were used to develop factors with which to scale the skeletal models to represent a range of patient demographics. Parametrically modelled mould sets enable the modification of tissue thickness to account for varying thoracic wall thicknesses observed in the thoracentesis demographic. Through the implementation of scaling factors based on skeletal growth rates from the literature to represent different patient groups, clavicle sizing accuracy ranging from 0.4%-1.3% was achieved, and intercostal space measurement accuracy of 0.7%-2.8% was achieved as compared to target values from the literature. Improvements to simulated tissue were observed, with a 28.54% improvement in terms of peak force, 20.17% for impulse, and 36.31% for pulse width, when compared to the THM-30, a currently available popular model.

## DEDICATION

This thesis is dedicated to my family. To my siblings, Alana and Alex, for your endless support throughout the years, I am eternally grateful. To my amazing parents, Elias and Antoinette Khayat, who are both incredible inspirations, supporters, and the greatest role models anyone could ask for. Without you, this thesis would not exist. Thank you.

# ACKNOWLEDGEMENTS

TABLE OF CONTENTS

# LIST OF FIGURES

## LIST OF TABLES

# LIST OF APPENDICES

# LIST OF ABBREVIATIONS AND SYMBOLS

| | |
|---|---|
| .catpart | Catia Part |
| .obj | Object Filetype |
| .sldprt | Solidworks Part |
| .step | Step Filetype |
| .stl | Stereolithography |
| ABS | Acrylonitrile Butadiene Styrene |
| AM | Additive Manufacturing |
| ANOVA | Analysis of Variance |
| CAD | Computer-Aided Design |
| CHF | Congestive Heart Failure |
| cm | Centimeter |
| CT | Computed Tomography |
| df | Degrees of Freedom |
| FDM | Fused Deposition Modelling |
| hrs | Hours |
| HSD | Honest Significant Difference |
| Hz | Hertz |
| Kg | Kilogram |
| mm | Millimeter |
| MRI | Magnetic Resonance Image |
| N | Newton |
| n | Number |
| N·s | Newtons per second |
| NIDDKD | National Institute of Diabetes and Digestive and Kidney Diseases |
| PC | Participant Confidence |
| PPE | Personal Protective Equipment |
| PS | Performance Score |
| PT | Procedure Time |
| Q | Quartile |
| REB | Research Ethics Board |
| s | Second |
| SPSS | Statistical Package for the Social Sciences |
| USD | United States Dollar |
| UV | Ultraviolet |
| WiDACS | Wireless |
| wt | Weight |
| yr | Year |
| σ | Standard Deviation |

CHAPTER 1

Introduction

## 1.1. Defining Learning Curves, Introducing Medical Simulators

Errors in medical procedures are listed as the third leading cause of death in the United States [1], [2]. Estimated rates of medical errors ranging from 5.6% in New York [3] to 16.5% in Southern Australia have been reported; 13.7% of these resulting in permanent disability, and 4.9% in death. In excess of 50% of these cases were determined to have been preventable [4].

There are several contributing factors to the resultant 400,000 annual deaths and 3.5 million annual permanent disabilities in the United States [5]. A primary factor is described by Bari et al., who interviewed medical residents about their workplace errors. Of the residents interviewed, 52% attributed their errors to a lack of experience with the procedure they were performing [6]. This lack of experience can be directly related to the widely reported concept of a learning curve (the rate of skill mastery), which is prevalent in the clinical practice of surgical skills [7], [8].

Clinical-skills learning curves vary depending on the measured parameters they describe [9]. Standard curves typically plot performance time or success rate, along with the number of trials. Success rate-based curves typically resemble Figure 1.1-1, which shows a steep initial region, indicating rapid learning but low skill level (i.e. success rate below the acceptance standard). A secondary region is observed where the curve's slope flattens, indicating slower learning approaching the acceptance standard. A tertiary region typically follows, showing a plateau,

indicating skill mastery (i.e. success rate firmly above the acceptance standard, which depends on the procedure) [7], [10].
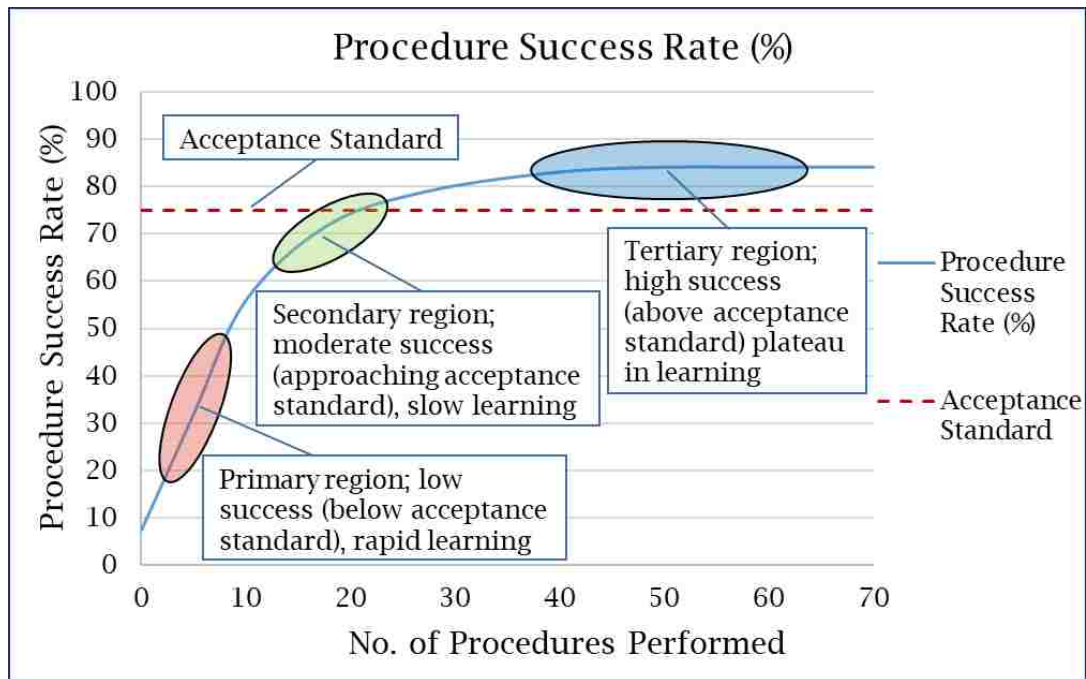


**Figure 1.1-1: Typical procedure success rate clinical learning curve**

Experiential learning is essential to clinical education. Aristotle historically stated that "[clinicians] do not seem to be made by a study of textbooks" [11]. Contemporaneously, the importance of skill development through deliberate practice is echoed in many studies [7], [8], [10], many of which compare clinical performance data (i.e. success rate %, procedure time) and clinician experience (i.e. procedures performed). These studies conclude that practical clinical experience is directly related to better performance in medicine. Furthermore, lack of experience increases the incidence of clinical error [6]. As such, investigations of clinical learning curves have been conducted to reduce patient risk during clinical procedures performed by less experienced clinicians [7], [12]-

[14]. Many of these studies aim to shorten the learning curve—to increase the slope of the initial region, achieving skill mastery in fewer trials.

The need for experiential learning via live-patient practice in residents who are still in the early stages of the clinical learning curve (i.e. initial region, lacking experience) poses difficult moral questions. Paradoxically, without an alternative to practicing on patients, in order to improve the skills of a clinician and reduce patient risk (i.e. to progress to tertiary region, with a high success rate), the clinician must practice the procedure on patients, subjecting them to elevated risk. While it is ultimately necessary to practice the procedures on live patients to master the skills, it is optimal to have prior experiential training.

One solution adopted by the medical community is the implementation of practical-skills training simulators. Medical training simulators are simplified representations of patients that mimic features critical to the delivery of care [15]. They are designed to be incorporated into medical education curricula as practice tools, as alternatives to practicing on live patients. Through the representation of skeletal structures, venous maps, and tissue layers, these models provide simulations of human anatomy [16]. The effectiveness of these simulators is demonstrated in multiple studies [14], [17], [18], investigating their use in various applications. These studies reconfirm that one of the primary benefits of medical simulation training is that the high-risk, initial regions of the learning curve (i.e. before skill mastery has been achieved) are shifted away from patients [17]. In addition to reducing the risk associated with practicing on patients, these simulators increase knowledge retention of the trained skills for clinicians, such

that clinical skills may be repeated successfully up to one year post-intervention [18].

While training simulators help mitigate learning curve risks, a compromise is associated with their use. In order to address learning curve issues for the largest number of patients undergoing a wide array or procedures, the design of these models must balance simulator fidelity (anatomical accuracy and functionality), with manufacturability and cost. The effect of fidelity variation (the simplification of simulator features) is dependent on the simulator and its application [19]. For many procedures, low-fidelity simulators are sufficient to allow for progress along the learning curve (progress to secondary or tertiary regions) [19], [20]. Others however, require high-fidelity simulation [21], [22]. One such application is in the training of necessary force exertion [23], such as in thoracentesis simulation training, which requires manual insertion of a needle into simulated tissue that surrounds skeletal structures [24]-[28].

## 1.2. Background

Based on the literature defining force-exertion training as a case that benefits from high-fidelity simulation [23], an investigation into existing thoracentesis simulators was performed to assess their fidelity (Chapter 1.2.2). Criteria for analysis of existing solutions are based on background research on the thoracentesis procedure, patient demographics, and key functional constraints of existing simulators.

## 1.2.1. General Thoracentesis Procedure

Thoracentesis is a procedure performed to treat pleural effusions, which are the excessive pooling of fluid in the pleural space, which is the space between the membranes of the lungs and the chest wall (Figure 1.2.1-1) [29], [30].
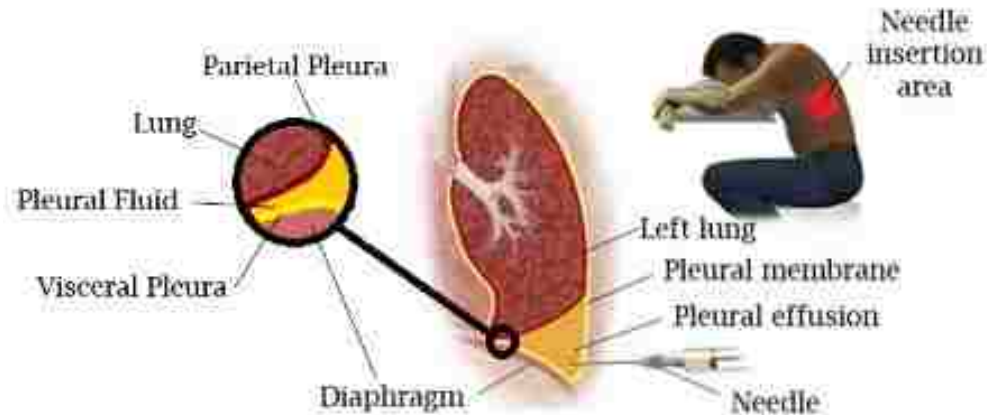


**Figure 1.2.1-1: Pleural effusion (adapted from [31])**

The procedure begins with a palpation sequence, which starts with the tracing of the mid-clavicular line along the back, down one to two intercostal spaces (depending on fluid level) from the pointed base of the scapula (inferior angle) [32]-[34], which correlates to the 7th rib [35]-[37]. This palpation is performed to identify the optimal insertion site for a catheter needle, which is inserted normally through the thoracic wall, along the upper edge of the rib (Figure 1.2.1-2) to drain fluid from the chest cavity [34].
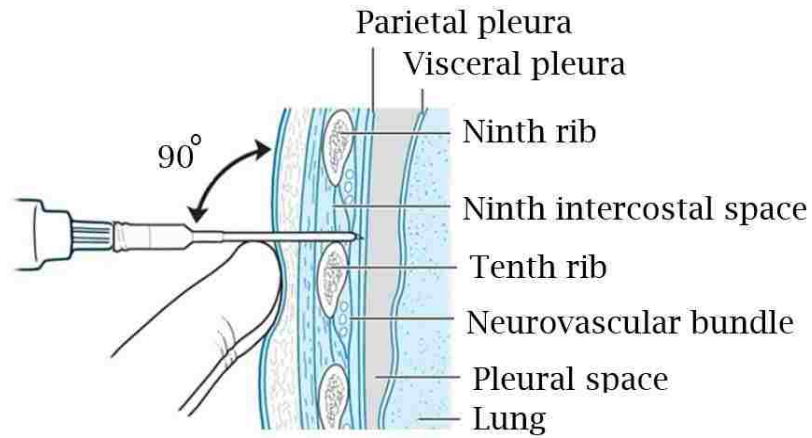
**Figure 1.2.1-2: Insertion of thoracentesis needle/catheter (adapted from [34])**

Through the removal of this fluid, pressure equilibrium and space within the chest cavity are re-established, restoring proper lung function and relieving symptoms including coughing, chest pain and difficulty breathing [35]. Alternatively, thoracentesis may be performed as a diagnostic test, where the doctor studies the sample obtained from the procedure to diagnose heart failure, lung disease, cancer, or infection [29], [30], [39].

In the event of procedural error, pneumothorax (introduction of air into the pleural space), hemothorax (introduction of blood into the pleural space), and lacerations of the kidney or spleen may occur. These errors have an 11% occurrence rate when performed by residents learning the procedure [40]. Minor complications, including dry taps (unsuccessful fluid removal) and subcutaneous hematoma (pooling of blood under the skin, outside of blood vessels) are more common, with a 15% occurrence rate [40]. These rates increase to 30% when performed by newer, less experienced residents, which demonstrates a clear correlation between experience and performance [33]. Furthermore, in a study where experienced emergency physicians were observed during thoracentesis procedures, only 60% were able to accurately identify key landmarks necessary to

optimal site determination for needle insertion on a test subject with palpation (i.e. mid-clavicular line, inferior angle of scapula, upper edge of ribs) [41].

These error rates may be due to the fact that traditionally, residents were only able to practice clinical thoracentesis skills on live patients for the first time [42], [43]. Based on studies which outline practice vs. performance [7], [10], alternative educational methodologies, in the form of training simulators, have been explored and implemented to allow for progress along the thoracentesis learning curve for residents [44]-[49]. The effectiveness of these simulators however, is dependent on their fidelity [21]-[23]. To determine criteria by which to evaluate simulator fidelity, patient demographics were analyzed.

## 1.2.2. Demographic and Design Constraints

178 000 thoracenteses are performed on patients with pleural effusions in the United States annually [50]. This population can be broken down into sub-groups based on age and physical constitution in terms of thoracic wall thickness. Mynarek et al. explored the age distribution of patients and showed that there is a skewing of the population towards the 40-70-years age groups, with a peak in the 50-59 years' group (Figure 1.2.2-1, in red), which includes 22% of cases reviewed in the study. A notable spike is observed however, in the 0-9 years' age group, representing 19% of the thoracentesis-requiring population (Figure 1.2.2-1, in red) [51]. Despite this, the majority of the simulators further analyzed in Table 1.2.2-1 (Chapter 1.2.3) are designed to simulate the average adult male, representing a mere 8.2% of the population of the study (Figure 1.2.2-1, in green).
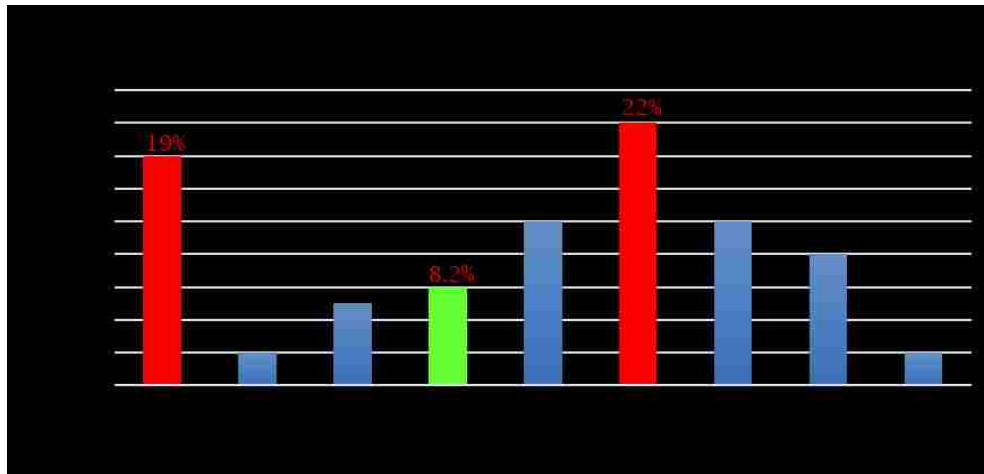
**Figure 1.2.2-1: Thoracentesis age distribution (adapted from [51])**

While these simulators have been proven to be effective for the demographic they represent [48], [49], they fail to represent the majority of the thoracentesis-requiring demographic. This is problematic because these younger (0-9 years of age) patients may be more susceptible to infection than adults, as pneumonia is the leading cause of pleural effusions in children [52]. Anxiety also poses a problem for thoracentesis with children due to the invasive and painful nature of the procedure; flinching and trembling are common, which may increase the likelihood of error [53]. The potential severity of these nervous reactions is so significant that it frequently requires the administration of drugs to calm patients [53]. Practicing on an adult-sized simulator, which does not represent this age group's skeletal anatomy, may not adequately prepare the resident for the execution of the procedure, nor may it quell any anxiety associated with performing the procedure on a patient more susceptible to infection. Based on a conservative estimate, which does not take into account the potentially elevated error percentages due to these factors (anxiety, flinching, etc.), approximately 10,000 thoracenteses performed on children in the United States are subject to

some sort of complication (Eq. 1). This estimate is based on average error rates for new residents performing the procedure (30%) [40], total annual U.S. thoracenteses performed (178,000) [50], and the percentage of the demographic represented by children (19%) [51].

Eq. 1)

$$(0.19) * (0.30) * (178,000) = 10,146$$

When performing thoracentesis one of the key success criteria is the depth of needle insertion. There are organs which can be punctured, including the lungs [54]. A study by Harcke et al. outlines the thickness of the thoracic wall among military personnel of similar fitness levels, where a range of 3.07cm to 9.35cm was found within an age range of 10 years (horizontal needle insertion) (Figure 1.2.2-2), [55]. For normal insertions (representative of proper thoracentesis procedure) a range of 2.66cm to 8.02cm was found. Additional reporting on thoracic wall thicknesses from Jones et al. [56] describes a lower range of 2.40cm, further expanding the range of tissue thicknesses. Figure 1.2.2-2 highlights key regions encompassing the extremes of the thoracic wall thicknesses.
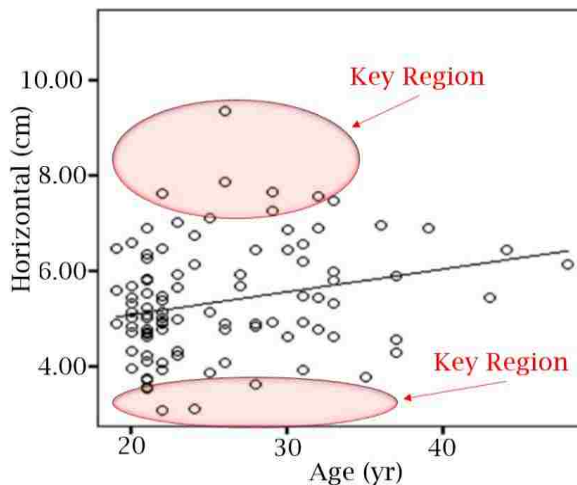


Figure 1.2.2-2: Chest wall thickness in military personnel (adapted from [55])

The variation in thoracic wall thickness is further amplified by Canadian obesity rates [57]. Data from the Childhood Obesity Foundation show that more than 59% of adults and 26% of children from ages 2-17 are overweight or have obesity. The distribution of children with obesity in the United States is detailed in Figure 1.2.2-3 [58].
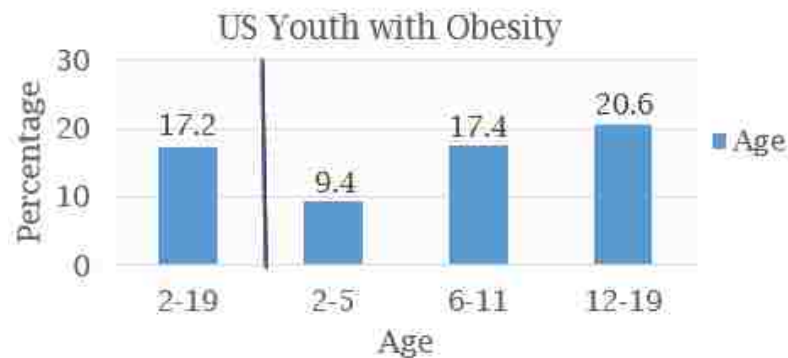


**Figure 1.2.2-3: U.S. youth with obesity (adapted from [58])**

Furthermore, congestive heart failure (CHF), which is linked to obesity, is the leading cause of pleural effusions requiring thoracentesis, with 33% of pleural effusions being attributed to CHF [59].

Based on patient demographic characteristics and outlined procedures, 3 elements are influential on simulator fidelity. These three elements are:

- Skeletal completeness; ability to properly perform the palpation procedures outlined by the United States Marine Corps [32] and Berg et al. [33].
- Skeletal scale; ability to represent patients of different sexes and ages, outlined by Mynarek et al. [51].

10

- Tissue re-configurability; ability to represent patients with varying thoracic wall thicknesses, and varying tissue compositions (i.e. varying musculature and adipose tissue thickness), outlined by Harcke et al. [55], Jones et al. [56] and the NIDDKD [57].

With key factors for evaluating simulator fidelity, an analysis was performed to determine whether or not currently available simulators adequately represent the characteristics of the thoracentesis-requiring demographic (Table 1.2.2-1). In this table, a score of 5 indicates complete fulfillment of the category, 4 indicates complete fulfillment of category, but lacking quality or accuracy. A score of 3 is indicative of fulfillment of most of the necessary elements, with reasonable accuracy. A score of 2 is indicative of minimal fulfillment of the category, with partial visual realism. A score of 1 indicates a very poor fulfillment of the category, with poor accuracy and completeness, while 0 indicates no fulfillment whatsoever.

**Table 1.2.2-1: Thoracentesis training simulator fidelity assessment scores**

| Model & Maker | Image | Skeletal Completeness (/5) | Tissue Reconfigurability (/5) | Patient Demographic Representation (/5) |
|---|---|---|---|---|
| Thoracentesis and Thoracostomy Ultrasound Model<br><br>Blue Phantom | [24] | 1<br><br>No clavicle, no scapula | 0<br><br>Single layer, non reconfigurable | 2<br><br>Only available in one size; 30-50 yr. male |

| | | 2 | 0 | 1 |
|---|---|---|---|---|
| THM-30<br><br>SIMULAB | [25] | No clavicle, flat ribs, scapula 24.4% shorter than simulator target patient representation | Single layer, non reconfigurable | Only available in one size; 18-100 yr. adult (no sex is given) |
| Adult Thoracentesis Simulator<br><br>MEDIQUIP | [26] | 3<br><br>No clavicle | 0<br><br>Single layer, non reconfigurable | 2<br><br>Only available in one size; 30-50 yr. male |
| Ultrasound-Guided Thoracentesis Simulator-Strap-On Set<br><br>ERLER ZIMMER | [27] | 2<br><br>No clavicle, no scapula | 0<br><br>Single layer, non reconfigurable | 1<br><br>Only available in one size; 30-50 yr. adult (no sex is given) |
| MW4: Ultrasound Guided Thoracentesis Simulator<br><br>Kyoto Kagaku America Inc. | [28] | 2<br><br>No clavicle, no scapula | 0<br><br>Single layer, non reconfigurable | 2<br><br>Only available in one size; 30-50 yr. male |
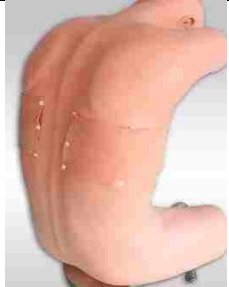
Through this analysis of current models, it has been determined that the palpation sequence (List 1) [32], [33] cannot be properly executed, due to a lack of key anatomical landmarks including the scapula or clavicle in certain models. The varying ages (and associated statures) of patients requiring thoracenteses are not accounted for, as all simulators analyzed are only available in one patient

configuration, representing 8.2% of the total demographic [51]. Variations of thoracic wall thickness are not accounted for in current simulators analyzed [55]-[57]. It was also noted that most models have a single-layer tissue, whereas the human thoracic cross section contains 4 discrete layers (skin, adipose tissues, muscle, pleura). Multiple-layer interactions, particularly those involving the skin, are influential on needle insertion resistances [59], [60]. The implications of the single-layer representation in the THM-30 are detailed in Chapter 3.2, where a cadaveric and THM-30 simulator needle insertion experiment is presented. To summarize, the experiment concludes that two layers of simulated tissue are necessary to accurately represent the human thoracic cross section. This experiment also serves to provide key needle insertion resistive forces for human tissues, which were unavailable in the literature.

The implications of the lack of patient demographic representation (fidelity) in currently available simulators are explained by Issenberg et al. [62], who determined that simulators capturing multiple clinical scenarios (i.e. healthy child, vs. overweight adult) are more beneficial to the user than those capturing few, emphasizing the importance of a versatile, adaptable simulator.

## 1.2.3. Design and Fabrication Strategies and Limitations

Currently, thoracentesis training simulators are produced by machining and moulding processes [63], [64]. Manufacturing using these conventional means is efficient in terms of mass production of elements [65]-[67]; however, these techniques often require significant product and process knowledge beforehand, given the time and overhead needed to design and fabricate mould sets [66], [68]-[70]. These processes involve static designs and fabrication moulds, which are

13

difficult to change after initial completion [71]. The implications of this approach are simplified, low fidelity and static models such as the THM-30 (SIMULAB), which is the model currently in use at the Schulich School of Medicine & Dentistry-Windsor Campus, and the model used for comparisons in this study [25].

Technological advancements have led to alternative design and fabrication tools and techniques, specifically additive manufacturing (AM) and parametric computer-aided design (CAD). These tools and techniques have been established in the automotive and other industries, and are gaining in popularity in the medical community [72]. Lichtenberger et al. implemented CAD and AM in the development of medical training simulators for ultrasound-guided joint injections and nerve block injections, noting that customizability to represent specific patient types was facilitated, due to the flexibility of the CAD files in terms of overall detail and features [73]. No such strategies have been applied in the development of thoracentesis training simulators, however similarities between the simulators developed by Lichtenberger et al. and thoracentesis training simulators (i.e. needle insertion apparatuses, with silicone tissues and static skeletal structures), indicate that the implementation of CAD and AM may be beneficial in the development of a thoracentesis training simulator thoracic wall.

## 1.3. Problem Statement

Medical training simulators offer an effective means of progressing along the learning curves for clinical skills without subjecting patients to elevated risk associated with a lack of experiential learning [7]-[11], [12], [14]. However, for simulators designed for force perception purposes, such as thoracentesis needle

insertion simulators, high fidelity models yield better training results [23]. Current thoracentesis simulators are insufficient in terms of patient demographic skeletal size representation, anatomical landmark palpation capabilities, and tissue representation. This lack of fidelity can be attributed to the conventional means by which these simulators are designed and fabricated [63], [64].

## 1.3.1. Hypotheses

The aim of this research is to address the shortcomings of currently available simulators by implementing a flexible CAD- and AM-centered methodology to design and fabricate a high fidelity thoracic wall representation. Hypotheses pertaining to an increase in thoracic wall fidelity are:

$H_1$: Tissue re-configurability (ability to be modified to represent different characteristics) will be achieved in terms of tissue thickness, and needle insertion resistive properties of the cadaver subject will be replicated by obtaining experimental needle insertion data from a cadaver patient, and implementing a variable-hardness silicone.

Thoracic wall thickness has been shown to be highly variable, ranging from 24mm to 80.2mm [55], [56], within an age group of 10 years; not accounting for obesity rates [57]. Needle insertion forces are dependant on tissue layer composition, and thickness [59], [60]. Conventional simulators do not account for the variation in tissue thickness, and no literature is available which documents the needle insertion force properties of a thoracic wall. The implementation of parametric relationships into custom mould sets is expected to allow for the development of a reconfigurable model, in terms of thoracic wall thickness.

Needle insertion forces of the thoracic wall developed in this thesis are expected to more accurately represent the characteristics of a cadaver subject, than the THM-30 training simulator. To measure this, needle insertion experiments will be performed.

$H_{1.1}$: Simulated thoracic wall representations require more than one artificial tissue layer to represent the cadaver subject.

Literature describing interactions of layers with each other is indicative of a potential oversimplification of the 4-layer human thoracic wall with a single uniform tissue layer; as is the currently available simulator standard. The dominance of skin on insertion forces (peak force, in particular) is described in the literature, further reinforcing the theory behind the need for more than one simulated tissue layer [59], [60].

$H_{1.2}$: Furthermore, it is hypothesized that the needle insertion property representation of the THM-30 simulated tissue will be statistically different than the cadaver subject in terms of peak force (N), impulse (N·s) and pulse width (s).

Due to single layer constitution and the absence of skin [59], [60], as well as an overall lack of tissue thickness [55], [56], it is expected that the THM-30 will not provide sufficient resistance to needle insertion to replicate realistic human needle insertion procedures.

While not a hypothesis, it is speculated that anatomical landmark palpation capabilities will be improved as a result of incorporating a clavicle to the skeletal assembly, and appropriately sizing models. This speculation is based on thoracentesis palpation procedures which outline key reference anatomy for the determination of optimal needle insertion site [32]. These elements include the mid-clavicular line, which is dependant on clavicle length. Palpation down 1-2 intercostal spaces from the inferior angle of the scapula is necessary to determine appropriate needle insertion level, however currently available models seldom have a scapula, and if so, are typically improperly sized for the target patient representation [51]. The maintaining of anatomical reference relationships (scapula's inferior angle's correlation with the 7th intercostal space [35]-[37]), the appropriate sizing of the clavicle, and intercostal space width are the quantified measures, and are expected to facilitate proper palpation procedure.

## 1.4.    Methodology Overview

Educational training tools serve to enable clinicians to perform procedures more effectively, increasing patient safety [17]. In order to provide optimal training, product features and constraints must be determined with an understanding of human physiology and the dynamics of the human system. Thus, biomechanical engineering solutions require the integration of human physiological and anthropometric data, as well as collaboration with medical experts to ensure that the design will meet the needs of the user and patient [74].

Biomechanical solutions to medical problems are becoming increasingly popular due to their ability to address problems in different ways. Using a

biomechanical approach centered on advanced CAD and AM techniques, splints and braces [75] have been created to alleviate a variety of issues, including arthritis and degenerative musculoskeletal disorders [76]. Applications extend to incorporation in surgery [77], modelling and recreating organs [78], as well as to developing educational training models [73]. Using these tools, complex devices can be designed, fabricated, updated and refined, avoiding long design and fabrication times associated with conventional methods [80]. While these engineering tools provide the ability to rapidly prototype and customize, they must be coupled with medical insight to appropriately address the complexity of medical applications. Knowledge from the medical field of study, combined with human physiological data are integrated into Engineering technology-driven design and fabrication processes. Incorporating anthropometric and experimentally-obtained data, along with medical design constraints (patient characteristics) from the literature into a unified solution serves to identify key features and constraints. Once constraints and features are identified, flexible CAD and AM tools are used to design and fabricate a thoracic wall representation for a thoracentesis training simulator of higher fidelity than currently available. This cross-disciplinary approach is to ensure that appropriate product features and constraints are defined early in the design process, and can be effectively implemented into final products. The approach taken in this study is detailed in Figure 1.4-1, which represents an expansion on previous work by Kalami et al., who utilized a similar approach to develop custom-fitted finger exo-skeleton braces [75].
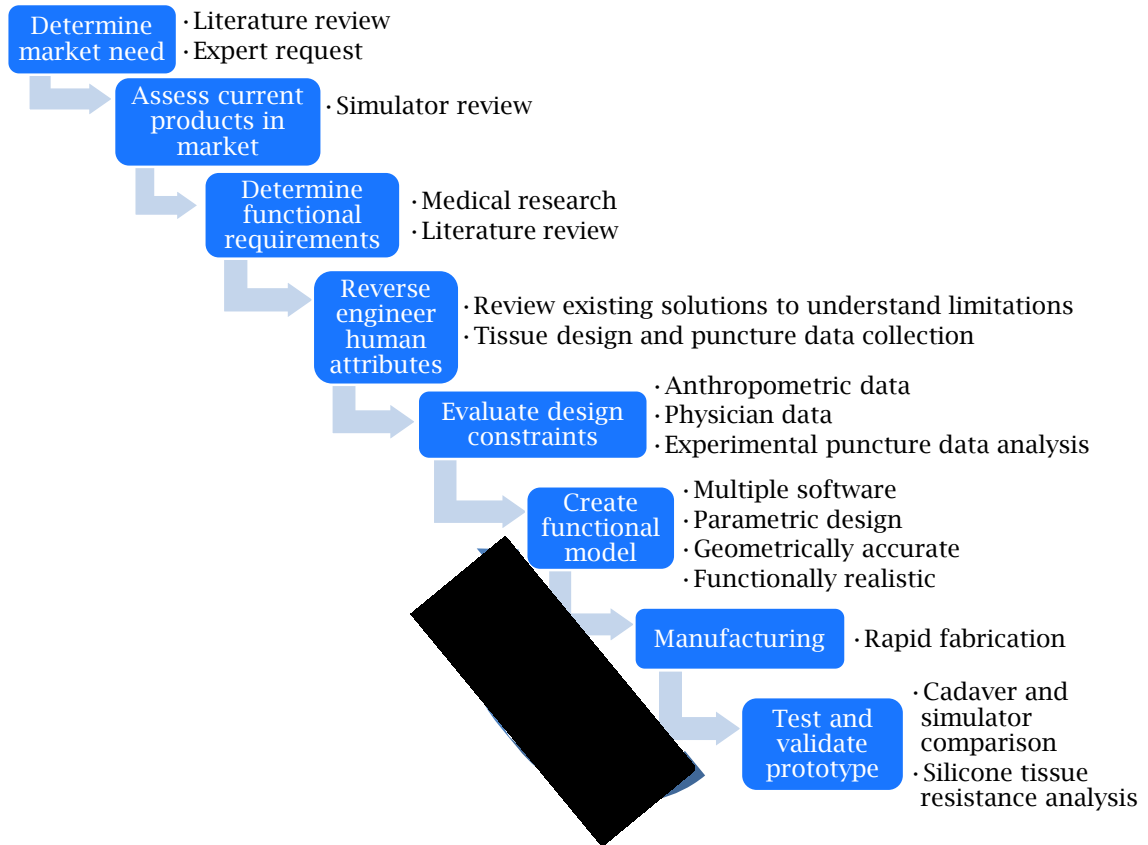
**Figure 1.4-1: Design and fabrication approach for the development of a reconfigurable thoracentesis training simulator (adapted from [75])**

The effectiveness of this approach lies in leveraging the synergy of these design and fabrication tools rather than the capabilities of the individual tools alone. By implementing an alternative dynamic design and fabrication process, a high fidelity thoracic wall representation with reconfigurable tissues was developed and evaluated. Final element evaluation was performed by comparing the elements developed in this research, the model currently in use at the Schulich School of Medicine & Dentistry-Windsor Campus [25], anthropometric data from the literature, and experimentally-obtained cadaveric needle-insertion data. Anatomical palpation capabilities (i.e. skeletal completeness with respect to palpation sequence), skeletal scale accuracy (i.e. clavicle length for a 2 yr. old

19

male) and tissue needle insertion characteristics (i.e. resistive forces, tissue thickness) were compared to determine whether the elements developed with the methodology outlined in Figure 1.4-1 are of superior fidelity to the THM-30 simulator [25]. Design re-configurability was verified by comparing anatomical landmarks of various target patient representations, and overall process time and cost was compared to estimated conventionally-acquired results from a local moulding company [79].

## 1.5.   Project Scope

Key elements to improving the overall fidelity of a thoracic wall representation, specifically, the skeletal structures and tissues, are shown in Figure 1.5-1.
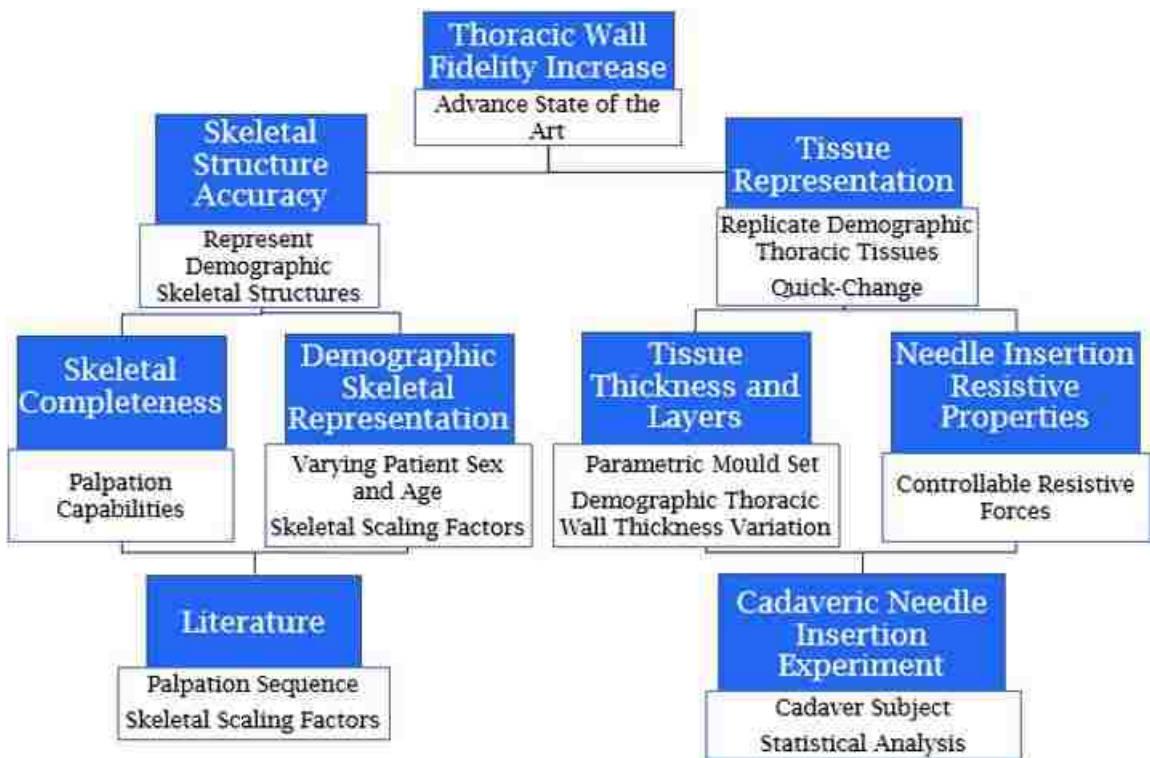


**Figure 1.5-1 Project scope for thoracentesis training simulator thoracic wall fidelity increase**

Literature on training simulators [23], thoracentesis procedure [32], [33] and patient demographic [51], [55], [57] demonstrates a need for an increase in fidelity with respect to tissues (force-perception aspect) and skeletal structures (for landmark palpation and patient size representation) [51]. Furthermore, a more flexible design and fabrication approach is needed in order to facilitate the development of subsequent iterations on the models, to represent the variations in demographic physical characteristics [51]. These are addressed in two forms; the first being parametric design and scaling factor implementation, and the second being a quick-change element for final product tissue interchangeability.

## 1.6.    Motivation

The initial attention to thoracentesis practice and simulators outlined in this study came from a request from Anna Farias (lead anatomist at the Schulich School of Medicine & Dentistry-Windsor Campus, leader of a medical team comprised additionally of Lakshmi Kamala and Sarah Zhang, also from the Schulich School of Medicine & Dentistry-Windsor Campus) [81] for a better simulator. From the literature, thoracentesis procedures are subject to elevated error rates, with up to 30% of thoracentesis procedures performed by new clinicians having complications [40]. In a study performed by Bari et al., 40% of new residents who had recently performed a clinical error attributed them to a lack of experience with the procedure being performed [6]. In response to these error rates, thoracentesis training simulators have been implemented into medical curricula, and have helped improve performance through experiential learning [48], [49]. However, simulators which have a force-perception aspect (i.e. needle insertion thoracentesis) benefit from high fidelity [23]. Upon analysis of

currently available thoracentesis training simulators (Table 1.2.2-1), it has been determined that they do not sufficiently represent the patient demographic in terms of tissue thickness or layer composition [55], [57], skeletal size variation [51], nor are they anatomically complete in terms of skeletal landmarks (i.e. clavicle, scapula) according to outlined palpation procedures (List 1) [32], [33]. The need for better training simulators for medical residents is the driving force for this research, in hopes of reducing the error rates associated with this procedure, and improving overall patient safety.

## 1.7. Document Map

Chapter 2 presents a review of all literature necessary to understand the limitations of current thoracentesis training models, medical training as a whole, as well as key information influential on design and fabrication strategies.

Chapter 3 presents a detailed methodology of how the design and fabrication constraints determined through the literature review, as well as a cadaveric needle insertion experiment, are incorporated into a dynamic system, centered on CAD and AM techniques.

Chapter 4 presents final products of the skeletal and tissue design and fabrication strategies, as well as comparisons between the elements developed with the proposed approach, the conventionally-developed simulator [25], and a cadaver subject.

Chapter 5 contains limitations of this thesis, along with a summary of contributions to the field, future work, and conclusions drawn.

# CHAPTER 2
## Literature Review

## 2.1. Procedure Specifics and Patient Characteristics

A standard thoracentesis procedure is outlined by Pulmonary Central [82] and the John Hopkins Medical Health Library [29], however specialists often deviate slightly per their personal preference and case specifics (i.e. patient scarring, physical restrictions) [83]. The effects of the variability in execution of this procedure are theorized to be statistically insignificant; however, no study has been performed to determine the impact of the slight deviations on a large scale. Detailed procedural checklists have been developed by the United States Government [32] and Berg et al. [33], and are presented in List 1, in Appendix A. There are typically 3 patient postures preferred for the procedure [84]:

- Seated, leaning forwards, with arms suspended onto a table
- Lying on bed, with arm up and behind head
- Lying on side, with arms resting under head

The seated position is the most commonly used, as it allows for the spacing out of the ribs to allow for easier needle insertion, as well as improving overall patient comfort [29], [85].

Ultrasound guidance may be used during thoracentesis procedures, as it allows for more accurate fluid level determination, as well as a reduction in overall error rates [86]. However, this is not yet universally performed, as it requires an additional skilled technician, as well as the ultrasound equipment itself [87]. Manual palpation however, is performed in all thoracentesis

procedures. This is done to determine the insertion site, as well as to identify landmarks influential on insertion technique, including the lower edge of the ribs, which must be avoided, as they are surrounded by neurovascular bundles [34], [39]. A simplified summary of the procedure is seen in Figure 2.1-1 [82], and a summary of the unassisted posterior palpation sequence is in Figure 2.1-2 [29], [34]-[39].
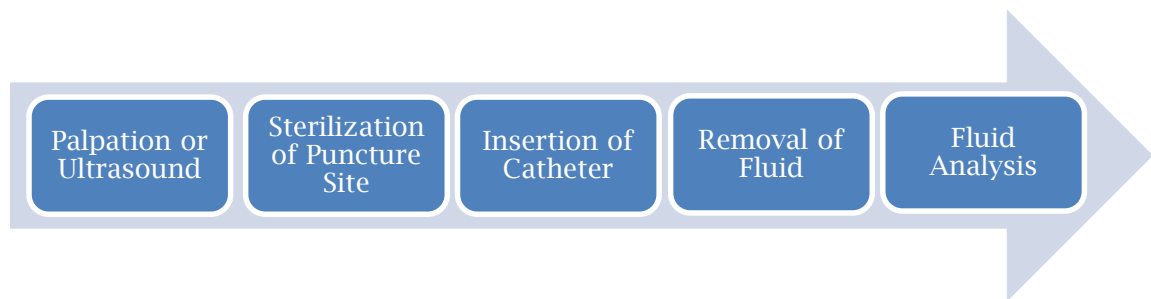


Figure 2.1-1: Summarized thoracentesis procedure [29], [30], [34]-[39]
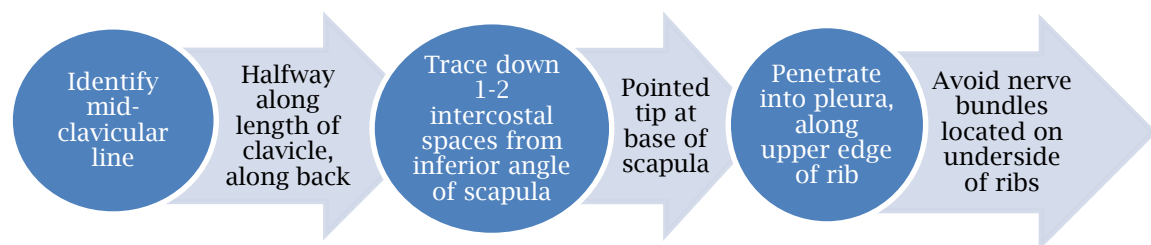


Figure 2.1-2: Summarized thoracentesis palpation sequence [29], [32]-[39]

Thoracentesis patient age demographic has been outlined by Harcke et al. [55], with spikes in the 0-9 years of age (19%) and 50-59 years of age (22%) groups. The variations in patient stature are exemplified by Weaver et al. [88], who used computed tomography (CT) scans to track landmarks, determining that the rib cage grows significantly from 6 months to 20 years of age. Growth slows between 20-30 years of age, and overall rib cage size remains relatively constant between 30-100 years of age (Figure 2.1-3). The results are reinforced by Subit et al., who

found that the growth of the ribs between 0-20 years of age can be approximated as linear, before approaching a plateau in adulthood [89].

| Age | Size |
|---|---|
| ⬛ → 3 Years<br><br>🫒 → 20 Years<br><br>🟡 → 30 Years<br><br>🟠 → 50 Years |  |
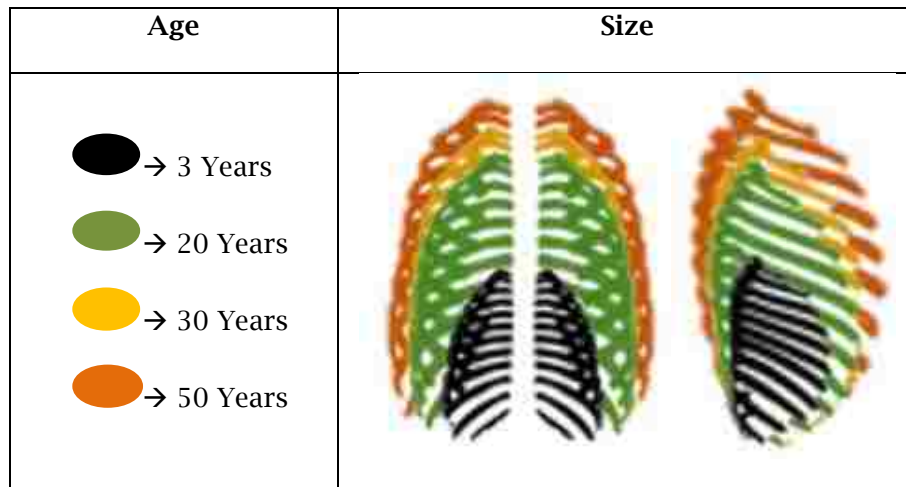
**Figure 2.1-3: Rib cage growth from 3 years to 50 years of age (adapted from [88])**

While specific growth rates for the rib cage are not detailed in the literature, Figure 2.1-3 illustrates that the overall size of a young patient from the 0-9 years' age group is visibly considerably smaller from the age group represented in the majority of thoracentesis training simulators (30-39 years old), and even more so from the most common age group for thoracentesis procedures, the 50-59 years' old group (Figure 2.1-3). Intercostal space measurements for children are not clearly documented in the literature, however data for adult males and females are documented by Kim et al. [90], showing mean values of 14.9mm ± 3.6mm for males and 14.2mm ± 3.5mm for females. Measurements were taken along the posterior axillary line, in the 9th intercostal space (Figure 2.1-4).
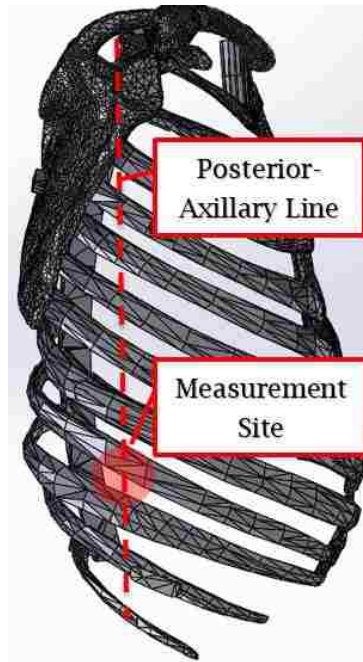
**Figure 2.1-4: Intercostal space measurement site**

McGraw et al. [91] analyzed digital chest radiographs of males and females from birth to 18 years of age, and found that females achieve approximately 80% of clavicle length by 9 years of age, while males achieve this growth percentage by 12 years of age (Figure 2.1-5). Furthermore, the growth was found to be approximately linear up to 12 years of age for both males and females (8.4mm/yr.). Beyond 12 years of age, growth rates differ based on sex, but remain linear (5.4mm/yr for males, 2.6mm/yr for females). No significant difference was observed between the lengths of the left and right clavicle in normal patients. McGraw et al. also described mean clavicular lengths for adult males and females, being 161.29mm ± 10.69mm, and 149.16mm ± 12.2mm, respectively.
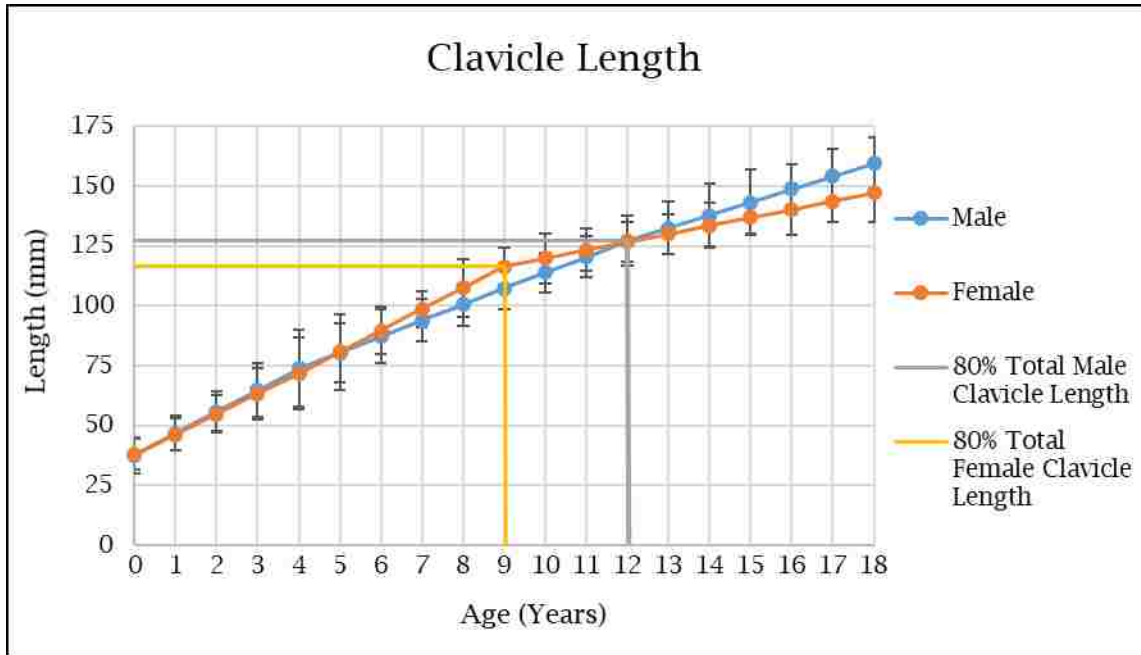
**Figure 2.1-5: Growth of male vs. female clavicle from 0-18 years of age (adapted from [91])**

The growth rates of the scapula, which is a key landmark for palpation (Figure 2.1-2), are not clearly described in the literature. However, through analysis of medical images and literature, Cunningham et al. [92] found that full growth of the scapula is typically achieved by 23 years of age. Sobush et al. [35], the Loyola University Medical Education Network [36], and Lewandowski [37] found that the inferior angle (pointed base) of the scapula (Figure 2.1-2) is consistently located at the 7-8th intercostal space, maintaining this relation to the rib cage, regardless of growth. This relationship is further reinforced by Canavese et al., who performed a comprehensive review of the literature, and summarized that the various skeletal structures in the thoracic cage may grow at slightly different rates, but maintain functional skeletal relationships (and therefore, relative positioning to each other) regardless of age or size [93]. These summaries indicate that although the rate of growth of specific structures varies slightly, the relative positioning of landmarks remains consistent.

27

## 2.2. State of the art

Conventionally, medical residents are taught thoracentesis skills in a three-tiered approach, outlined in Figure 2.2-1 [94]. However, thoracentesis error rates ranging from 11% to 33%, outlined by Berg et al. [33], Brauner et al. [40] and Seneff et al. [95] have led to the development of thoracentesis training simulators [24]-[28]. These simulators have been implemented into medical curricula in an attempt to provide experiential training for residents prior to performing the procedure on real patients [18], [48], [49].



**Figure 2.2-1: Conventional procedural skill training methodology for thoracentesis [94]**

The effectiveness of currently available thoracentesis training simulators as a means of allowing for clinician progress along the learning curve has been investigated by Jiang et al. [48] and Wayne et al. [49]. Wayne et al. showed the improvements in written (32.12%) and clinical (36.6%) skills exams after a 4-hour training session, incorporating a thoracentesis training simulator (Figure 2.2-2) [49].
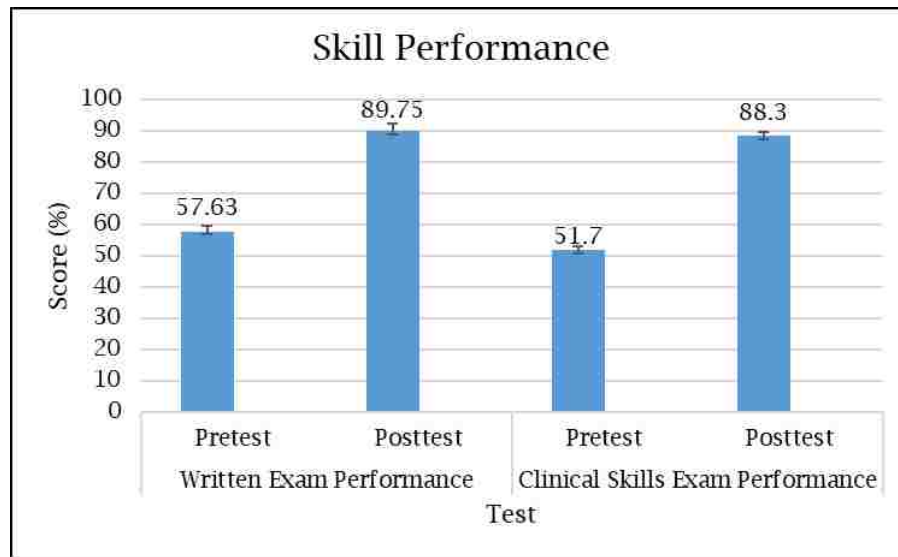
**Figure 2.2-2: Skill performance pre and post-test (adapted from [49])**

Jiang et al. investigated the knowledge and skill retention of residents trained with thoracentesis training simulators. By conducting a brief training session, followed by a 5-run trial, scores on procedure time (PT), performance score (PS), and participant's confidence (PC) were graded immediately, at the 6-month mark, and again at the 1-year mark. Results indicated significant improvement in all three categories, particularly in the first 3 tests. Approaching the 4th and 5th test, scores migrated towards a plateau, indicating full understanding and skill mastery. Retesting at the 6-month mark yielded results similar to the 4th and 5th tests, indicating a relationship between the use of the simulators for training and skill and knowledge retention. Comparing performance of residents trained with the simulator, against those who had no such training one year later showed superior performance in the trained group. Results for the PS, PC, and PT tests are shown Figure 2.2-3, Figure 2.2-4 and Figure 2.2-5 [48].
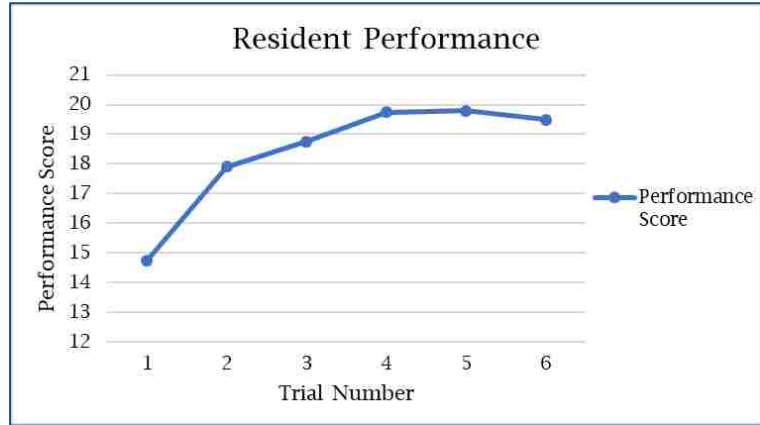
**Figure 2.2-3: Performance score on 5 test trials, as well as the 6th (retest) (adapted from [48])**
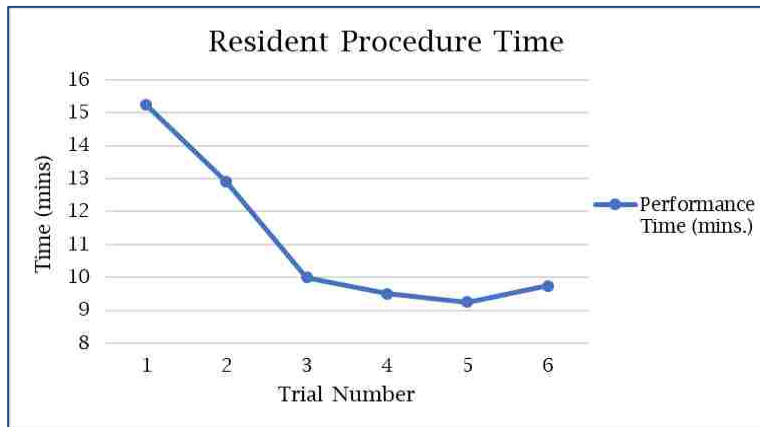


**Figure 2.2-4: Performance time on 5 test trials, as well as the 6th (retest) (adapted from [48])**
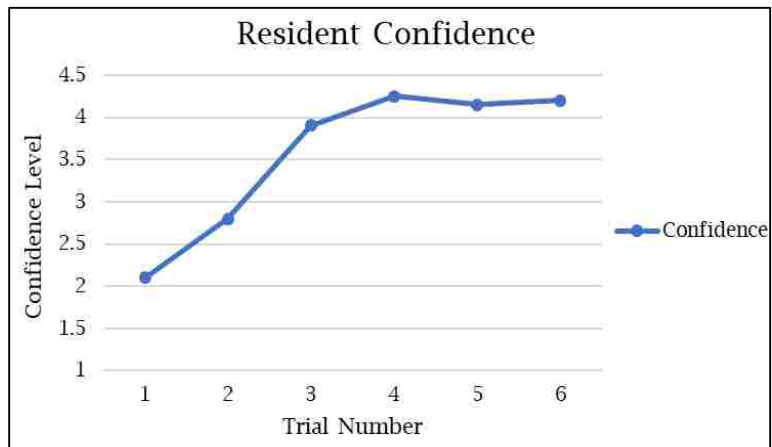


**Figure 2.2-5: Performance time on 5 test trials, as well as the 6th (retest) (adapted from [48])**

Most participants stated that four trials were sufficient for proper understanding and confidence performing this procedure. Concluding statements from the study indicated that clinical competency in first year medical residents who received simulation training was superior to those who did not [48]. These studies reinforce Berg et al.'s [33] claims that practical training improves long-term skill and knowledge retention. With the use of training simulators, residents no longer need to practice on patients to achieve skill mastery. Furthermore, thoracentesis training simulators have been well received by residents, as shown by a study by Shanks et al., where 94% of residents felt that simulators should be used to learn technical skills for thoracentesis, and 89% felt that supervised practice and feedback with the simulator would be beneficial as well [47].

While thoracentesis training simulators have proven to be effective, it must be noted that all results are based on training and evaluation on the *same* training simulator, with *identical* physical characteristics (i.e. tissue thickness, skeletal size, etc.) [49]. This is problematic due to the variations in patient physical characteristics deemed influential on thoracentesis procedures, previously described in Chapter 1.3 and further exemplified in Mynarek et al. [51] and Harcke et al.'s [55] studies, which outline the variations in age and physical characteristics of patients undergoing thoracentesis procedures. With varying physical statures, ranging from underweight to obese, and a demographic encompassing new-borns to the elderly, key haptic cues (needle insertion depth, needle insertion resistive forces, intercostal spacing) for the procedure itself vary from patient to patient. Currently available thoracentesis training simulators do not account for many factors outlined in the literature, including:

- Skeletal landmark completeness for palpation [32], [33]

- Skeletal size associated with age and sex (overall scale of patient representation) [51]

- Varying tissue thickness associated with stature and obesity [55], [57]

- Tissue needle insertion resistance properties

As the aim of this thesis is to improve patient thoracic wall representation in simulators, a quantitative analysis of a popular model, the THM-30 [25] was performed, to provide a baseline for comparison to elements developed in this study (Figure 2.2-6, Table 2.2-1). Values from the literature are from anthropometric tables and other studies which present information on patients of the same target representation as the THM-30 (adult, approximately 30 yrs. of age (unspecified by manufacturer)).
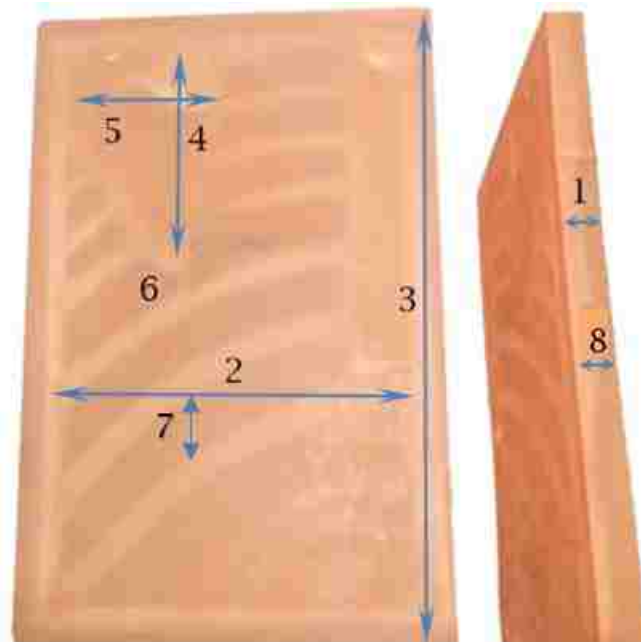


**Figure 2.2-6: THM-30 Numerical measurement references**

Table 2.2-1: THM-30 Property Comparison to Literature Values for Adult

| Characteristic | Number | THM-30 | Literature | % Difference |
|---|---|---|---|---|
| Thoracic wall thickness (mm) | 1 | 20.3 | 24-80.2 [55], [56] | 16.7-77.4 |
| Chest breadth (mm) | 2 | 177.8 | 170.5 ± 1.5 [96] | -4.28 |
| Overall thoracic cage height (mm) | 3 | 267.0 | 315 ± 79.9 [96] | 15.2 |
| Clavicle length (mm) | N/A | N/A | 161.3 ± 10.7 [91] | |
| Scapula height (mm) | 4 | 114.5 | 151.4 ± 11.4 [97] | 24.4 |
| Scapula width (mm) | 5 | 76.2 | 102.4 ± 6.6 [97] | 25.6 |
| Inferior angle-corresponding intercostal space | 6 | 4 | 7 [35]-[37] | |
| 9$^{th}$ Intercostal space width (mm) | 7 | 27.5 | 14.9 ± 3.6 [90] | 84.6 |
| # of ribs | N/A | 9 | 12 [98] | 25 |
| Thoracic index (thoracic depth/thoracic width) | N/A | 0 (flat) | 0.75 [99] | |
| Needle insertion resistive force (N) | N/A | N/A | N/A | |
| # of tissue layers | 8 | 1 | 4 [100] | 75 |

Elements from Figure 2.2-6 and Table 2.2-1 influencing the factors which are not accounted for in current simulators, which will be discussed in Chapter 2.4, are:

- Thoracic wall tissue thicknesses
- Clavicle and intercostal space length/width
- Scapula height inferior angle corresponding intercostal space
- Needle insertion resistive forces

These elements are key factors which must be incorporated into the design approach. To address the issues outlined through the comparison of the THM-30, other simulators, and factors deemed influential on thoracic wall fidelity from the literature, a review of design and fabrication methodologies for training simulators was performed.

33

Conventional design and fabrication strategies include stamping, machining, and injection moulding [101]. While effective for the mass production of parts, the small-batch production of parts with varying geometries (i.e. to represent the thoracentesis demographic with drastic physical differences between patients) is difficult. The THM-30 thoracentesis training simulator [25] is an example of a product developed with these conventional methodologies, as exhibited by the product features typical to injection moulded parts; including perimeter flash (number 1; Figure 2.2-7) and residual signs of mould gates (number 2; Figure 2.2-7). Flash is residual liquid material which has seeped into cracks between the two mould plates (parting line) caused by a variety of reasons, including improper mould alignment, improper mould pressure, or improper venting, and is common in the injection moulding of liquid silicone parts which exhibit lower viscosities than other materials [102], [103]. Edge gates, which are the most common type of gate used for flat parts with two halves (indicated by the parting line around the perimeter), leave a "scar" on the surface of the part, which is caused by residual material from the injection process [104].
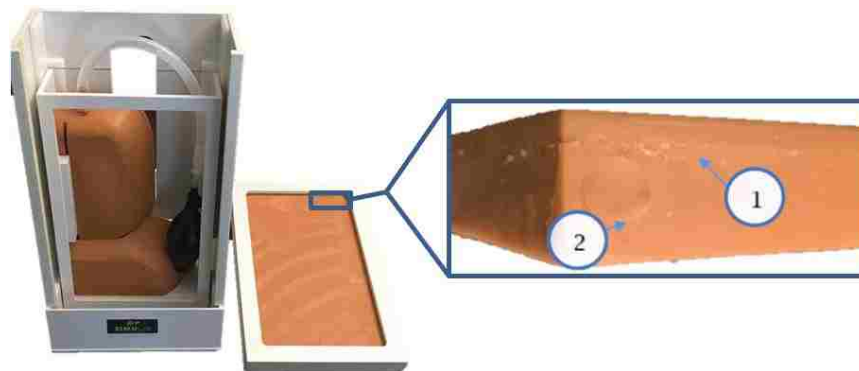


**Figure 2.2-7: Signs of injection moulding on THM-30 thoracic wall representation**

## 2.3. Additive Manufacturing and Computer-Aided Design in the Medical Field

Technological advancements, particularly in the fields of CAD and AM, enable the design and fabrication of increasingly adaptable and complex parts. The implementation of CAD and AM into the medical field shows promise, with the versatility of these tools and techniques being exemplified by the varying successful applications, ranging from the development of patient-specific surgical implants and prostheses, to detailed anatomical models, as described by Ventola et al. [78].

The customizability of products developed using CAD and AM is of notable benefit to the representation of patients, specifically for the purpose of medical training simulation. Malyala et al. reconfirmed the versatility of CAD and AM in the medical field previously demonstrated by Ventola et al. [78], and developed patient-specific surgical training models from computed tomography (CT) and magnetic resonance imaging (MRI) files [77]. These studies demonstrate the ability to utilize medical imaging files (CT, MRI) to develop physical models with varying physical characteristics. The versatility in terms of patient representation is further exemplified by Lichtenberger et al.'s development of nerve block and joint injection simulators [73]. These simulators, developed using AM and CAD, demonstrate the potential effectiveness of these tools for the development of a thoracentesis training simulator, as the models both contain skeletal structures fabricated with AM processes, which are encased in silicone tissues and shaped in custom moulds.

In the development of these simulators [73], [77], several trends were observed. CT scan files were frequently used to generate CAD models for skeletal structures, as they provide accurate representations of patient anatomy [77]. These models were typically simplified to reduce on computational intensiveness (i.e. processing time and power needed to manipulate models), due to software limitations described by Chwatko et al. [105], specifically; meshing element limits. This was performed by modifying the object (.obj) files, which provide a detailed representation of surface geometry from the medical scans, in the form of triangulated surface meshes [106]. These modifications typically involve taking an average of the triangulated surface meshing elements, or removing unnecessary skeletal structures entirely. Model simplification and mesh refinement is further detailed by Bucking et al. [107], who describe the process of converting medical imaging data to anatomical models with CAD and AM. The smoothing operations are performed to reduce roughness in surface representations of smooth features caused by low-resolution medical scan uploads. To smooth these rough surfaces, multiple software can be used, including Autodesk Meshmixer [108], Windows 3D Builder [109], and FreeCAD [110]. Files can then be converted to formats which are modifiable in CAD software, including .step, .stl, or other software-specific file types. Typically, software selection is based on software capabilities and operator proficiency. Commonly used software include Catia V5 [111] (Antunes et al., modelling of foot skeletal and tissue models) [112], Solidworks 2016 [113] (Chwatko et al., modelling of right hip) [105], and Autodesk NetFabb [114] (Olszewski et al.), modelling of mandible [115].

Parametric relationships are defined between dimensions, surfaces and or features to enable geometry to change or adapt automatically, in response to a change of another feature or dimension [116]. While these relationships have not been incorporated into CAD models for use in the development of medical training simulators, they are frequently used in automotive and industrial systems design [117]-[119]. Shah et al. [117] and Camba et al. [119] demonstrate the incorporation of parametric relationships into industrial design systems to reduce on redesign time and difficulty. The key highlight from these studies is the reduction in redesign time to represent similar systems, with a focus on "design reusability". This reusability is demonstrated by the manual alteration of a dimension or feature, followed by the automatic reconfiguration of the system to accommodate the change. This automatic alteration of the system geometry holds promise for implementation in a custom moulding set, which could be readily modified to provide different silicone tissue dimensions. By implementing parametric relationships, static models become dynamic, facilitating the development of models representing different physical characteristics [120].

In order to leverage the design flexibility of parametric CAD modelling, AM is frequently used to rapidly prototype designs. AM can be broken down into 7 main families. Common to all families, is the dissection of intricate 3-dimensional models into 2-dimensional layers, comprised of boundary (perimeter) and fill (interior) regions [121]. The families are summarized below [122]:

- Material extrusion (fused filament): Material is heated, liquefied, and extruded by a printing head onto a platform. Models are built layer by layer, depositing additional material atop previously hardened layers.

- Powder bed fusion: Powder material is initially spread onto a platform. A laser fuses the first layer, after which the platform descends, more powder is spread atop the model, and the laser fuses the next layer.

- Material jetting: Material droplets are deposited by a printer head onto a platform, and are then allowed to cool, or be cured with UV light. Subsequent layers are deposited atop the cured structures.

- Binder jetting: Utilizes a powder material and a binding agent. Powder material is spread atop a platform, onto which binder material is deposited by an extruder. Subsequent layers are fabricated by lowering the platform, and spreading additional powder atop the model.

- Directed energy deposition: A multi-axis arm (4 or 5 axis) moves around a fixed object, depositing either powder or wire-form material, which is melted using an electron beam or plasma arc.

- Vat photopolymerization: Utilizes an ultraviolet (UV) light to cure resin on the surface of a reservoir, forming a model on a platform which descends deeper into the reservoir to allow for the curing of subsequent layers.

- Sheet lamination: Material is positioned onto a platform, and the required cross-sectional layer is cut out from the sheet of material. Subsequent layers are formed by adding additional material, bonding the layers together, and cutting the next cross section.

Commonly used AM processes in the development of medical training simulators are material extrusion, binder jetting, and sheet lamination. Olszewski et al. [115] used sheet lamination to develop a human mandible for measurement comparison purposes. For this application, structural integrity was not a

necessary quality, meaning the lightweight paper model was acceptable. Lichtenberger et al. [73] utilized binder jetting technology to fabricate nerve-block injection simulators. For this application, colour was needed in prints, as certain elements were not encased in silicone, and needed realistic visual appearance. The most common AM family used in the development of medical training simulators is material extrusion. Malyala et al. [77] and Thielen et al. [123] developed models for the rib cage and cranial skeletal structures using polymeric materials. Of note from these papers, was the ability to accurately represent human bone and cartilage using different infill patterns [123]. Furthermore, structural properties highlighted through the use of the polymer (ABS model material) were noted to have high strength to weight ratio, which may be beneficial for bones which will be subjected to pressure through palpation.

Summarizing insights gained which form the general approach for the development of a reconfigurable, high fidelity thoracic wall:

- CT scan file conversion to obtain accurate skeletal models
- Conversion of CT scan .obj files to CAD file type (.step, .sldprt, .catpart)
- Parametric relationship for moulds, to render static models dynamic in terms of tissue thickness
- AM for skeletal structures and moulds for silicone tissues

## 2.4. Application-Specific Design and Fabrication Strategies

A frame for the approach to the work in this thesis is provided by Kalami et al. [75] (Figure 2.4-1). This research outlines the steps in which a CAD and AM system was used to develop patient-specific custom finger and hand braces. The research implements these tools and techniques, along with parametric design.

By incorporating a virtual representation of the finger, parametric relationships were updated to result in a modified brace, tailored to the specific patient's characteristics. The steps outlined by Kalami et al., along with the review of the literature, provide a foundational outline to the approach in this thesis.
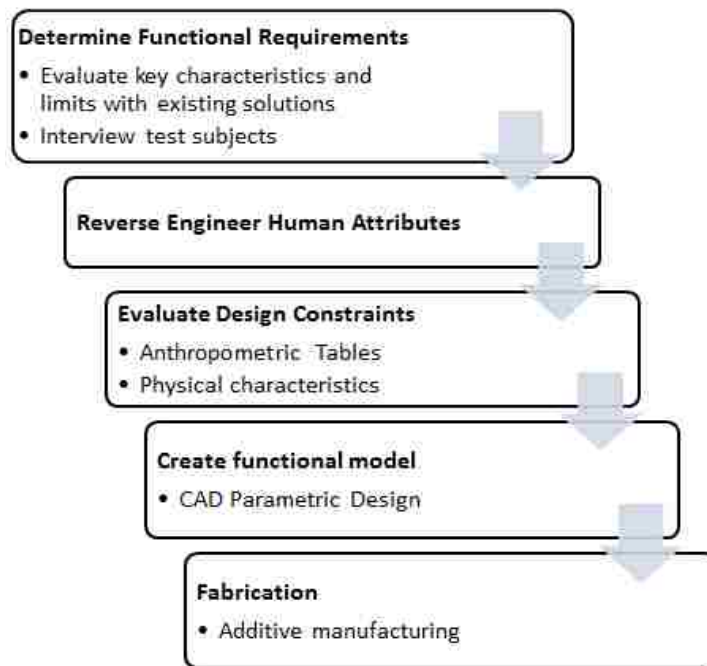


**Figure 2.4-1: Generalized procedure for the development of custom finger braces (Kalami et al. [75])**

To optimize the methodology in Figure 2.4-1 for the application in the development of a reconfigurable, high fidelity thoracic wall representation, decisions on aspects shown in Figure 2.4-2 must be made.
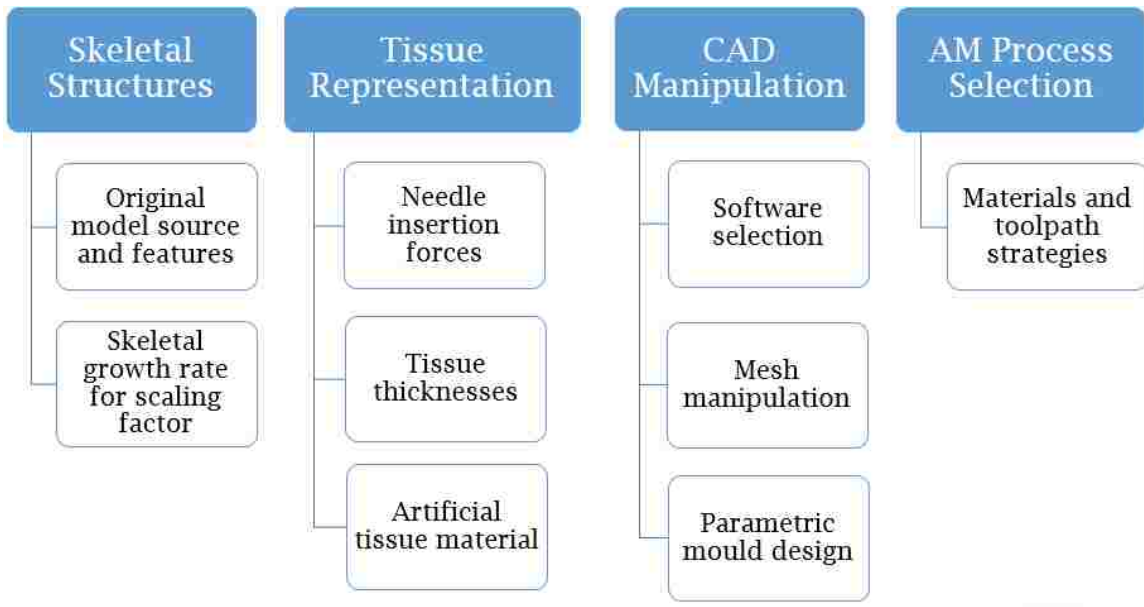
**Figure 2.4-2: Design and fabrication decisions**

Gaps common to both the literature and the simulator analysis from Table 2.2-1, are the realism of needle insertion resistive forces, the parametric/reconfigurable design for medical training simulators, as well as the quick-change/adaptability of models. These elements are comprised within the project scope (Figure 1.5-1), and along with the anatomy lessons learned, are influential in CAD and AM decisions.

## 2.4.1. Skeletal Structure Constraints

CT scan files are the most frequently used source of medical imaging in the development of patient-specific CAD models. Multiple open-source models are available, with varying degrees of anatomical completeness, and accuracy [124]-[127]. Based on the need for a clavicle, rib cage, and a scapula, three individual models were selected to represent the right side of the thoracic cavity, as unilateral pleural effusions are more frequently observed on the right side [128].

Individual models for the rib cage, clavicle, and scapula for an adult male were selected as the baseline, as they most accurately represent largest group in the target demographic (50-59 years of age) [51]. However, to leverage the reusability of models detailed by Shah et al. [117] and Camba et al. [119], the same models will be used to represent the entire demographic; being scaled according to growth factors for the clavicle, from McGraw et al. [91] (Table 2.4.1-1).

Table 2.4.1-1: Detailed clavicle growth rates from McGraw et al. [91]. Starred values indicate 80% of total respective clavicle growth

|  | Measured Clavicle Length (mm) | | Approximated Growth Rate (mm/yr) | |
|---|---|---|---|---|
| Age | Male | Female | Male | Female |
| 0 | 37.6 | 37.8 | 9.06 | 8.49 |
| 1 | 44.8 | 48 | 9.06 | 8.49 |
| 2 | 55.5 | 53 | 9.06 | 8.49 |
| 3 | 57.9 | 58.8 | 9.06 | 8.49 |
| 4 | 69.6 | 67.2 | 9.06 | 8.49 |
| 5 | 85.8 | 86 | 6.67 | 8.95 |
| 6 | 96.4 | 98.7 | 6.67 | 8.95 |
| 7 | 103.1 | 102.8 | 6.67 | 8.95 |
| 8 | 110.8 | 110.7 | 6.67 | 8.95 |
| 9 | 112.8 | 113.8* | 6.67 | 3.41 |
| 10 | 120 | 122.8 | 6.67 | 3.41 |
| 11 | 123.4 | 125.2 | 6.67 | 3.41 |
| 12 | 127.4* | 130.4 | 5.38 | 3.41 |
| 13 | 141.2 | 139.3 | 5.38 | 3.41 |
| 14 | 145.2 | 139.4 | 5.38 | 3.41 |
| 15 | 150.5 | 143.3 | 5.38 | 3.41 |
| 16 | 155.1 | 143.6 | 5.38 | 3.41 |
| 17 | 161 | 145.6 | 5.38 | 3.41 |
| 18 | 161.2 | 149.2 | 5.38 | 3.41 |

Table 2.4.1-1 is based on further elaboration on the clavicular growth rate averages from McGraw et al., also shown in the table. The decision to use the growth rates of the clavicle for all of the skeletal structures was made based on

the thorough documentation of the growth rates of the clavicle, the limited information regarding size and age of the scapula and rib cage, as well as the literature describing the constant positional relationships maintained from birth to skeletal maturity [37]. While the rib cage exhibits slight growth from 20-30 years of age, along with changes in shape (varying thoracic index; which is the ratio of rib cage depth-to-width), for the purpose of this thesis, these will be assumed to be negligible. This assumption is based on the fact that the palpation procedure only necessitates accuracy with respect to the clavicle length (to identify the mid-clavicular line) and the association of the inferior angle of the scapula with the $7^{th}$ rib, to palpate down 1-2 intercostal spaces (to the $8^{th}$ or $9^{th}$ intercostal space) [32], [33], [35]-[37]. This decision is further reinforced by an anatomy-based rationale. Analyzing images such as Figure 2.4.1-1 [129] and considering the linear growth of the rib cage and clavicle, as well as the positional relationships that are maintained throughout skeletal growth, it is assumed that since there are no additional structures within the connection of the rib cage, clavicle, and scapula (other than the acromio-clavicular joint and sterno-clavicular joint), scapular growth is directly related to the rib cage and clavicle.
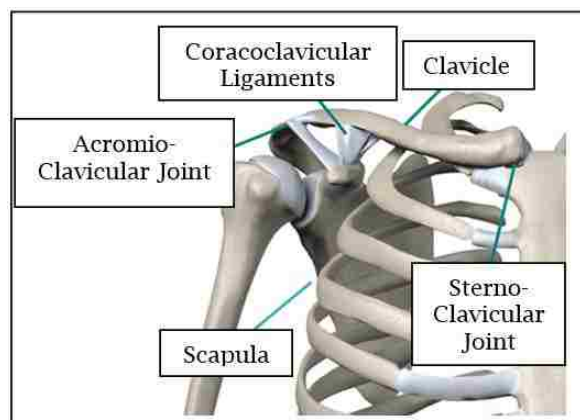


**Figure 2.4.1-1: Chest girdle skeletal structure (adapted from [129])**

To confirm the linearity of the growth rates of the clavicle described by McGraw et al., comparisons between measured clavicle lengths in their study, and lengths predicted by the growth rates detailed in Table 2.4.1-1 will be made. The use of these clavicle-based scaling factors on the remainder of the assembly will be investigated by comparing intercostal space measurements detailed by Kim et al. [90], and the scaled rib cage models. These comparisons will be made for 3 target patient representations; a 2 year-old male, an 18 year-old female, and a 30 year-old male (Table 2.4.1-2). These groups were selected for comparison as they encompass the youth peak in the demographic breakdown [51] (0-9 years of age), the post-pubertal-growth phase (9-18 years of age), as well as the target demographic for the THM-30 simulator (adult, approx. 30 years of age) [25]. Due to the unavailability of pediatric intercostal spacing literature, only clavicle measurements will be compared for the 2-year-old male patient representation. Comparisons of intercostal space widths are contingent on the assumption of negligible post-pubertal growth, which is a limitation of this aspect of the research, due to limited literature available pertaining to the topic.

Table 2.4.1-2: Landmark measurements for selected patient demographics [90], [91]

| Landmark / Patient | Clavicle Length (mm) | Intercostal Space Width (mm) |
|---|---|---|
| 2 Yr. Old Male | 55.5 | |
| 18 Yr. Old Female | 149.2 | 14.2 |
| 30 Yr. Old Male | 161.2 | 14.9 |

## 2.4.2. Tissue Representation

Based on the need for a high fidelity representation of the haptic (relating to the sense of touch; force perception) element of the training simulator outlined by Crofts et al. [23], and the varying physical characteristics of the thoracentesis-requiring demographic, a variable representation of the needle insertion forces, and overall tissue cross-section is necessary.

Needle insertion characteristics on various tissues have been widely investigated. Poniatowski et al. [130], DiMaio et al. [131], Abolhassani et al. [132], Mavhash et al. [133], Jiang et al. [134], and Okamura et al. [135] have studied the effects of various factors on soft tissue needle insertion forces. In these studies, needle insertions were typically performed on bovine or porcine tissue samples (liver or brain) using needles with varying tip geometries (i.e. bevel tip, blunt tip, conic tip), equipped with tension/compression load cells to measure forces [132]. Jiang et al. [134] and Okamura et al. [135] performed analyses of variance (ANOVA) to statistically quantify differences or similarities between the means of values recorded. From these studies, several factors were identified as being influential on needle insertion characteristics, including insertion velocity, insertion depth, tissue layers, needle insertion angle, needle type and diameter. No literature was found pertaining to the distribution of thoracic wall tissues (i.e. adipose tissue thickness distribution trends). There was also a lack of literature available to determine the influence of operator age and sex on thoracic needle insertion forces, however, Perry et al. [136] investigated the influence of operator gender and age on pain felt by patients during needle insertion in the jaw region. This study determined that both age and gender had no influence on patient pain

during the procedure, indicating that technique was not directly influenced by either.

The use of porcine samples to mimic human tissues has been widely accepted, as the constitutions (tissue layers) are similar. However comparatively little research has actually investigated the needle insertion property similarities between the two. Brett et al. [59] and Holton et al. [60] investigated these properties, and found that the peak forces of the tissues (the skin, in particular) were over 200% higher in the porcine specimens than the human specimens (6.0N ± 0.7N for human skin vs. 12.9N ± 2.6N for porcine skin), using an epidural needle (which has an identical tip shape to a thoracentesis needle). These results indicate that for force-perception purposes, porcine studies may not be suitable.

Common to most studies, was the dominant influence of insertion velocity on forces measured. To account for this, mechanical needle-insertion apparatuses are frequently used to eliminate the variance in forces associated with fluctuating insertion velocities [130]-[135]. The use of these automated insertion mechanisms is of particular benefit to the mathematical simulation of needle insertion characteristics, as demonstrated by Okamura et al. [131], Mahvash et al. [133] and Simone et al. [137], who collected needle insertion data experimentally to create predictive mathematical models. Despite the extensive literature on the virtual simulation of tissues, comparatively limited literature is available regarding the physical recreation of simulated tissues. Wang et al. [138] and Forte et al. [139] however, investigated the use of synthetic materials to represent *in-vivo* (living) human tissue. Wang et al. prepared silicone samples mixed with varying concentrations of mineral oil to represent liver, muscle tissue, and adipose

tissues. Results from this study showed that the addition of oil in varying quantities to the silicone influenced the needle insertion characteristics, eventually reaching a critical threshold, where the characteristics mimicked human tissue (40 wt. % for the silicone formula used in this case).

While effective in the representation of individual tissue layers, few studies were found that sought to recreate a multi-layer representation of human tissues. This is largely due to the complexity of multi-layer tissue-needle interactions outlined by Mahvash et al. [133], Jiang et al. [134], and Gordon et al. [140]. These studies outline the varying forces for different tissue layers, highlighting the skin as the layer requiring the most force to penetrate, followed by muscle, and lastly, adipose tissues. This is exemplified by Abayazid et al. [141], who developed a secondary 2.5mm "skin" layer to be added to their simulated tissue, showing a 90.2% increase in insertion force rate, compared to the same simulated tissue without the addition of a simulated skin layer. Despite the influence of various layers on insertion characteristics, no literature was found which analyzed insertion criteria for the thoracic cavity; specifically, a cross-section containing the pleural membrane.

## 2.4.2.1. Needle Insertion Experiments

To account for the lack of literature pertaining to the needle insertion characteristics of the thoracic cavity, as well as the discrepancies between porcine and human needle insertion forces, a cadaveric needle insertion experiment was performed. The aim of obtaining needle insertion measurements from a cadaveric subject was to minimize the complexity of modelling human tissues outlined by Holton et al. [60], which includes the calculation of adjustment factors to account

47

for varying tissue characteristics between human and porcine subjects. While variations in tissue properties exist between cadaveric and living patients due to the cool temperatures and chemical changes associated with embalming, cadavers provide accurate representations of human anatomy (tissue layers, thicknesses) [59].

To summarize the highly complex tissue recreation, peak force (N), impulse (N·s), and pulse width (s) will be measured. Peak force will be measured to determine the maximal exertion on the needle needed to penetrate all 4 tissue layers. Impulse will be measured to compare the force exerted throughout the entire puncture of tissues, and will provide a measure of the area under the force-time curve. Pulse width will be measured to account for, and to remove excessively varying insertion velocities, which are influential on the needle insertion characteristics [130]-[135].

Manual needle insertions will be performed, as during manual needle insertion (as is the case in clinical thoracentesis), the larger force needed to penetrate the tougher outer skin layer can result in a variable velocity profile throughout tissue puncture, whereas in automated insertions, velocity is typically constant throughout [131]-[133]. These variations in velocity throughout punctures are influential on overall force needed for needle insertion, as described by Brett et al., who investigated needle insertion resistive forces in different tissues [59]. To determine the influence of the multiple layers (skin, adipose tissues, muscle, pleura), as well as to statistically determine which layers must be synthetically modelled (given the single layer constitution of the THM-30 and other simulators), three different insertion sites will be used. One site will

contain the skin and adipose tissues, a second site will contain the muscle and pleura, and a third site will contain all 4 layers of the thoracic cross section (skin, adipose tissues, muscle, pleura). Data will be low-pass Butterworth filtered, to remove high-frequency noise data, and to obtain "smooth" readouts (flat band pass regions) [142]. The use of low pass filters is prevalent in the processing of human force data, as shown by Ford et al. [143], who investigated knee motion during force exertion. Results will be analyzed with a repeated measured analysis of variance (ANOVA) in SPSS, as per Jiang et al. [134] and Okamura et al. [135], with significance levels of $p<0.05$, to determine statistical differences between tissue layers.

Upon completion of the cadaveric testing, needle insertions using the same apparatus will be repeated on the THM-30 thoracentesis training simulator, to determine the realism of the needle insertion properties of the single-layer tissue. While the target gender representation of the THM-30 is not specified, the tissues of the cadaver are on the lower-end of the spectrum of thoracic wall thicknesses described in the literature (24mm-80.2mm; with a cadaver thoracic wall thickness of approximately 25mm). Given that the THM-30 tissue thickness is also near the lower end of the spectrum (20.3mm), this comparison should provide insight as to the quality of the tissue representation. Results from the cadaveric experiment will be used as targets for the recreation of synthetic silicone tissues, using a variable-hardness silicone, as per Wang et al. [138].

To develop these elements, custom mould sets will be designed and fabricated. Tissues will be represented using modifiable splines, to allow for modifications of tissue distribution, which, although not documented in the

literature, may prove to be necessary in the future. These tissues will be used to model mould sets, in such a way that parametric relationships will be established, allowing for the re-configuration of tissue thickness. An initial mould set will be developed to fabricate a static model (one patient configuration upon fabrication). A second mould set will then be developed, allowing for the incorporation of a quick-change tissue element. This quick-change feature will consist of an additional tissue layer, which can be added or removed post-fabrication, to represent a different thoracic wall thickness. This feature is further detailed in Chapter 3.3.

Lastly, upon completion of the elements developed in this study, testing on the tissues developed will be performed, and compared to results from the cadaver and the THM-30. The comparisons will consist of tissue thickness, and needle insertion resistive forces. A cross-sectional analysis of the tissues will also be performed, to investigate potential inconsistencies in the silicone curing (air bubbles, improperly mixed silicone), which may influence needle-insertion characteristics.

### 2.4.3. Software Selection

Multiple different CAD software are available for use, and frequently, several are used in conjunction, based on individual software strengths and weaknesses. While many software may be capable of performing the same task, operator proficiency is key. For this reason, only widely available and popular software will be selected for use, to maximize potential repeatability. Chapter 2.3 outlines several commonly used software for this application. Selected candidates, along with the reason for their selection are presented below:

- Windows 3D builder: Part axial rotation and trimming ease (for removing unnecessary skeletal structures)

- Windows 3D builder, FreeCAD, Autodesk Netfabb: Mesh modification, repair, and conversion capabilities

- SolidWorks, CatiaV5: Part and assembly importing and design capabilities

- SolidWorks: Parametric design capabilities, specifically for non-uniform surfaces

The selection for these software is supported by literature, as well as the fact that they are readily available; with temporary versions available for no cost to the user, and several being taught in schools. These factors increase the ease of reproducibility of results, as identical software can be used, using the same techniques. These techniques are further detailed in Chapter 3.1 and Chapter 3.3.

## 2.4.4. AM Process Selection

Desirable fabrication qualities for the development of medical training simulators are the rapid production of multiple iterations (to represent different patients), moderate-high accuracy, and a thermoplastic or polymer material use (lightweight, durable). Models should be conducive to silicone moulding (i.e. non-porous), and sustain mechanical stresses associated with manual palpation through tissues. Ideally, the process would enable automated fabrication, and eliminate the knowledge- and expertise-based needs associated with the fabrication of conventional moulds [66], [67]. From the literature, three AM families are candidates for use in this thesis. Sheet lamination, binder jetting, and

material extrusion have been successfully implemented in the development of various anatomical models by Malyala et al. [77], Lichtenberger et al. [73], and Thielen et al. [123] and Olszewski et al. [115], respectively.

Comparing the three candidates, sheet lamination is eliminated because of the need for post-processing (de-cubing), and the potential for porosity associated with poor layer bonding [122]. Binder jetting is eliminated due to the potential inconsistency of parts in terms of structural integrity, as the binder material used occasionally causes loaded parts to fail, which could occur during manual palpation [122]. Material extrusion is selected for its ability to rapidly produce structurally consistent plastic parts. With parametric models, the flexible manufacturing enabled by material extrusion enables the rapid and consistent fabrication of lightweight models; both for the skeletal structures, as well as the moulds [122].

Several material extrusion machine candidates were explored and compared [144]. Build envelopes for candidates range from small (8.54cm x 4.8cm x 13cm [145]) to very large (100cm x 100cm x 200cm [146]). Based on estimated physical characteristics of the largest model needed, being an adult male, with a thoracic cage height of approximately 27cm (Table 2.2-1), a mid-large sized build envelope was needed. Given the complexity of the rib cage anatomy, the selected machine had to be capable of utilizing both model, and support material. Support material is used to provide a base, onto which model material can be deposited, when the print overhang angle exceeds the 45-degree critical angle. This critical angle is documented by Ahn et al. [147] and Kranz et al. [148] as the angle at which additional layers of material can no longer be self-supported, and

risk toppling without supplementary support. Based on these factors, the Fortus 400mc was selected for use [149]. Ease of use and process automation are desirable characteristics, which are prevalent with the use of this model. Furthermore, the build envelope measures 40.64cm x 35.56cm x 35.56cm [149], which is large enough for the fabrication of models needed. Process parameters for the Fortus 400mc are summarized in Table 2.4.4-1 [149], which emphasizes the high degree of automation; and therefore user-friendliness of the system. For comparison to other potential mid-large sized printers, a popular model—the MakerBot Replicator 2X [150] is also summarized. Process parameters for the MakerBot Replicator 2X are common to the majority of open-source AM machines. While these machines provide more user control, the consistency and ease of use are superior with the Fortus 400mc.

Table 2.4.4-1: Fortus 400mc and MakerBot Replicator 2X process parameters [149], [150]

| Parameter | Fortus 400mc | | MakerBot Replicator 2X | |
|---|---|---|---|---|
| | Automated | User Defined | Automated | User Defined |
| Print duration | X | | X | |
| Placement | | X | | X |
| Feed rate | X | | | X |
| Power output | X | | X | |
| Orientation | | X | | X |
| Order | | X | | X |
| Temperature | X | | | X |
| Build platform levelling | X | | | X |
| Build platform-part adhesion | X | | | X |

Multiple materials compatible with the Fortus 400mc were explored to determine the optimal material to fabricate the models with. A summary of

potential candidates is presented in Table 2.4.4-2, which outlines the flexural strength (associated with manual palpation) of each material, along with their cost, which are key factors for decision making. Based on the review of materials, ABS-M30 [151] was selected, as it is the least costly material, while still providing mid-range strength qualities. This decision is reinforced by Malyala et al. [77], who used ABS model material to fabricate patient-specific medical models, noting the lightweight, high-strength qualities.

Table 2.4.4-2: Summary of material review [152]

| Material | Cost/Kg (CAD) | Flexural Strength | Density |
|---|---|---|---|
| ABS-M30 [176] | $39.23 | 48 MPa | 1.04 g/cm3 |
| ULTEM 9085 [177] | $170.23 | 68 MPa | 1.34 g/cm3 |
| Nylon[178] | $104.73 | 28.8 MPa | 1.08 g/cm3 |
| PC [179] | $98.18 | 68 MPa | 1.20 g/cm3 |

Support material, as the name implies, supports the model material during fabrication and is later broken off or dissolved in a caustic solution bath [153]. Based on a review of available support materials for the Fortus 400mc, SR-30 was selected, as it is the least costly material, which is both water soluble, and compatible with ABS-M30 [154]. The other candidate for use was SR-20 support material, however manufacturer guidelines suggest the use of SR-30 for use with ABS-M30 [155]. The use of SR-30 facilitates the removal of support material, by placing completed models into a caustic bath solution, as opposed to having to manually remove material with pliers.

In the fabrication of models with the Fortus 400mc, three part-fill settings are available. The settings are sparse, sparse-double dense, and solid-normal [156]. The sparse infill setting utilizes a unidirectional internal material deposition

strategy for individual layers, alternating directions between layers to reduce part density and weight. The sparse-double dense infill uses a bi-directional internal fill on each layer, giving more strength—at the cost of increased material usage when compared to the sparse setting. The solid-normal infill uses a dense fill pattern, reducing air gaps within the part and producing the strongest parts; at the cost of the most material consumption. In the fabrication of partial-fill models, perimeter layer and surface layer settings can be altered to add or remove solid layers to create a manifold (watertight) outer surface. These settings adjust the number of full-density toolpath passes surrounding the partial-density core regions of the model. This is important, particularly for the moulds, due to the porous nature of parts created with AM, outlined by Lam et al. [157], which could allow for silicone to permeate, potentially negatively influencing the curing process. For this application, a sparse setting will be used, with 3 contour passes, to reduce material usage, while maintaining manifold surfaces.

## 2.5. Summary

The research in this study aims to develop a high fidelity thoracic wall representation, with reconfigurable tissues, and complete skeletal structures for palpation. Key elements being addressed in this thesis, highlighted through a review of the literature are:

- Tissue thicknesses; based on the varying thoracic wall thickness of the thoracentesis-requiring population, the significant difference between the THM-30 simulator and the literature (16.7%-77.44%; not accounting for obesity factor) and the influence of tissue thickness on needle insertion forces (Table 2.2-1), [55], [57], [131], [138].

- Skeletal completeness; based on the palpation procedures outlined in the literature that use the mid-clavicular line as a reference for lateral site determination and the fact that there is no clavicle at all in the THM-30 simulator, off of which to make this reference (Table 2.2-1), [32], [33].

- Skeletal size; based on the palpation procedures, which use the pointed base (inferior angle) of the scapula as a reference for vertical site determination (7th intercostal space), the improper sizing of the scapula itself (24.37% difference) [55], [88], [91], as well as inaccurate intercostal spacing exhibited in the THM-30 (84.6% difference) [35]-[37], [90], (Table 2.2-1).

- Tissue needle insertion properties; based on the need for high fidelity in elements of a force-perception nature [23]. Target values were not found in the literature and are unavailable for the simulator, but will be determined experimentally.

Insights gained from the literature help define the approach, summarized in Figure 2.5-1.
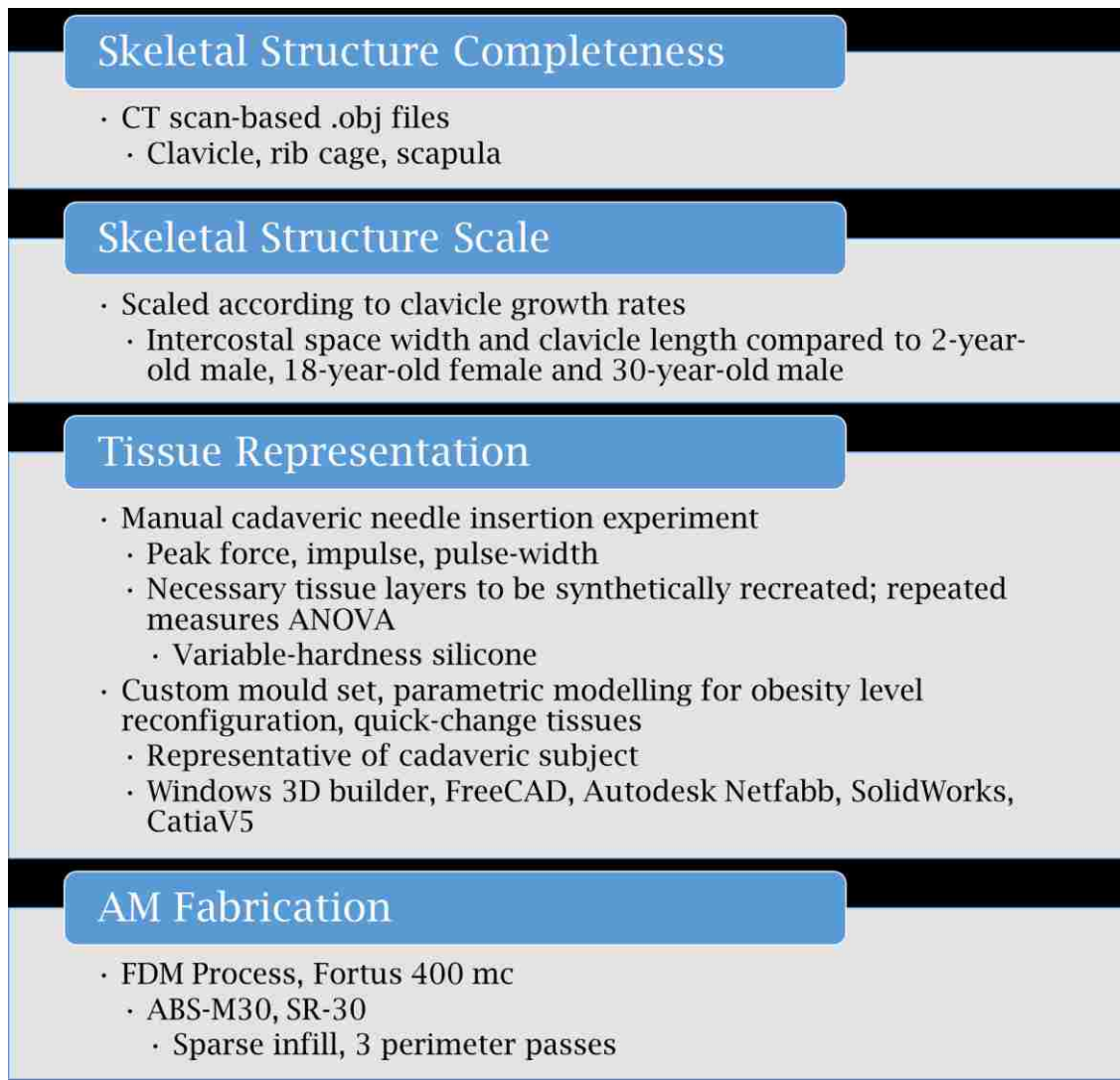
**Figure 2.5-1: Sumamrized approach for the design and fabrication of a reconfigurable thoracic wall representation**

The next chapter details the means by which this approach is followed and expanded on.

CHAPTER 3

Methodology

This chapter describes the methods followed throughout this thesis. Chapter 3.1 presents the steps by which computed tomography (CT) skeletal models essential to proper landmark palpation, outlined by the United States Government [32] and Berg et al. [33], were modified and combined into a reconfigurable skeletal assembly. The incorporation of skeletal scaling factors determined through the literature review is also presented [91]. Models obtained through the use of these scaling factors were then compared in terms of skeletal measurements to the THM-30, and values from the literature. Chapter 3.2 presents the cadaveric and THM-30 needle insertion experiments, which were performed to determine key tissue needle insertion resistive forces (peak force (N), impulse (N·s) and pulse width (s)) necessary to improving the fidelity of the tissues, as per Crofts et al. [23]. Chapter 3.3 presents the methodology to develop parametric mould sets used to shape silicone tissues. Quick-change elements are incorporated, both in terms of virtual model reconfiguration, as well as physical post-fabrication tissue reconfiguration. Chapter 3.4 presents a variable-hardness silicone "calibration" experiment, performed to simulate realistic cadaveric tissues in silicone. Chapter 3.5 presents the fabrication strategies used to obtain initial and subsequent prototypes, as well as an evaluation of the thoracic wall representation developed in this thesis.

## 3.1. Skeletal Structure Modelling

To develop a reconfigurable skeletal assembly, publically available models for an adult male were first obtained (Figure 3.1-1 (a), (b) and (c)) [163].

**Figure 3.1-1 (a): Rib cage object file [163], (b) Clavicle object file [163], (c) Scapula object file [163]**

Original models contained over 151000 triangular meshing elements, being used to construct surface geometry. These meshing elements can be likened to image resolution; excessively low resolution yields an unrecognizable image, whereas excessively high resolution imaging yields large file sizes, which may be unnoticeably different to the human eye compared to a mid-range resolution file. As skeletal models fabricated would eventually be encased in silicone tissues, a mid-range mesh density (1000-7500, depending on patient size) was targeted, as the "haptic resolution" would be diminished due to the silicone "buffer". To reduce the amount of meshing elements, which exceeded software limitations outlined by Chwatko et al. [105] (20,000 triangular meshing elements for SolidWorks 2009), models were trimmed and meshes were modified. The rib cage model was trimmed in half using Windows 3D Builder's "split" command, removing the left half; as pleural effusions are observed most frequently on the right side [128] (Figure 3.1-2). This software was selected for its ability to rotate, trim, and smooth the surface of models with ease.
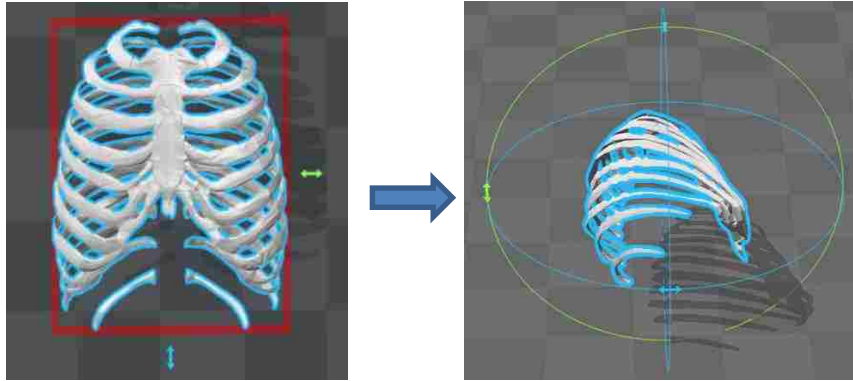
**Figure 3.1-2: Rib cage halving using "split" command in Microsoft 3D Builder**

Meshing modifications were then performed on the .obj models for the clavicle, halved rib cage and scapula to reduce the number of triangular meshing elements constructing the surface geometries. Surface meshes for all skeletal models were simplified using Microsoft 3D Builder's "smooth" function, which takes an average of the surface meshing elements, to reduce the total number of elements needed, resulting in a smoother surface geometry.

Meshes obtained through the initial splitting and smoothing operations had several errors, including missing or inverted faces and edges. Autodesk NetFabb's "extended repair" function was used to automatically repair the majority of the errors. Remaining missing or inverted faces which exceeded the threshold value for repair (0.5 mm default) were manually repaired in FreeCAD. FreeCAD was selected for its "evaluate mesh repair" function, which allows for the highlighting and manual repair of meshing errors.

With trimmed, simplified, and manifold (watertight) meshes completed, FreeCAD was used to fill the hollow surface geometries, resulting in solid body geometry. This was performed by using the "convert to solid" function, in the

meshing workbench. These solid models were then converted to .step format, using the "export" function in FreeCAD, yielding solid .step models, capable of being manipulated freely in Catia V5 and Solidworks 2016.

Resulting .step file skeletal models consisted of solid bodies, surrounded by surface meshes. These meshes were manually deleted in Catia V5, to expose the solid bodies for further manipulation. Catia V5 was selected for use for this application for the automatic highlighting of surface geometry, facilitating the identification and removal of surface mesh representations (Figure 3.1-3).
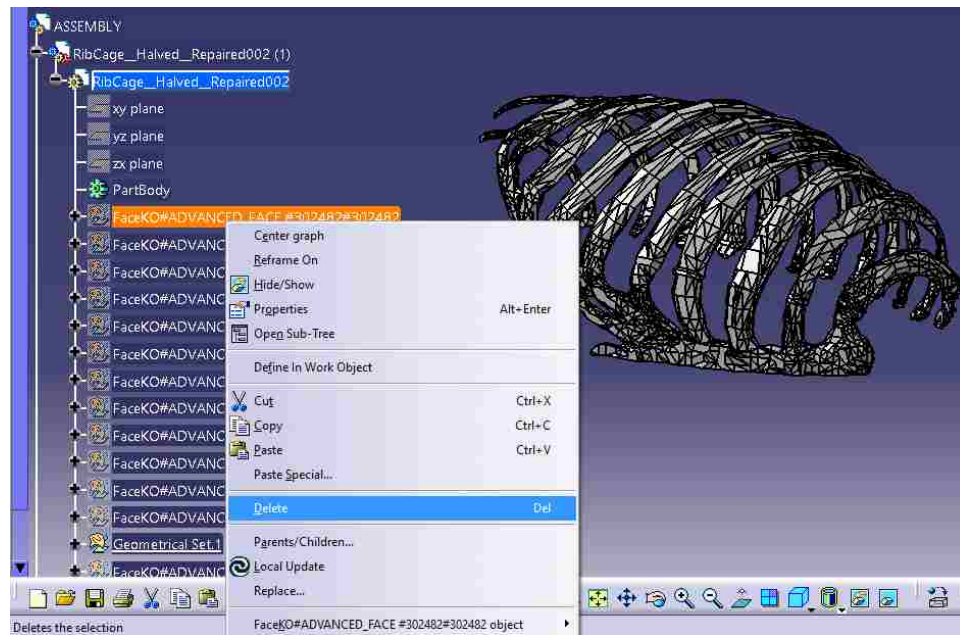


**Figure 3.1-3: Manual deletion of meshing surfaces in Catia V5**

An artificial spine representation was then modelled using Catia V5 software's "pad" command, to provide additional structural support during manual palpation, as well as to connect the 11th and 12th "floating" ribs to the rib cage structures, yielding the rib cage model depicted in Figure 3.1-4. The spine consists of a rectangular arc, drawn on a custom sketch plane, which was oriented using

the means of the endpoints of the ribs, coincident with the original trimming plane seen in Figure 3.1-2.
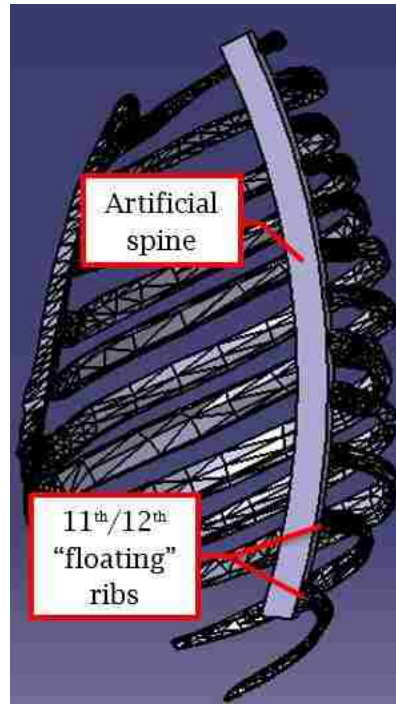


**Figure 3.1-4: Rib cage model spine modifications**

Completed models for the rib cage, scapula, and clavicle were then uploaded into an assembly in the Catia V5 "Product" workbench. Individual CAD models were oriented into the product assembly to align key anatomical reference points, including the inferior angle of the scapula, with the 7th intercostal space, and the clavicle with the sternoclavicular and acromio-clavicular joints (Figure 3.1-5).
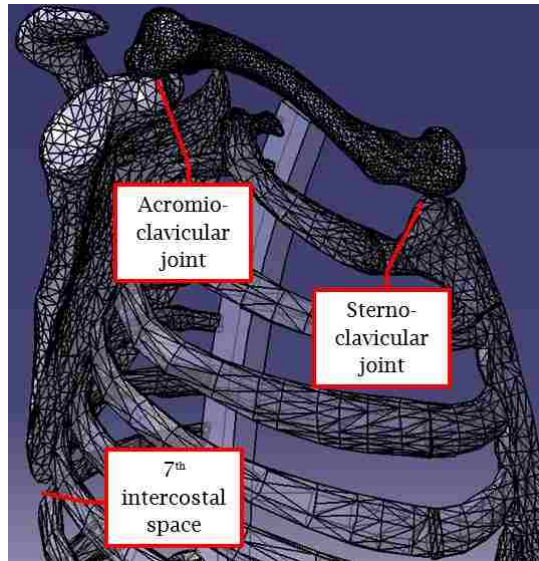
**Figure 3.1-5: Skeletal structure alignment for clavicle and scapula with rib cage landmarks**

Models were fixed into appropriate position with manually drawn and extruded columns, depicted in Figure 3.1-6. These columns served to join the three skeletal bodies into a single body, which upon fabrication, would maintain landmark alignment.
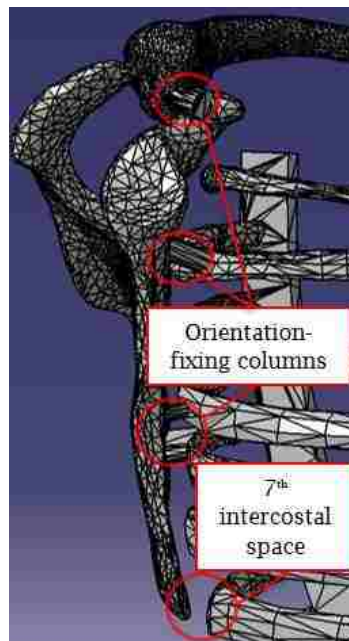


**Figure 3.1-6: Orientation-fixing columns**

To enable the representation of different patients' skeletal proportions, clavicle growth rates were used to develop input values for the "scale" function in Solidworks 2016. Initial "baseline" sizing for the skeletal structures was that of a 30 year old male, with a clavicle length of 161.2mm, as per Table 2.2-1 and Table 2.4.1-2. By implementing growth rates and percentages of total growth for the clavicle outlined in Table 2.4.1-1, input values for scaling functions for the skeletal assembly were determined. The skeletal assembly was imported into SolidWorks 2016, for to its ability to readly scale models, and its ability to establish parametric relationships with irregular surfaces (such as those in the human body). With an initial scaling factor of "1" representing a 30 year old male (assuming negligible growth after 18-years of age), different patients were then represented by altering the scaling factor, using the "scale" command. Uniform (identical in all 3 planes) scaling was performed to maintain landmark positional relationships regardless of overall patient stature being represented.

To determine if the growth rates documented by McGraw et al. [91] provided sufficient accuracy with respect to measured clavicle length, comparisons between predicted (according to initial clavicle length at birth, and detailed scaling factors), and measured clavicle lengths were made. A comparison was then made on the error between the predicted and measured values, and the standard deviations in the reported values from McGraw et al.. Intercostal spacing measurement comparisons were then performed between the thoracic wall developed in this thesis, the THM-30 and measurements from Kim et al. [90]. Clavicle comparisons were performed for 3 target patient representations; a 2-year-old male, an 18-year-old female and a 30-year-old male and intercostal space measurements were compared for the 18-year-old female and 30-year-old male.

Measurements were made on the CAD models using the "measure" command in SolidWorks 2016, and using a caliper for the THM-30 and fabricated skeletal models.

## 3.2. Tissue Investigation and THM-30 Simulator Analysis Experiment

In this experiment, the needle insertion characteristics of the THM-30 [25], and a 70 year-old female cadaver patient were investigated using a manual needle-insertion apparatus. The goals of this experiment were to determine the statistical significance of the tissue layers of the cadaver subject, to determine resistive forces for individual layers and the entire thoracic cross section of the cadaver subject and the THM-30 simulator.

### 3.2.1. Participants and Subject

The cadaveric needle insertion experiment was conducted with 5 participants (2 males, 3 females) ranging in age from 23 to 50 with no clinical experience in the procedure. The THM-30 needle insertion experiment was performed by 5 males aged 23-25, also with no clinical experience. Statistical grouping of participant data was not performed as age and gender are not directly influential on needle insertion technique [136]. Participants performed manual needle insertions on an adult female, formalin-fixed cadaver subject, which accurately represented *in-vivo* (living) tissue layer thicknesses [59]. All identities were protected and consent to use data was given. A Research Ethics Board (REB) application was approved for the use of cadavers (Appendix D) and a respectful working environment was maintained at all times. The participant pool is a

current limitation of this study, as with only 5 participants, errors may be amplified. Furthermore, a consistent group of participants for all needle insertion experiments performed in this thesis would be beneficial in eliminating any potential bias. Furthermore, additional cadaver subjects would be beneficial, to obtain a larger data pool.

### 3.2.2. Instrumentation and Data Acquisition

The data were collected by fitting a thoracentesis needle (Bound Tree Medical, Dublin, OH) [165]  onto a metal base (Figure 3.2.2-1) which slid into a metal sleeve containing a Forsentek Compression Cell with a load capacity of 50kg (Forsentek Co. Limited, Longgnng Dist., Shenzhen China) [166]. The calibrated load cell was pressed against by the base of the needle during insertion, collecting data with a sampling rate of 1000 Hz, converting compression data to voltages. Voltages were converted to  Newtons with a custom WiDACS (Wireless Data ACquisition System) [167], which was powered by a Pocket Juice portable power pack (UbuyEZ, Temecula, CA) [168]. This receiver then transmitted the data to the WiDACS Logger software (Cort Research and Innovation Inc., Tecumseh, On. Canada) [167] on the HP G15 Workbook (Palo Alto, California, United States) [169] and displayed it with default settings, including a gain factor of 3.818 (based on necessary voltage for sensor activation) and a data acquisition offset of -5906.1 (based on system bias). Data were collected with a 1.5s pre-trigger time (time recorded before threshold value is reached), 2s post-trigger time (time recorded after threshold value is reached) and a trigger level (force threshold at which recording commences) of 1N. Data were then converted into Excel software files (Redmond, Washington, United States) [170].
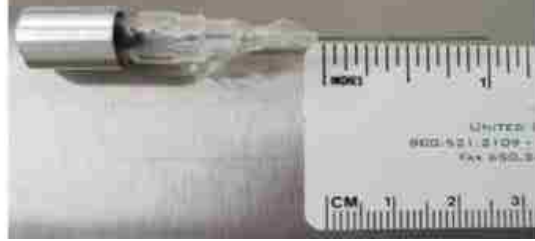
**Figure 3.2.2-1 (a): Thoracentesis needle**

### 3.2.3. Experimental Procedures and Protocol

All participants wore appropriate lab clothing and personal protective equipment (PPE). To separate tissue layers, in order to obtain data for individual tissues for statistical analysis, the cadaver specimen was prepared by making two perpendicular incisions approximately 12.5mm-deep, down to the muscle tissue and peeling back the skin and adipose tissues with forceps and a scalpel (Figure 3.2.3-1). Muscle tissues were measured to have a thickness of approximately 12mm, meaning the entire cross-section was approximately 25mm-thick. This preparation served to expose 3 different insertion "sites" (cross-sections with different layer constitutions).



**Figure 3.2.3-1: Preparation of the cadaver**

The tissues were pinned back using a clamp, and the three insertion sites were exposed (Table 3.2.3-1).

Table 3.2.3-1: Cadaveric needle insertion positions

| Position | Description | Image |
|----------|-------------|-------|
| 1[1] | Muscle-Pleura |  |
| 2 | Skin-Adipose Tissue |  |
| 3 | Entire Thoracic Wall |  |

[1] Position 1 is depicted with a lumbar puncture needle

All procedures were performed on the same day, within an hour of each other. Independent variables for this procedure were the position and trial number and dependent variables were the peak force (N), impulse (N·s) and pulse width (s). Peak force was measured to determine the maximal force exerted to perform the insertion. Impulse, which is the integration of the force-time curve, was measured to quantify the effect of the force on the tissues/needle over time, otherwise known as the change in momentum. Pulse width was measured to account for any operator deviation, where the needle may have been inserted excessively rapidly or slowly, leading to skewed results. All subjects were given the same instructions; to grasp the apparatus by the base, position it perpendicularly to the insertion site and wait for a verbal queue indicating zeroing of the WiDACS. Once the queue was given, participants firmly pressed down on the needle until complete insertion through the tissues involved was achieved. Once completed, participants removed the needle and repositioned it for the next test. Each participant performed 3 tests in the first location, using the same technique. Once complete, participants moved to the second and third sites and repeated the same procedure. For the second layer, which consisted of skin and adipose tissue, the tissues were held upright (perpendicular to the body) firmly, and horizontal insertions were performed. A total of 45 insertions (15 per site) were performed. Throughout all procedures, participants stopped pressing once all layers had been penetrated, indicated by a sudden drop in resistance, thereby eliminating the spikes in force data associated with the base of the needle striking the tissue. Control variables were minimized in this procedure by performing all tests in the same locations, on the same subject and in the same timeframe (within one hour).

Simulator needle insertions were performed to determine mean values for the three aforementioned criteria (peak force (N), impulse (N·s) and pulse width (s)). The simulator possessed a single, uniform cross-section layer for needle insertion, so position was unimportant in the collection of the data. For the simulator tests, participants performed insertions in an identical manner to the cadaver insertions, also waiting for the verbal queue before inserting through the tissue layer. Each participant performed 3 insertions into the THM-30, for a total of 15 insertions.

### 3.2.4. Data Analysis

Force data for both experiments were converted to Newtons and low-pass filtered using default settings with a 4th order Butterworth filter with a cut-off of 25 Hz, to provide a smooth (flat) pass band, by removing high frequency signals from external noise, as per Ford et al. [142]. Multiple trials were combined by eliminating outliers, identified automatically with Statistical Package for the Social Sciences (SPSS), by exceeding the threshold determined by logic outlined in Table 3.2.4-1 and replacing them with an averaged value of other trials for that position. Upon completion of these data treatment procedures, mean values were obtained for each position's results. Standard deviation was calculated with Excel 2016 using the "STDEV.P" function, which calculates standard deviation based on the entire population.

Table 3.2.4-1: Outlier identification logic in SPSS

| Quartile (Q) | % of Data Representation | Lower Outlier Criteria | Upper Outlier Criteria |
|---|---|---|---|
| 1 (Q1) | 25 | Q1-(Q3-Q1)*1.5 | Q3+(Q3-Q1)*1.5 |
| 3 (Q3) | 75 | | |

### 3.2.5. Statistical Analysis

Three 5 x 3 Repeated Measures ANOVAs (ANalysis Of VAriance) (5 participant levels x 3 position levels) were performed for the cadaver data, with position as the "within" variable (all instruction given is the same, as are the cadaver and locations used) and with no "between" variables. Significance was set at p<0.05. Tukey's HSD (Honest Significant Difference) test was used compare mean values and determine statistical significance of positions on measured variables. Mean values for peak force (N), impulse (N·s) and pulse width (s) were obtained for each position on the cadaver, as well as for the THM-30 needle insertions.

Values in Chapter 4.2 are reported in the following format: $F(\text{df}_{condition}, \text{df}_{error})$ = $F$-value, $p$ = $p$-value [171]. The $p$ value tests the null hypothesis (that is, that there is no statistical difference between means of groups analyzed). A $p$ value less than the significance threshold (.05), is indicative of a statistical difference between means. The $p$ value is determined with the F value, which is a ratio of the two mean squares from the groups being tested, also shows the degrees of freedom for the condition measured, as well as the error. An F value close to 1 is indicative of an accepted null hypothesis (meaning, no difference between groups), while a larger F value is indicative of statistical difference between groups [171]. In the event that results from the ANOVA violate sphericity (the assumption that variances between differences of the groups (position, in this case) are equal), indicated by a rejected Mauchly's Test of Sphericity (which occurs frequently, particularly with small sample sizes, as in this case), the Greenhouse-Geisser correction was used. The Greenhouse-Geisser correction adjusts the F

value degrees of freedom to account for the positive bias from the violation of sphericity, as per Laerd Statistics [172].

## 3.3.    Mould Development

To simulate the thoracic cross section of the human body, skeletal structures were encased in a silicone representation of tissues, as described by Lichtenberg et al. [73] and demonstrated by other popular medical training simulators (Table 1.2.2-1) [24]-[28]. Due to the lack of literature describing thoracic wall tissue distribution and outer thoracic wall shape, open-ended modelling techniques were implemented to ensure that models could be readily modified in the future.

To form the shape of the thoracic cross-section, an overmoulding solution was employed. Based on results from the cadaveric experimental needle insertions (Chapter 4.2), a dual-layer mould was needed to create a silicone representation of the human thoracic wall. To summarize, these results showed statistical similarities in the means of needle insertion characteristics (peak force, impulse, pulse width) between position 2 (skin and adipose tissue) and position 3 (entire thoracic cross section). This similarity indicated that the entire thoracic cross section could be statistically represented with position 2 (skin and adipose tissue) elements. However, the mean values for position 2 were consistently lower than those of position 3, indicating a need for additional tissue. The differences between position 1 (muscle and pleura) and positions 2, as well as the inclusion of position 1 elements within position 3 (muscle and pleura are contained within the entire thoracic cross section), indicated that the position 1 elements had to be represented separately from position 2. Thus, to statistically represent the

thoracic cross section (position 3), a dual layer cross section was needed (one layer for position 1 elements, and another for position 2 elements).

Using the skeletal structures as a frame, spline-representations of the thoracic wall cross-section were drawn in SolidWorks 2016 [113] on 6 evenly distributed sketching planes (50mm spacing) using the "plane" and "spline" commands, and then lofted using the "loft" command to generate an artificial tissue representation (Figure 3.3-1). Splines can be manually modified to represent varying tissue distributions, however, as no literature was found detailing dimensional distribution of tissues, it was modelled to be constant along the mid-clavicular line of the front and rear of the skeletal structures (key landmark regions). The initial default thickness of tissues was approximately 6.5mm on each side of the ribs (inner and outer).
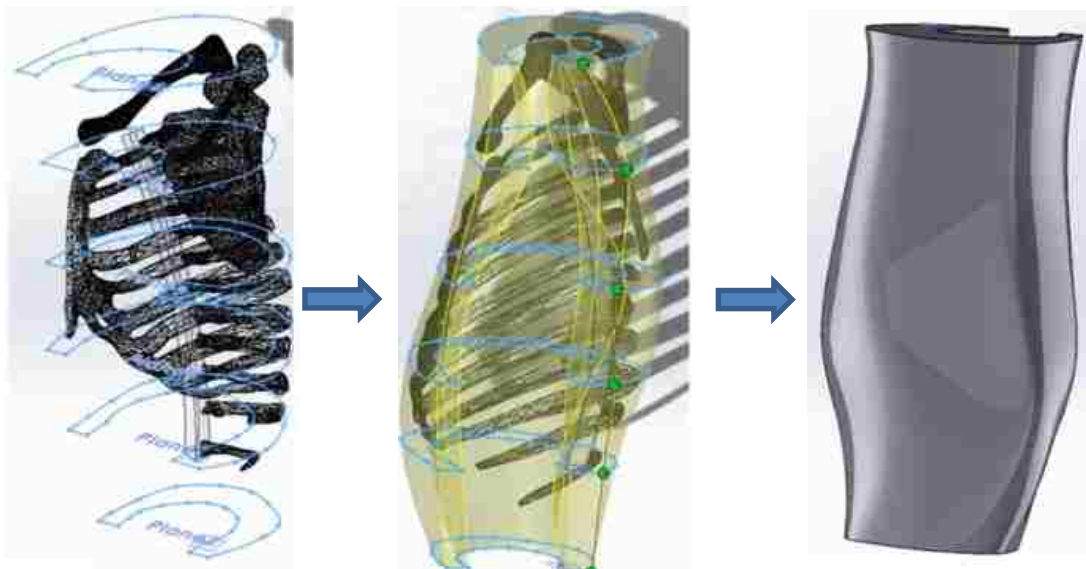


**Figure 3.3-1: Spline lofting for artificial tissue representation**

A rectangular mould block was modelled using the "extruded boss/base" command. The tissue and mould block were then inserted into an assembly together. From this tissue, a "negative" was generated in the mould-block, using

the "cavity" function, to house the skeletal structures during the silicone pouring (Figure 3.3-2 (a)). An insert was designed to provide the inner curvature of the thoracic cavity using the "extrude boss/base and extruded cut" commands to model elements 2 and 3 (Figure 3.3-2 (b)) and Table 3.3-1). Assembly features for the mould were modelled using the "extruded cut" command to model element 4 in Figure 3.3-2 (b) and Table 3.3-1.
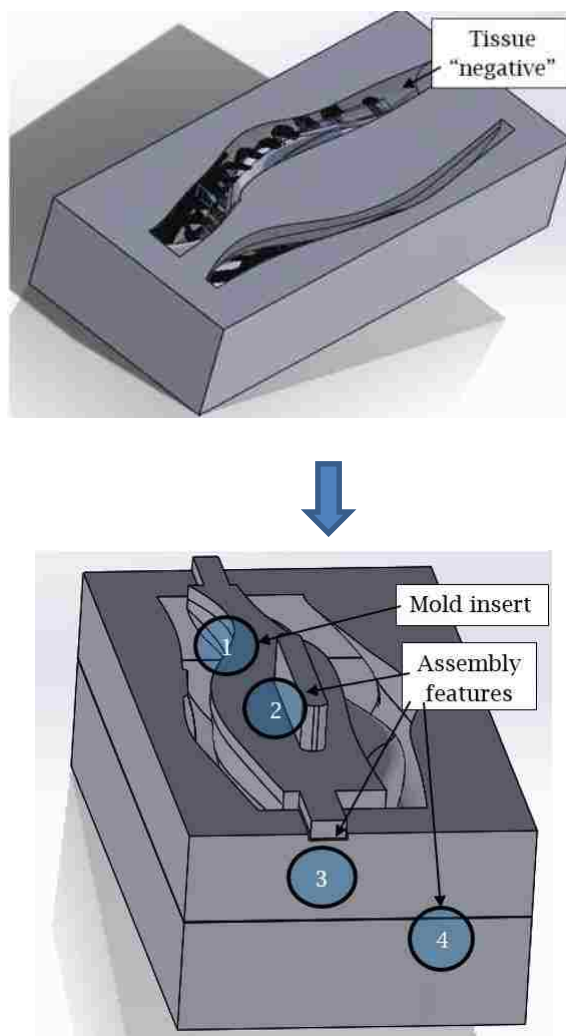


**Figure 3.3-2 (a): Tissue 'negative" (top), (b): Insert and assembly feature modifications (bottom)**

Table 3.3-1: Mould modification summary

| Element | Function |
|---------|----------|
| 1 | Provides inner shape and thickness of thoracic tissues, allowing for potential future placement of internal organs |
| 2 | Enables insert removal upon silicone setting |
| 3 | Accurately aligns mould insert |
| 4 | Allows for separation of mould upon silicone curing, enabling prototype removal |

Mould modifications for tissue thickness re-configurability were implemented using the "surface offset" command, to offset the outer surface of the tissue "sheet", which was parametrically linked to the mould set automatically through the use of the "cavity" command. Figure 3.3-3 depicts the surface offset, which allows for the representation of varying patient thoracic wall thicknesses.
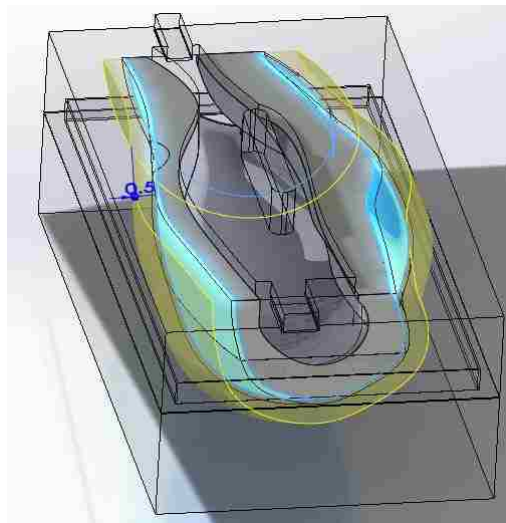


Figure 3.3-3: Parametric offset of tissue and mould

Due to the parametric relationship between the mould and tissue sheet, altering the tissue thickness results in the mould automatically adapting to fit the new shape. Model configuration for the target patient representation (adult female) necessitated a thoracic wall thickness of 25mm, as per cadaver

75

specifications. Additional thoracic wall thickness can be obtained by modifying the surface offset, to account for obesity in the demographic. Initial configuration allows for a horizontal thickness ranging from 0mm (no tissue) to 113.5mm, along the posterior axillary line (to accommodate peak in thoracic wall thickness in Harcke et al.'s study [55], as well as additional adipose tissue from potential obesity) (Figure 3.3-4), based on the initial mould block size. Additional thickness may be achieved by modifying the mould block; however, to save material a minimal block size (202mm x 407mm x 417mm) was used (Figure 3.3-5 (a) and (b)). Silicone pouring strategies are outlined in Chapter 3.5.1.
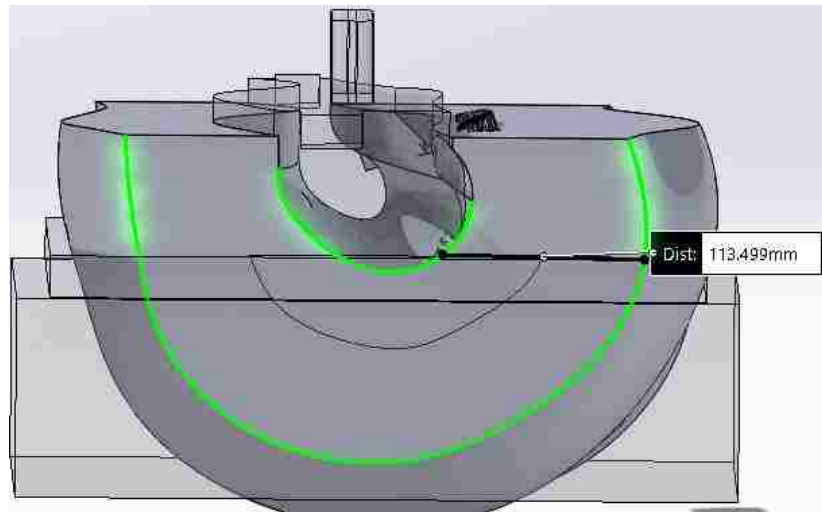


Figure 3.3-4: Maximal thoracic wall thickness for initial mould configuration
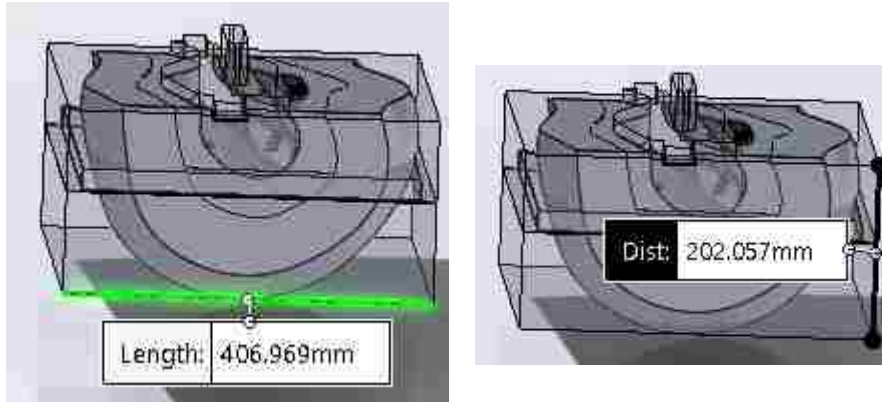
**Figure 3.3-5 (a) and (b): Dimensions of intiial mould block configuration**

### 3.3.1. Quick-Change Mould Modifications

To further leverage the adaptability of CAD modelling, a quick-change element was developed using SolidWorks 2016. This quick-change element allows for post-fabrication (silicone pouring) tissue re-configurability. Modifications were incorporated to the artificial tissues and mould base (Figure 3.3.1-1). The "extruded boss/base" command was used to model "pegs", used for alignment into the mould, resulting in extruded pegs into the actual silicone tissue (4 in Figure 3.3.1-1). Peg "negatives" were incorporated into the artificial tissue design, using "extruded boss/base" commands, and an "up to surface" constraint to obtain automatically adapting pegs that maintain contact with the mould shape, regardless of the tissue sizing (3 in Figure 3.3.1-1). These pegs served to provide alignment features upon silicone pouring (the pegs in the tissue result in negatives into the silicone outer layer, and the negatives form extruded pegs into the inner tissue, allowing for insertion into each other). An additional groove in the artificial tissue and corresponding mould was modelled using the "extruded

77

boss/base" and "extruded cut" commands. Modification functions are summarized in Table 3.3.1-1.
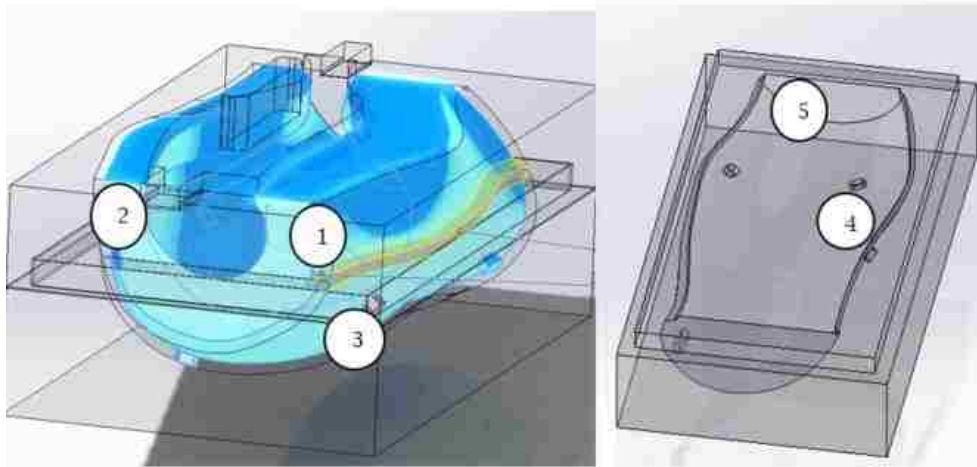


**Figure 3.3.1-1: Quick-change mould modifications**

**Table 3.3.1-1: Quick-change mould modifications function summary**

| Element Number | Description |
|---|---|
| 1 | Horizontal artificial tissue slots for locking in edges of outer tissue |
| 2 | |
| 3 | Artificial tissue locking "pegs" and spacers for creating peg "negatives" in outer tissue |
| 4 | Mould "negatives" for creating pegs in inner tissues to lock into peg "negatives" in outer tissue |
| 5 | Horizontal ribs for creating "negative" in inner tissue for alignment of edges with outer tissue ribs |

To assess tissue re-configurability, comparisons between tissue thicknesses detailed in the literature, the THM-30 and the thickness range of the parametric mould sets was performed. This was performed on the CAD models using the "measure" command in SolidWorks 2016, and using calipers on the THM-30 and fabricated models from this thesis.

### 3.3.2. Mould Optimization

To reduce overall material usage and to accommodate build envelopes of smaller printers, mould optimization was performed. Based on the cross sectional analysis of the tissues presented in Chapters 3.5.1 and 4.6.2, ambient room temperature and pressure were appropriate for the silicone pouring (no need for vacuum curing detailed by Alderson [173]). The lack of the need for vacuum indicated that only minimal strength (and therefore, minimal material) was needed for proper silicone pouring in this application.

Initial deletion of faces using the "delete face" command in SolidWorks 2016 was performed, leaving only the upper and inner surfaces of the mould base, and lower and inner surfaces of the mould top (Figure 3.3.2-1). The "thick surface" command was used to extrude the surfaces of the moulds, with a thickness value of 6.35mm (Figure 3.3.2-2 (a) and (b)).
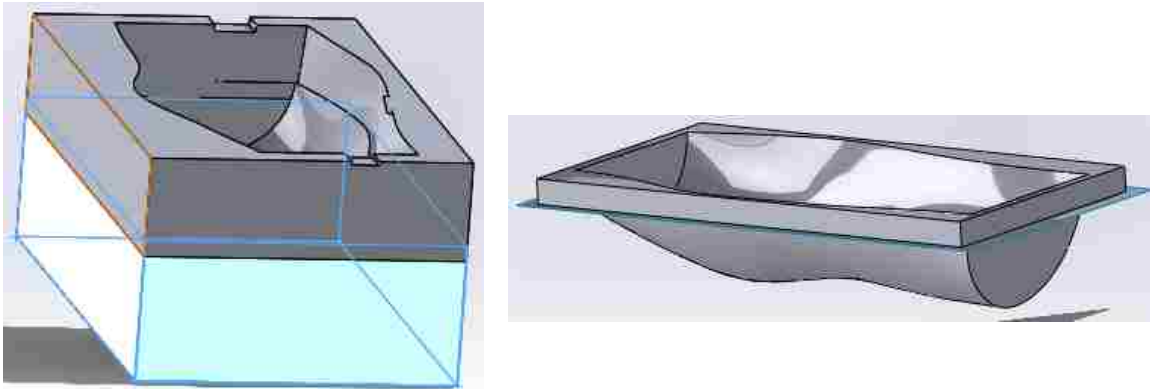


**Figure 3.3.2-1 (a): Deletion of perimeter faces, (b) Remaining inner and upper surfaces of mould base**
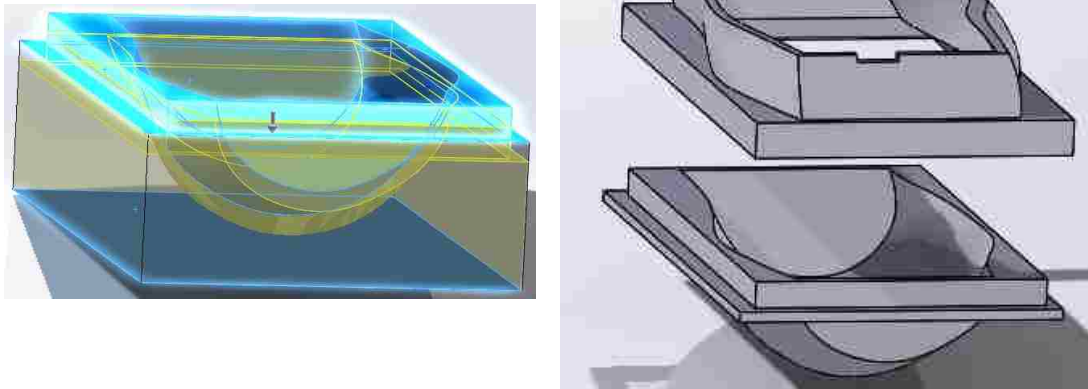
**Figure 3.3.2-2 (a): "Thickening" of mould faces to obtain solid body, (b): Upper and lower thickened mould elements**

Supports were then incorporated to the mould base to maintain neutral orientation (prevent rolling) during the silicone curing process. For these supports, rectangular profiles were extruded using the "extruded boss/base" command (Figure 3.3.2-3).
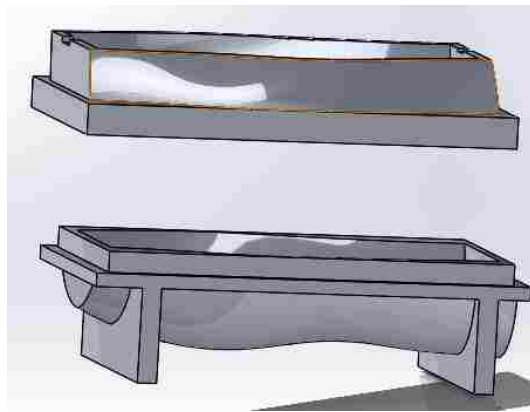


**Figure 3.3.2-3: Mould base supports**

The mould insert and artificial tissue representations were hollowed using the "shell" command with a boundary thickness of 2.54mm (Figure 3.3.2-4). The thickness for these two elements was defined to minimize material use, as the elements would not be subjected to load throughout the silicone curing process.
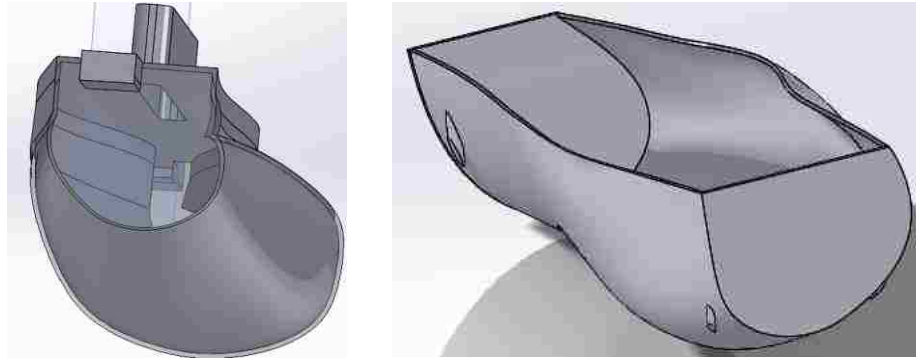
**Figure 3.3.2-4: "Shelled" artificial tissue and mould insert**

Completed mould elements were then split along a central plane, using the "split" command, to accommodate for smaller build envelopes (Figure 3.3.2-5). Upon completion, separated mould elements were adhered together using an epoxy resin, as per Cordes [174].
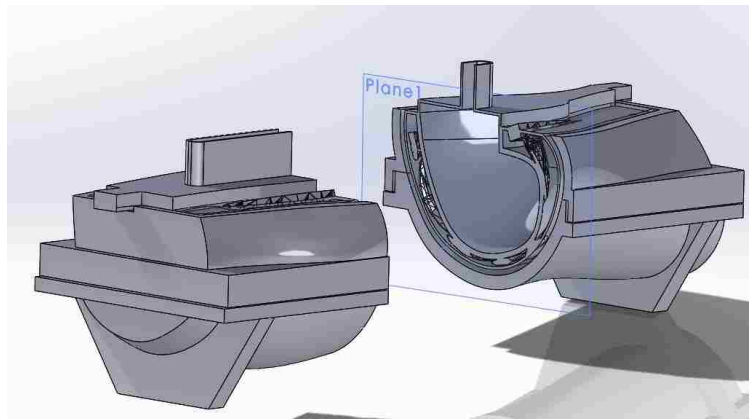


**Figure 3.3.2-5 Split mould set for fabrication using smaller build envelopes**

Upon completion of mould optimization, a comparison of material used for fabrication was performed. Measurements for model volume were performed using the "mass properties" tool in SolidWorks 2016 (Figure 3.3.2-6).
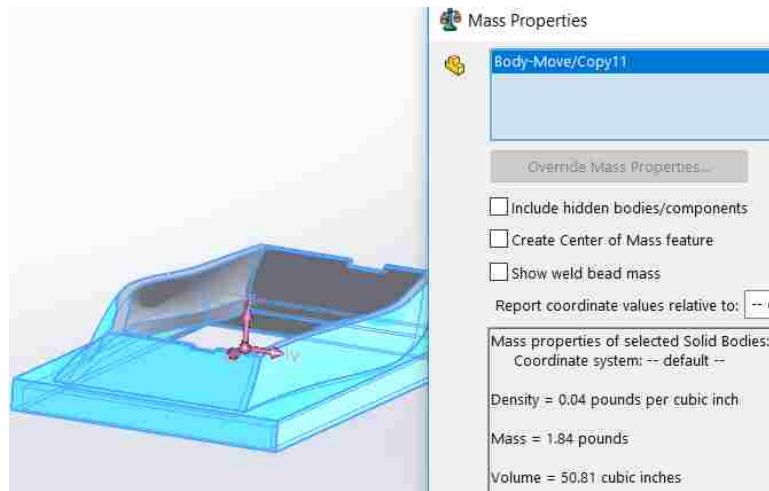
**Figure 3.3.2-6: Measurement of mass properties of mould top**

## 3.4.    Silicone Tissue "Calibration"

The use of a variable-hardness silicone [180] enabled the tailoring of mixtures to simulate different tissues, with different properties, as previously demonstrated by Wang et al. [138]. A variety of ratios of oil-silicone (Table 3.4-1) were mixed to obtain different 15mL, 12.5mm-thick samples (Figure 3.4-1) to be punctured and compared to the cadaver and THM-30 values. In so doing, controllable individual layer needle insertion forces were obtained, and correlated to cadaver tissues.

Initial silicone durometer was calibrated using a proprietary blend directly from the company (exact composition unknown) to represent the characteristics of human skin [180]. As per company recommendation, addition of oil was performed in 1 drop (equivalent to 1.01%) intervals to determine optimal consistency for the representation of muscle tissue (which was not an available proprietary blend directly from the company). Furthermore, recommendations from a different company (with a similar product) recommended that oil

percentages not exceed 10%, thus an initial range of 0% to 8.08% oil content was tested [181].



Figure 3.4-1: Isolated silicone layers with varying constitutions

Table 3.4-1: Silicone sample oil content

| Sample | % Oil |
|--------|-------|
| 0      | 0     |
| 1      | 1.01  |
| 2      | 2.02  |
| 3      | 3.03  |
| 4      | 4.04  |
| 5      | 5.05  |
| 6      | 6.06  |
| 7      | 7.07  |
| 8      | 8.08  |

To obtain values for comparison with the cadaver, a similar needle insertion experiment was repeated on the tissues developed in this thesis.

### 3.4.1. Participants

This experiment was conducted with the same 5 male participants (aged 23-25, with no clinical experience) who participated in the THM-30 needle insertion experiment. Participants performed manual needle insertions into the silicone samples to determine appropriate silicone-oil ratios to represent the peak force

(N), impulse (N·s) and pulse width (s) of the position 1 (muscle, pleura) and 2 (skin, adipose tissues) tissues from the cadaver

### 3.4.2. Instrumentation and Data Acquisition

Identical instrumentation and data acquisition techniques detailed in Chapter 3.2.2 were employed in this experiment.

### 3.4.3. Experimental Procedures and Protocol

All silicone testing procedures were performed on the same day, within an hour of each other. The independent variables for this procedure were the trial number and sample number, and dependent variables were the peak force (N), impulse (N·s) and pulse width (s).

Subjects were given the same instructions; to grasp the apparatus by the base, position it perpendicularly to the insertion site (center of the silicone sample) and wait for a verbal queue, indicating zeroing of the WiDACS. Once the queue was given, participants firmly pressed down on the needle until complete insertion through the tissues involved was achieved, indicated by the sudden drop in resistance, as well as observation of the needle penetrating through the silicone. Once completed, participants removed the needle and repositioned it for the next test. Each participant performed 3 tests in each sample, for a total of 15 insertions in each sample (150 total insertions).

### 3.4.4. Data Analysis

Identical data analysis techniques as detailed in Chapter 3.2.4 were used in this experiment.

### 3.4.5. Statistical Analysis

Statistical analysis was performed to eliminate outliers (identified using the logic previously outlined in Table 3.2.4-1) to determine values for peak force (N), impulse (N·s) and pulse width (s) for the silicone samples and to correlate silicone compositions to cadaveric tissues. Three 5 x 11 (5 participants, 11 samples (9 silicone samples, with the addition of the position 1 and 2 cadaveric insertion results for comparison)) Repeated Measures ANOVAs were performed to determine any statistical similarities between silicone samples and the cadaver insertions. Significance for the ANOVAs was set at $p < 0.05$. Tukey's HSD (Honest Significant Difference) was used compare mean values for peak force (N), impulse (N·s) and pulse width (s) and determine statistical significance of oil-silicone ratios on measured variables.

### 3.5. Fused Deposition Modelling of Models

With adaptable designs created, Fused Deposition Modelling (FDM) with a Fortus 400mc was used to fabricate all of the structures modelled (skeletal and mould components). ABS-M30 [151] was used as the model material. Solid infills were used for skeletal structures to maximize strength and partial infills (partial part density via strategic toolpaths) were used for the mould structures to reduce overall weight and manufacturing cost/time. 3 perimeter passes were used to ensure impermeability of mould structures, so as not to offset silicone compositions upon pouring. SR-30 support material [155] was used in the fabrication to support parts with intricate geometries (Figure 3.5-1) or angles exceeding the allowable free-hanging print threshold (approximately 45˚,

depending on material and extrusion characteristics [147], [148]). Post-fabrication processing was performed to remove support material from fabricated models using a CleanStation soluble-support caustic bath [153].
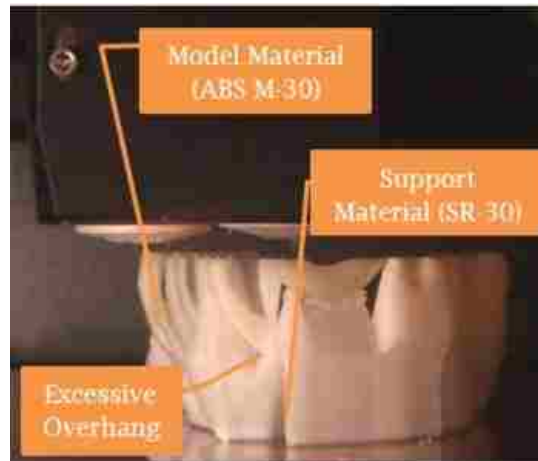


**Figure 3.5-1: Additive manufacturing of rib cage**

### 3.5.1. Silicone Tissue Fabrication and Evaluation

Utilizing the optimized mould set, a two-staged silicone pouring process was performed. By inserting the external tissue insert into the larger mould set, and pouring an initial silicone layer into the gap (Figure 3.5.1-1 (a)), which was present due to the size difference between the two (equivalent to position 2 elements, with a thickness of 12.5mm), an initial silicone layer was obtained (Figure 3.5.1-1 (b)). A composition corresponding to the cadaver position 2 needle insertion resistive forces was used (determined in Chapters 3.4 and 4.3). A second pour was performed, removing the tissue insert and inserting the skeletal structures between the first silicone tissue representation and the remainder of the mould. The internal insert was also implemented to provide shape to the inner surface of the thoracic wall representation (Figure 3.5.1-1 (b)). A composition

86

corresponding to the position 1 cadaveric needle insertions was used for this second layer (Chapter 3.4 and 4.3). The product of the second pour is the addition of the position 1 (muscle and pleura) elements to the initial tissue, representing position 2 elements (skin, adipose tissues).
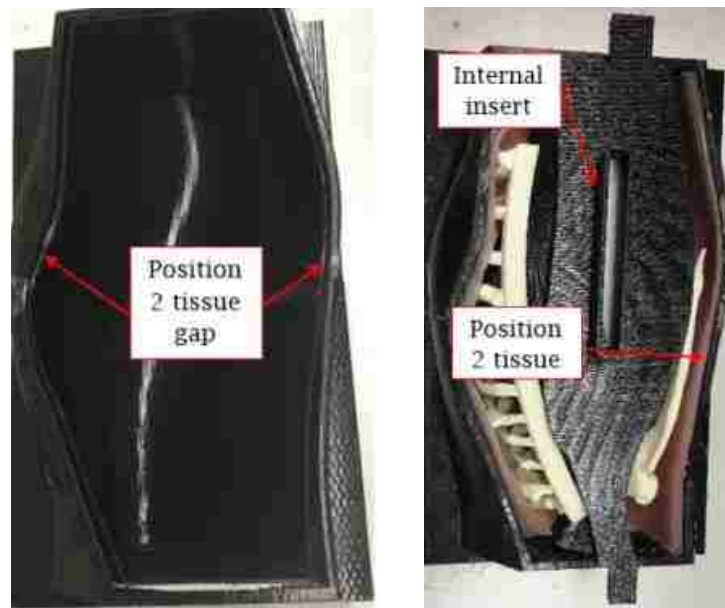


**Figure 3.5.1-1 (a): Mould set gap for pouring of first silicone layer, (b) Preparation for second silicone pour of two-pour overmoulding procedure**

Following this, insertions were performed on the thoracic wall representation fabricated with the selected tissues, which was modelled to represent the tissues of the cadaver patient. Tissue thickness was 25mm, with 12.5mm-thick layers representing the position 1 and 2 elements.

The thoracic wall representation testing was performed in an identical manner as the THM-30 needle insertion testing; with the same participants, at the same time of day and under identical conditions. Using tissues which were correlated to individual tissue layers, a combined cross-section was evaluated, and compared to the THM-30 and the cadaver position 3 tests. Insertions were

performed into the 9th intercostal space, along the mid-clavicular line of the fabricated model (Figure 3.5.1-2).



**Figure 3.5.1-2: Needle insertion site on thoracic wall representation**

Data analysis techniques were identical to the other experiments. Repeated Measures ANOVAs were performed to determine if the combination of the two silicone compositions, correlated to the position 1 and 2 elements of the human thoracic cross section was appropriate (indicated by statistical similarity in results). Three 5x2 (5 participants, 2 samples (combined silicone layers corresponding to tissue layers, and the cadaver results)) Repeated Measures ANOVAs were performed, with a significance of p=0.05. Tukey's HSD (Honest Significant Difference) was used compare mean values for peak force (N), impulse (N·s) and pulse width (s) and determine the statistical correlation (if any) between the dual-layer silicone tissues developed in this thesis, and the position 3 (entire cross section) tissues of the cadaver subject.

Upon completion of these elements and testing, a cross-sectional analysis of the insertion site was performed to ensure no inconsistencies (bubbles, improperly mixed silicone) were present, thereby offsetting results. This was performed with a band-saw, to saw through the structures along the mid-clavicular line, to expose the site of needle insertion. Results from this cross-sectional analysis were influential on the development of the optimized mould set previously described in Chapter 3.3, specifically, on the amount of material (and associated strength) needed for the mould sets.
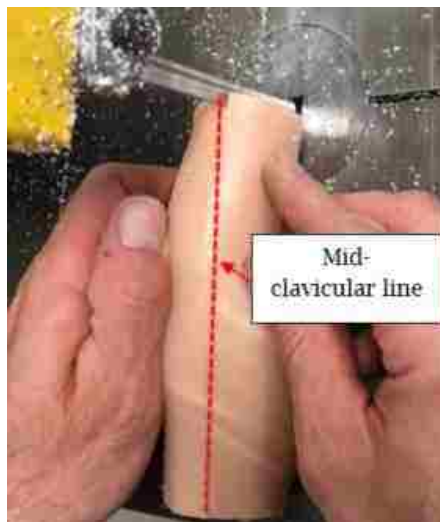


**Figure 3.5.1-3: Cross-sectional analysis preparation of simulated thoracic wall representation**

Upon completion of all design and fabrication as well as evaluation of tissues and landmark orientation and accuracy, a comparison between the cadaver insertions, the THM-30 insertions, and the tissues developed in this thesis was performed. An additional comparison of time and cost needed for the proposed approach, and a conventional approach was also performed, using an estimate from a local engineering company [79]. The following chapter presents results for all methodologies described in this section.

# CHAPTER 4

## Results and Discussion

By following the methodology detailed in Chapter 3, three different patient CAD models and two patient thoracic walls; including all necessary skeletal landmarks and tissues, were developed. This chapter presents the results of individual sections in Chapter 3.

### 4.1. Skeletal Structure Modelling

Through the steps outlined in chapter 3.1, individual CT scan models were transformed into a scalable skeleton. Original files were trimmed and modified to generate simplified meshes, resulting in a 90.34% decrease in total meshing elements. These meshes were refined, and converted to solid models in Figure 4.1-1 (a), (b) and (c).
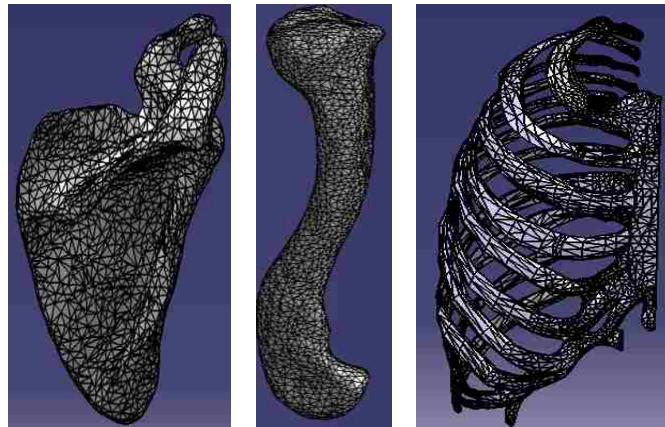


**Figure 4.1-1 (a): Scapula model, (b): Clavicle model, (c) Rib cage model**

An assembly was created from these models (Figure 4.1-2). Scaling factors from McGraw et al. [91] were used alongside initial clavicle lengths to develop Table 4.1-1, which lists scaling factors with which to scale the entire skeletal

assembly. Scaling factors to represent the three target patient representations (2-year-old male, 18-year-old female and 30-year-old male) are highlighted in yellow in Table 4.1-1.



Figure 4.1-2: Completed skeletal assembly

Table 4.1-1: Clavicle-based scaling factors for scaling of skeletal assembly. Starred values indicate 80% of total skeletal growth

| Age (years) | Male | | | Female | | |
|---|---|---|---|---|---|---|
| | Clavicle Length (mm) | Growth Rate (mm/yr.) | Scaling Factor Input | Clavicle Length (mm) | Growth Rate (mm/yr.) | Scaling Input Factor |
| 0 | 37.6 | 9.06 | 0.236 | 37.8 | 8.49 | 0.237 |
| 1 | 46.66 | 9.06 | 0.293 | 46.29 | 8.49 | 0.290 |
| 2 | 55.72 | 9.06 | 0.349 | 54.78 | 8.49 | 0.343 |
| 3 | 64.78 | 9.06 | 0.406 | 63.27 | 8.49 | 0.397 |
| 4 | 73.84 | 9.06 | 0.463 | 71.76 | 8.49 | 0.450 |
| 5 | 80.51 | 6.67 | 0.505 | 80.71 | 8.95 | 0.506 |
| 6 | 87.18 | 6.67 | 0.547 | 89.66 | 8.95 | 0.562 |
| 7 | 93.85 | 6.67 | 0.588 | 98.61 | 8.95 | 0.618 |
| 8 | 100.52 | 6.67 | 0.630 | 107.56 | 8.95 | 0.674 |
| 9 | 107.19 | 6.67 | 0.672 | 116.51* | 3.41 | 0.731 |
| 10 | 113.86 | 6.67 | 0.714 | 119.92 | 3.41 | 0.752 |
| 11 | 120.53 | 6.67 | 0.756 | 123.33 | 3.41 | 0.773 |
| 12 | 127.2* | 5.38 | 0.798 | 126.74 | 3.41 | 0.795 |
| 13 | 132.58 | 5.38 | 0.831 | 130.15 | 3.41 | 0.816 |
| 14 | 137.96 | 5.38 | 0.865 | 133.56 | 3.41 | 0.837 |
| 15 | 143.34 | 5.38 | 0.899 | 136.97 | 3.41 | 0.859 |
| 16 | 148.72 | 5.38 | 0.933 | 140.38 | 3.41 | 0.880 |
| 17 | 154.1 | 5.38 | 0.966 | 143.79 | 3.41 | 0.902 |
| 18-100 | 159.48 | 5.38 | 1.000 | 147.2 | 3.41 | 0.923 |

A comparison of the error between the predicted (according to growth rates in Table 4.1-1) and measured values, and the standard deviations in the reported values from McGraw et al. [91] is presented in Figure 4.1-3 and Figure 4.1-4, with error percentage and standard deviations referencing the secondary axis (% Variance).
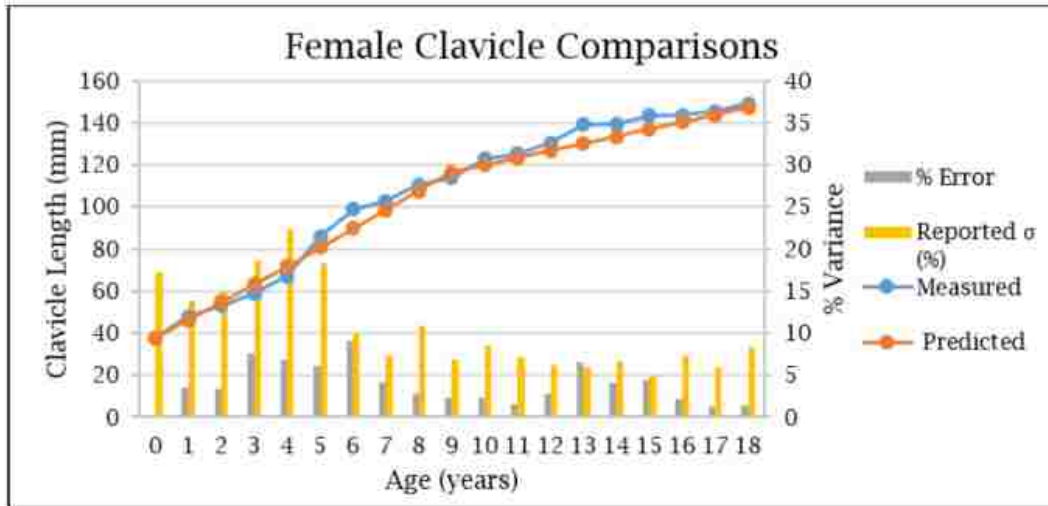


Figure 4.1-3: Female clavicle comparisons between calculated error (between measured and predicted lengths), and reported standard deviations
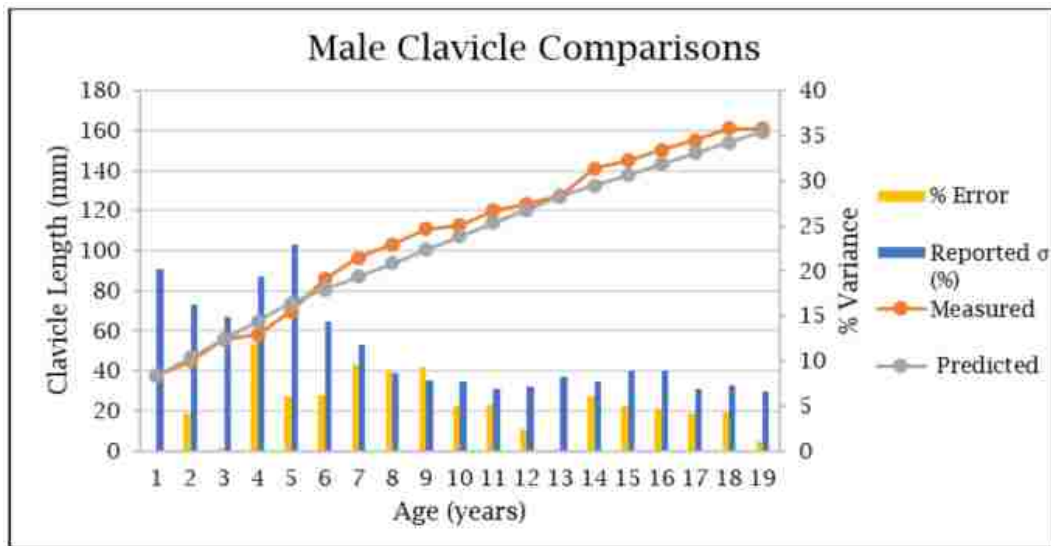


Figure 4.1-4: Male clavicle comparisons between calculated error (between measured and predicted lengths), and reported standard deviations

Intercostal spacing measurements from scaled skeletal structures representative of the 18-year old female and 2 year old male are presented in Figure 4.1-5 (a) and (b).
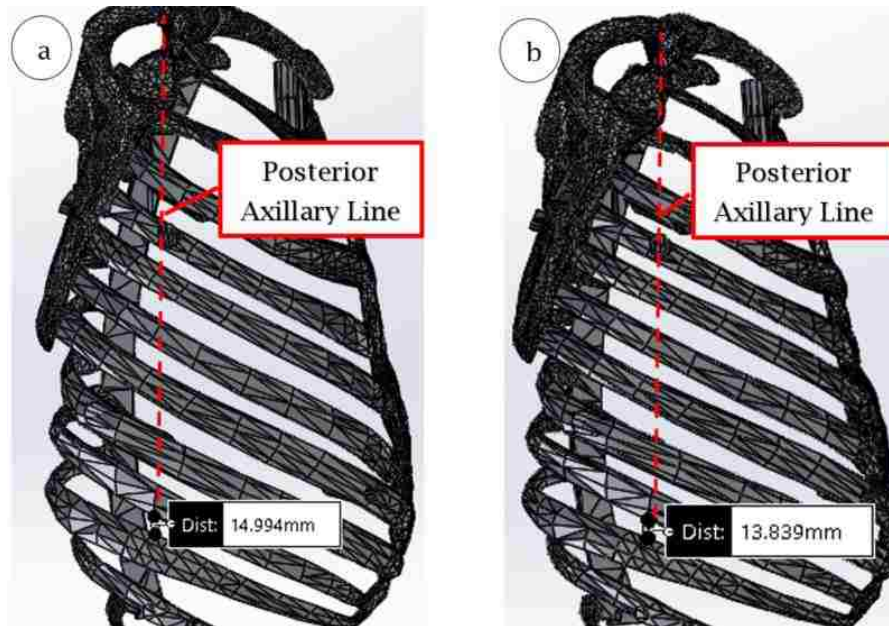


**Figure 4.1-5 (a): Intercostal spacing measurement alonge posterior axillary line with scaling factor of 1, to represent a 30 year old male. (b): Intercostal spacing measurement along posterior axillary line with scaling factor of 0.923, to represent an 18-year-old female**

Comparisons between clavicle and intercostal space measurements for the three target patients from the literature and skeletal assemblies developed in this thesis are presented in Table 4.1-2. Also included in this table are the intercostal spacing measurements from the THM-30 for reference.

Table 4.1-2: Skeletal landmark comparisons

| Landmark / Patient | Clavicle Length (Literature) (mm) | Clavicle Length (Scaled) (mm) | % Difference | Intercostal Space Width (Literature) (mm) | Intercostal Space Width (Scaled) (mm) | % Difference | THM-30 Intercostal Space Width (mm) |
|---|---|---|---|---|---|---|---|
| 2 Yr. Old Male | 55.5 | 55.7 | 0.40 | | | | |
| 18 Yr. Old Female | 149.2 | 147.2 | 1.3 | 14.2 | 13.8 | 2.8 | 27.5 (93.7% and 99.3% difference for female literature and scaled, respectively) |
| 30 Yr. Old Male | 161.2 | 159.5 | 1.1 | 14.9 | 15.0 | 0.70 | (84.6% and 83.3% difference for male literature and scaled, respectively) |

## 4.2.    Cadaver and THM-30 Experimental Needle Insertion Results

This section presents results from needle insertions on the THM-30 and the cadaver patient. All SPSS data readouts are presented in Appendix B.

### 4.2.1. Outlier Replacement and Positional Means

Tests for the cadaver insertions identified one outlier, which was replaced (position 1, trial 14, peak force) with the mean value of remaining trials for that position. Cadaveric insertion mean-values for position 1 (muscle, pleura), 2 (skin, adipose tissues) and 3 (entire cross section) are presented in Figure 4.2.1-1, Figure 4.2.1-2 and Figure 4.2.1-3.
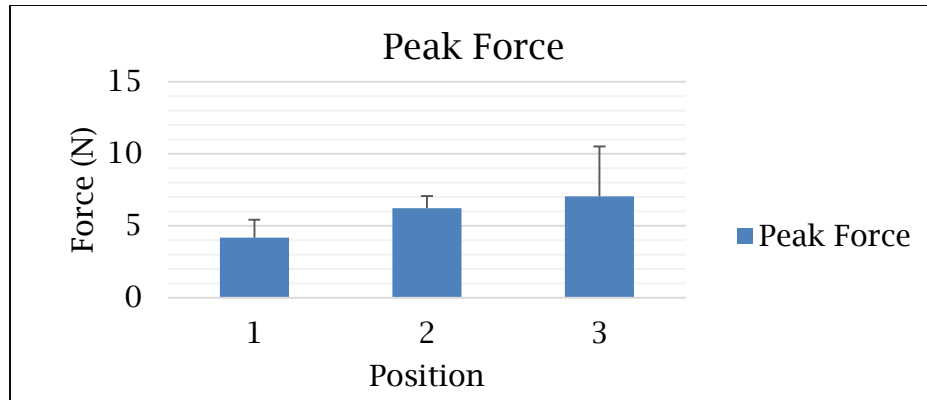
**Figure 4.2.1-1: Peak force mean values of cadaver needle insertions for position 1-3**
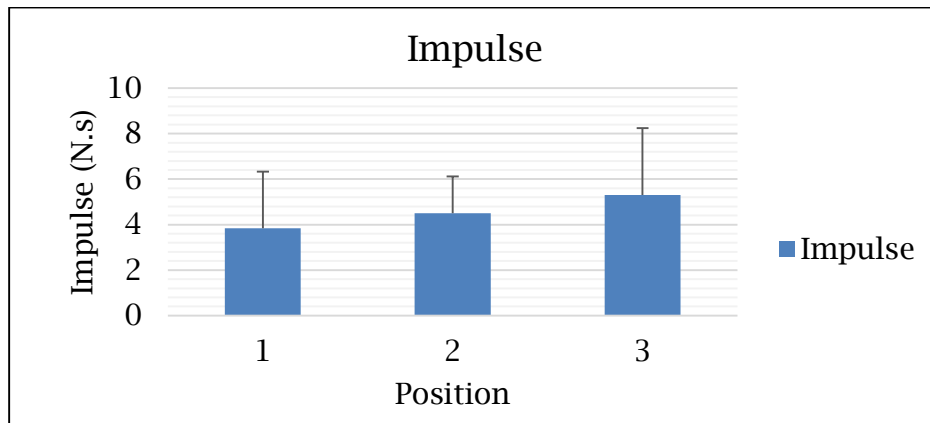


**Figure 4.2.1-2: Impulse mean values of cadaver needle insertions for position 1-3**
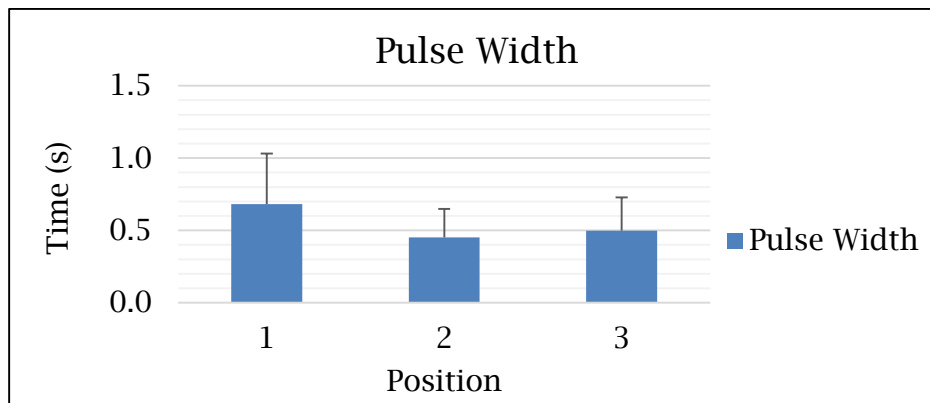


**Figure 4.2.1-3: Pulse width mean values of cadaver needle insertions for position 1-3**

Figure 4.2.1-1, Figure 4.2.1-2 and Figure 4.2.1-3 depict the dominance of the position 2 (skin, specifically) tissues on the needle insertion characteristics of the

human thoracic cross section, reconfirming trends observed in the literature showing greater influence of the skin compared to muscle and adipose tissue [137], [138], [144], [141]. Furthermore, position 2 tissues exhibited peak forces consistent with those from the literature (average peak force of 6.23 N for cadaveric tissue vs. 6.0N for living [60]), indicating potential similarities between cadaver and living tissues, further reinforcing the decision to obtain cadaver data. Peak force and impulse are consistently lower in the position 1 elements, compared to position 2 elements (4.17N and 3.85N·s, compared to 6.23N and 4.50N·s). The position 3 elements (containing both position 1 and 2 elements within) are consistently more similar to position 2 than position 1 (29.23% and 12.42% closer for peak force and impulse, respectively). While needle insertion into tissue is complex, it would be expected for values to double (or at the very least, increase proportionally to the values of position 1) upon insertion into the entire thoracic cross section, however this trend is not observed. The dominance of position 2 on thoracic needle insertions is also exemplified by the pulse width. Mean values of position 2 and 3 are 46.19% closer than those of 1 and 3. This is likely due to the nature of manual needle insertions, which are subject to varying insertion velocities. With the larger force associated with the puncture of position 2, compared to position 1, momentum generated by the hand forcing the needle through the skin carries the hand through the remainder of the softer tissues (position 1) more rapidly. These trends are further reinforced in chapter 4.3.2.

Outliers from the THM-30 punctures identified and replaced were: trial 3 (peak force), trial 5 (impulse and pulse width), and trial 6 (impulse and pulse width). A comparison between values from the THM-30 needle insertions, and the position 3 insertions from the cadaver is presented in Table 4.2.1-1.

Table 4.2.1-1: Mean values and differences between cadaver (position 3) and THM-30 needle insertions

| | Peak Force (N) | σ (N) | Impulse (N·s) | σ (N·s) | Pulse Width (s) | σ (s) |
|---|---|---|---|---|---|---|
| **Cadaver** | 7.04 | 3.47 | 5.30 | 2.94 | 0.50 | 0.23 |
| **THM-30** | 5.03 | 0.19 | 4.22 | 0.41 | 0.83 | 0.09 |
| **% Difference** | 28.55 | | 20.38 | | -66.00 | |

Graphical representations of comparisons between the position 3 insertions and the THM-30 punctures are illustrated in Figure 4.2.1-4, Figure 4.2.1-5 and Figure 4.2.1-6. A supplementary graphical representation of the means of the simulator and cadaver insertion curves is provided in Figure 4.2.1-7. This figure was obtained by manually aligning all of the curves by peak force, trimming insignificant trailing ends, averaging the curves, and overlaying them.
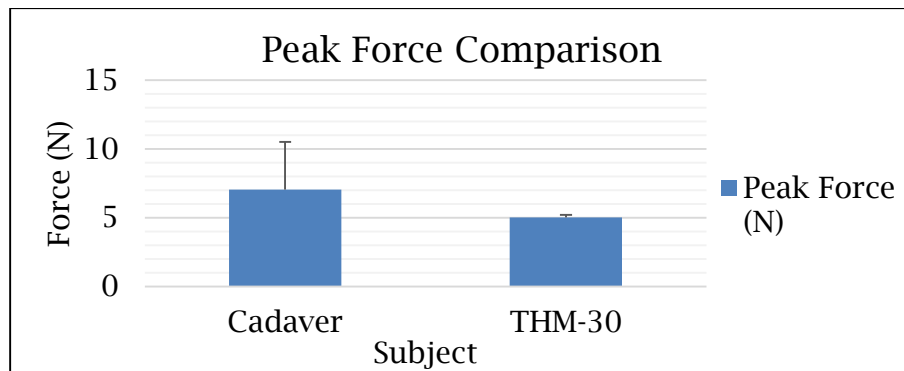


Figure 4.2.1-4: Peak force comparison between cadaver position 3 and THM-30 needle insertions
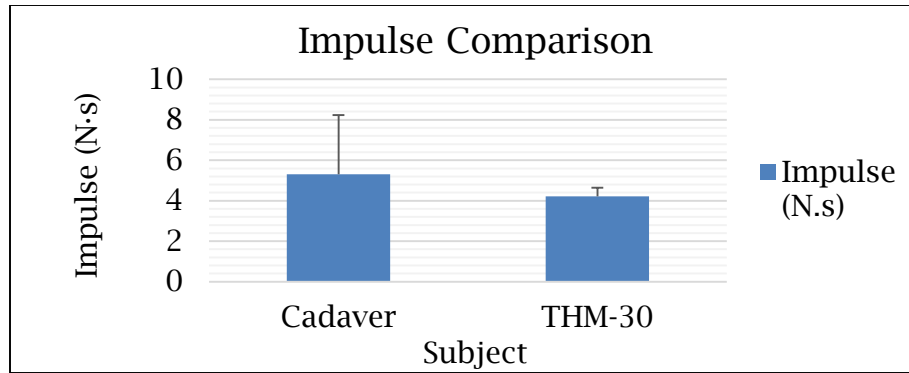
**Figure 4.2.1-5: Impulse comparison between cadaver position 3 and THM-30 needle insertion**
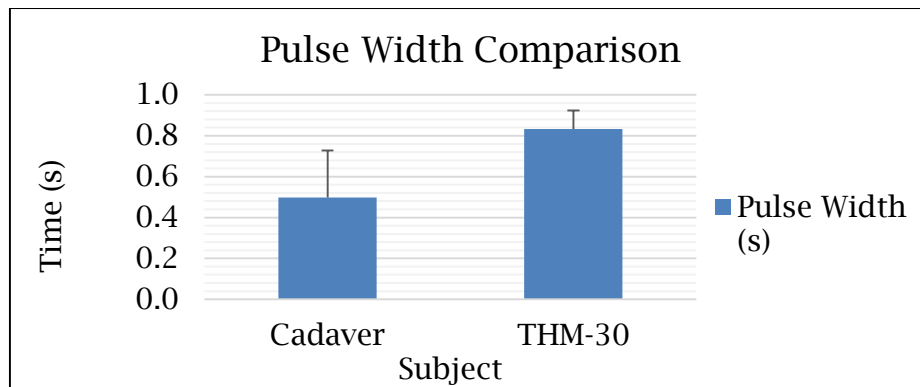


**Figure 4.2.1-6: Pulse width comparison between cadaver position 3 and THM-30 needle insertions**
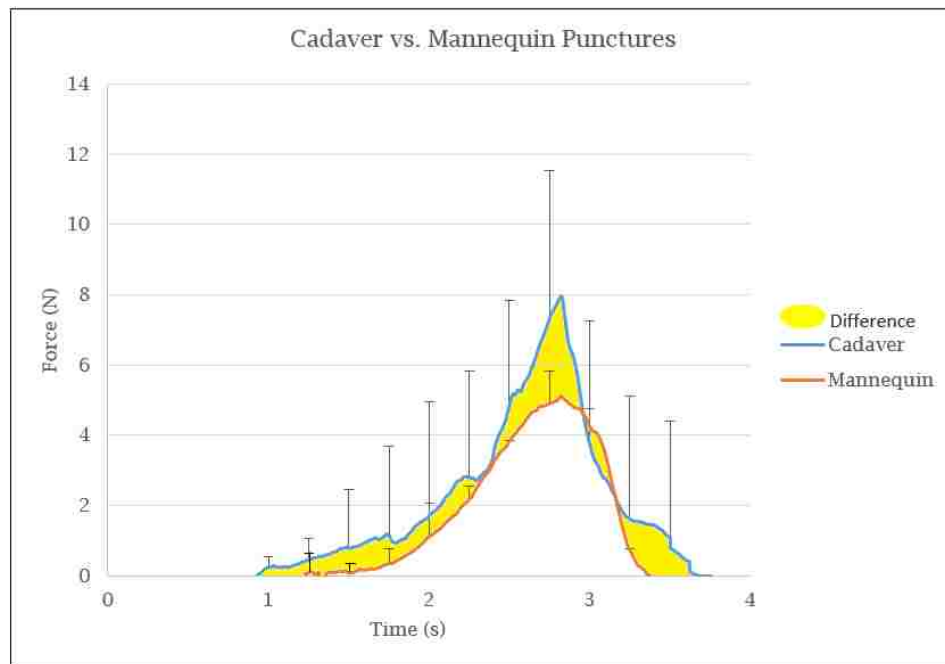


**Figure 4.2.1-7: Manually processed position 3 cadaver and THM-30 simulator puncture curves**

98

Manually integrated impulse values for the cadaver and THM-30 simulator were 6.34 N·s and 4.43 N·s, respectively, and peak forces were 7.95 N and 5.12 N. Comparing these values, impulse and peak force were 30.1% and 35.6% lower for the THM-30, compared to the cadaver subject. Additional analysis of the curves in Figure 4.2.1-7 shows differences in overall shape and number of peaks in the curves. The "steps" along the cadaver curve are representative of changes in tissue characteristics (i.e. skin vs adipose tissue), indicated by sudden changes in resistive forces felt. Each of these steps is influential on the haptic element of the needle insertions felt by the clinician's hand, however they are not observed in the THM-30 insertion curve. Furthermore, the variances in values observed in the comparisons in Figure 4.2.1-4, Figure 4.2.1-5 and Figure 4.2.1-6 are also observed in this figure, with significantly greater variances in peak force values from the cadaver needle insertions, which is speculated to be due to the inclusion of the skin tissues (along with the overall 4 tissue layer system).

### 4.2.2. Cadaver Positional Relationship Determination

5X3 Repeated Measures ANOVAs reveal a main effect of "position" in all three criteria for the cadaver needle insertions. For the peak force analysis, Mauchly's Test of Sphericity was violated ($p$=.004<0.05). The Greenhouse-Geisser correction was used to produce a more accurate reporting of data ($F_{(1.173,11.730)}$=15.649, $p$=0.001<.05). For impulse, Mauchly's Test of Sphericity was satisfied ($p$=.489>.05) and a correlation between means of positions was observed ($F_{(2,20)}$=3.687, $p$=.043<.05). Data from pulse width satisfied Mauchly's Test of Sphericity ($p$=.742>.05) and a correlation between means of positions was observed

(F(2,20)=5.965, *p*=.009<.050). Results from Tukey's pairwise comparisons for the cadaveric needle insertions are summarized in Table 4.2.2-1, with bolded values indicating similarities between tissues.

Table 4.2.2-1: Tukey's pairwise comparison results for cadaveric needle insertions

| Peak Force | | | Impulse | | | Pulse Width | | |
|---|---|---|---|---|---|---|---|---|
| Positions | Mean Difference | Sig.[b] | Positions | Mean Difference | Sig. [b] | Positions | Mean Difference | Sig. [b] |
| 1-2 | -2.058[*] | 0 | **1-2** | **-0.659** | **0.166** | 1-2 | .230[*] | 0.006 |
| 1-3 | -3.060[*] | 0.001 | 1-3 | -1.516[*] | 0.035 | **1-3** | **0.167** | **0.054** |
| **2-3** | **-1.003** | **0.181** | 2-3 | -0.858 | 0.185 | 2-3 | -0.063 | 0.341 |

*. The mean difference is significant at the .05 level.
b. Adjustment for multiple comparisons

The ANOVA results show that the means of positions 1 and 2, and 1 and 3 are statistically significantly different for two criteria (peak force and pulse width, and peak force and impulse). This difference means that they are statistically unrelated, and therefore cannot be grouped together.

Positions 2 and 3, however, are statistically similar in terms of all 3 criteria, meaning that they can be statistically grouped. This similarity indicates that the cross-section of the thoracic wall can be represented by the two-layer system (skin, and adipose tissue) developed. Position 2 alone, however, has lower mean values than position 3 (representative of the entire thoracic cross-section) in all three criteria, meaning that more tissue is needed in order to provide sufficient needle insertion resistance.

The statistical difference between positions 1 and 2 indicates that the two must be modelled separately, meaning at least one layer must consist of muscle and pleura. Given that both positions 1 and 2 are contained within position 3, a

layer representing position 1 and a second layer representing position 2, grouped together should statistically represent the entire thoracic cross section.

Based on these results, the final simulator must contain 2 layers, as opposed to the single layer found in currently utilized simulators, indicating further lack of existing simulator fidelity. These determinations are critical aspects to the design of the overmoulding components detailed in Chapters 3.3 and 4.4. Target values for the overall puncture of the dual layer simulator are those from position 3; however, if differences present themselves in the final comparison values, layers can be individually compared to positions 1 and 2, to determine the source(s) of error. It must be noted that trends observed in this experiment are contingent on the use of this specific cadaver patient, and may not be universally constant to all cadaver experiments.

## 4.3.  Silicone Tissue Evaluation

With target values for tissue needle insertion resistive forces, synthetic silicone tissues were used to emulate those of the human body. All SPSS data readouts are presented in Appendix C.

### 4.3.1. Outlier Replacement and Silicone Sample Mean Values

Needle insertions on the 9 samples yielded 7 outliers (sample 2, insertion 12, peak force; sample 2, insertion 1, impulse; sample 5, insertion 5, peak force; sample 7, insertion 1, pulse width; sample 8, insertion 13, impulse; sample 8, insertion 10, pulse width; sample 8, insertion 12, pulse width). These outliers were replaced with the mean values of the remainder of the trials for that sample.

Results from adjusted individual silicone sample needle insertions are presented
in Table 4.3.1-1, and Figure 4.3.1-1, Figure 4.3.1-2 and Figure 4.3.1-3.

Table 4.3.1-1: Silicone sample needle insertion mean values

| Sample | Peak Force (N) | σ | Impulse (N.s) | σ | Pulse Width (s) | σ |
|--------|------|-------|---------|-------|-------|-------|
| 0 | 6.229 | 0.640 | 4.034 | 0.807 | 0.623 | 0.118 |
| 1 | 4.148 | 0.290 | 2.719 | 0.819 | 0.687 | 0.195 |
| 2 | 3.305 | 0.234 | 1.782 | 0.474 | 0.614 | 0.208 |
| 3 | 2.915 | 0.240 | 1.609 | 0.599 | 0.572 | 0.167 |
| 4 | 2.579 | 0.202 | 1.536 | 0.496 | 0.610 | 0.168 |
| 5 | 1.890 | 0.182 | 1.022 | 0.340 | 0.551 | 0.119 |
| 6 | 1.372 | 0.147 | 0.561 | 0.168 | 0.394 | 0.083 |
| 7 | 1.210 | 0.088 | 0.562 | 0.107 | 0.469 | 0.107 |
| 8 | 1.108 | 0.067 | 0.358 | 0.167 | 0.379 | 0.145 |
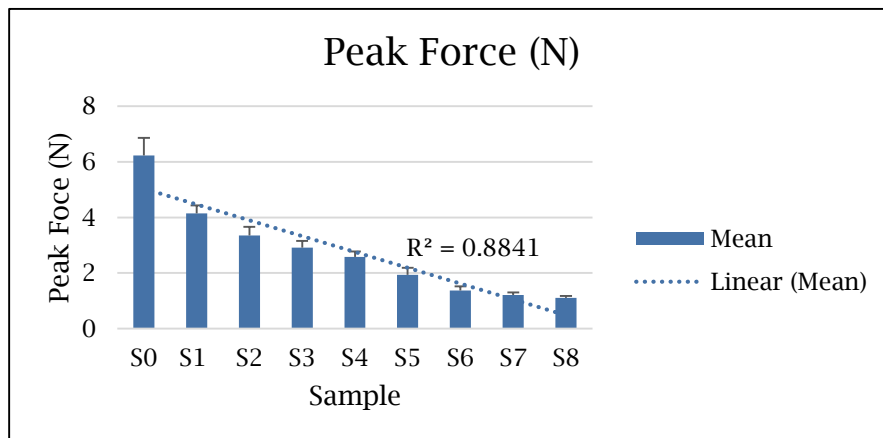


Figure 4.3.1-1: Peak force means for silicone sample needle insertions
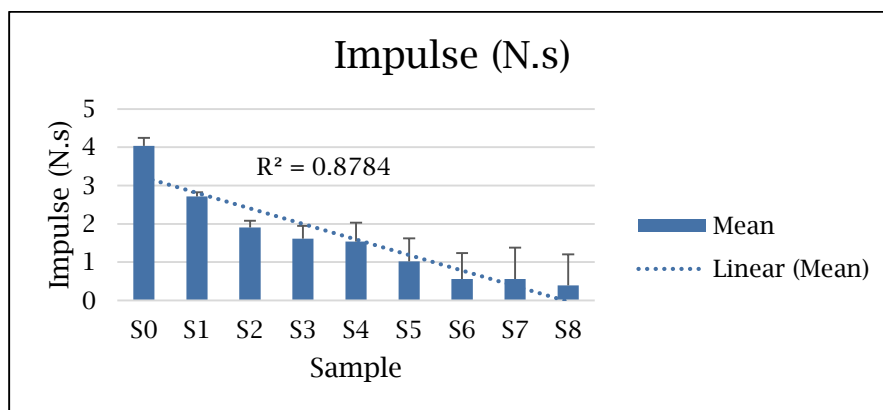


Figure 4.3.1-2: Impulse means for silicone sample needle insertions
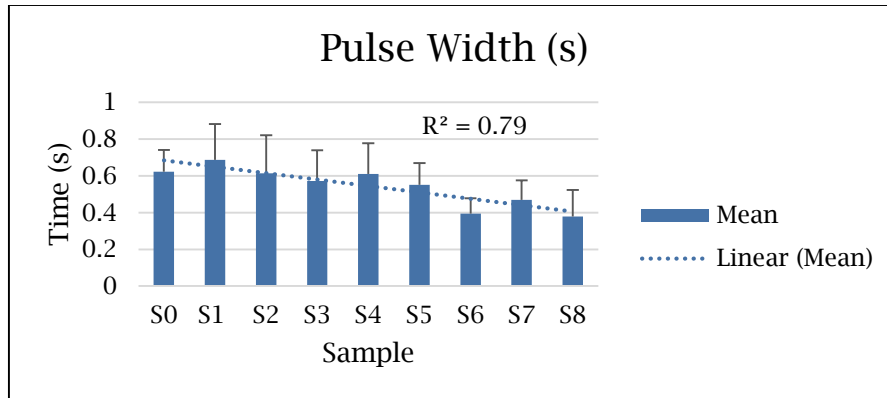
**Figure 4.3.1-3: Pulse width means for silicone sample needle insertions**

From the above figures, linearity is observed in terms of all 3 criteria (using Excel 2016's "Linear Trendline" tool). The addition of oil correlates to a decrease in needle insertion resistance, in a controllable (linear) manner.

### 4.3.2. Silicone Sample-Cadaveric Tissue Correlation

5X3 Repeated Measures ANOVAs reveal a main effect of sample in all three criteria for the silicone sample needle insertions. For the peak force analysis, Mauchly's Test of Sphericity was violated ($p$=.002<0.05). The Greenhouse-Geisser correction was used and produced a more accurate reporting of data ($F_{(2.822, 28.215)}$=249.146, $p$=0.001<.05). For impulse, Mauchly's Test of Sphericity was violated ($p$=5.839E-8>.05). The Greenhouse-Geisser correction was used and produced a more accurate reporting of data ($F_{(2.363, 23.626)}$=57.534, $p$= 2.6444E-10<.05). Data from pulse width also violated Mauchly's Test of Sphericity ($p$= 3.641E-10>.05). The Greenhouse-Geisser correction was used and produced a more accurate reporting of data ($F_{(3.436, 34.361)}$=8.493, $p$=0.135E-3<.05). Results showing statistical similarities from Tukey's pairwise comparisons pertaining to the cadaveric needle insertions (position 1 and position 2) and the silicone samples are summarized in Table 4.3.2-1.

**Table 4.3.2-1: Pairwise comparisons of position 1 and 2 of cadaveric insertions with silicone samples**

| Peak Force | | | Impulse | | | Pulse Width | | |
|---|---|---|---|---|---|---|---|---|
| Position / Sample | Mean Difference | Sig.[b] | Positions | Mean Difference | Sig. [b] | Positions | Mean Difference | Sig. [b] |
| Cadaver 1- Sample 1 | .021 | .929 | Cadaver 1- Sample 0 | -.88 | .860 | Cadaver 1- Sample 0 | .056 | .529 |
| Cadaver 2- Sample 0 | .177 | .519 | Cadaver 1- Sample 1 | 1.126 | .058 | Cadaver 1- Sample 1 | -.006 | .948 |
| | | | Cadaver 2- Sample 0 | .570 | .245 | Cadaver 1- Sample 2 | .067 | .490 |
| | | | | | | Cadaver 1- Sample 3 | .108 | .221 |
| | | | | | | Cadaver 1- Sample 4 | .071 | .373 |
| | | | | | | Cadaver 1- Sample 5 | .130 | .136 |
| | | | | | | Cadaver 2- Sample 3 | -.121 | .062 |
| | | | | | | Cadaver 2- Sample 5 | -.099 | .117 |
| | | | | | | Cadaver 2- Sample 6 | .058 | .353 |
| | | | | | | Cadaver 2- Sample 8 | -.018 | .749 |
| | | | | | | Cadaver 2- Sample 9 | .073 | .227 |

\*. The mean difference is significant at the .05 level..073
b. Adjustment for multiple comparisons

The above data demonstrates a strong correlation of the position 1 elements of the cadaver (muscle, pleura) with silicone sample number 1 in terms of all criteria. Position 2 elements of the cadaver (skin, adipose tissue) are correlated to sample 0 in terms of two criteria (peak force, impulse). Based on these similarities, sample 1 was designated to represent position 1 elements and sample 0 was selected to represent position 2 elements, reconfirming the accuracy of the "proprietary blend" from the company.

## 4.4. Mould Design

Based on literature describing the influence of multiple tissue layers on needle insertion forces, and experimentally-obtained insight, a dual-layer silicone model was required to accurately simulate the thoracic tissues of the human body. A two-pour moulding strategy was implemented, with the first pour consisting of the position 2 elements (skin, adipose tissues), and the second, the position 1 elements (muscle, pleura). Outer mould elements are depicted in Figure 4.4-1 (a) and (b) and inner components in Figure 4.4-2 (a) and (b). Element functions are detailed in Table 4.4-1.
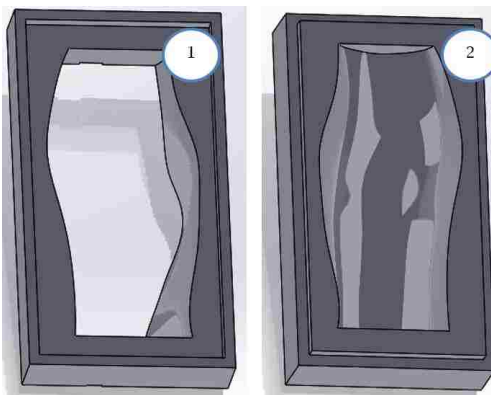


**Figure 4.4-1 (a): Top mould component, (b): Bottom mould component**



**Figure 4.4-2 (a): Tissue spacer insert, (b): Inner thoracic cavity mould**

Table 4.4-1: Mould element functions

| Element | Function |
|---|---|
| 1 & 2 | Top and bottom mould components: Provide shape of outer prototype, forming a seamless seal, while locking into position with raised and recessed edges |
| 3 | Tissue spacer insert: Allows for two-shot moulding, used in first shot to develop outer skin (position 2 elements) with variable thickness through spacer manipulation |
| 4 | Inner thoracic cavity mould: Provides appropriate spacing and shape of inner thoracic cavity |

Tissue modification and assembly scaling are depicted in Figure 4.4-3 and Figure 4.4-4, where parametric relationships result in automatically modified mould elements, representative of a different obesity level. Figure 4.4-3 depicts the initial configuration. In Figure 4.4-4, a surface offset command is illustrated, resulting in a newly adapted mould width.
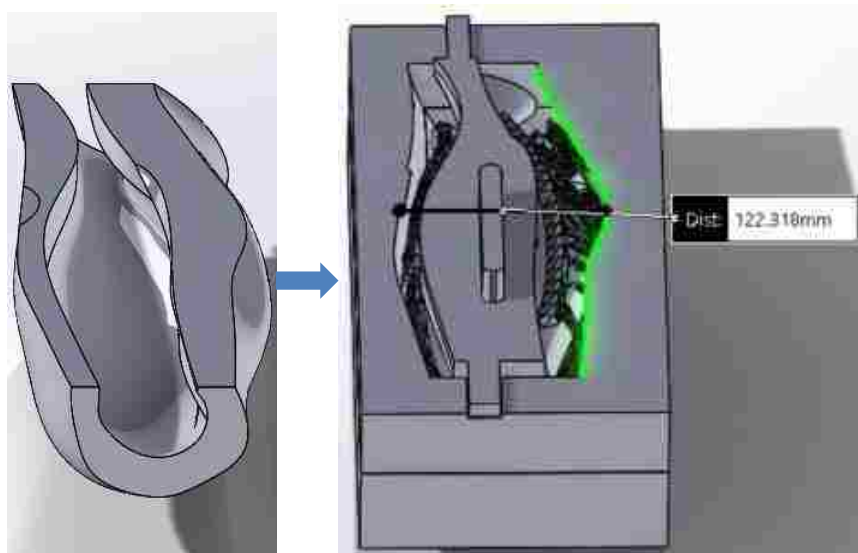


Figure 4.4-3: Initial mould obesity configuration
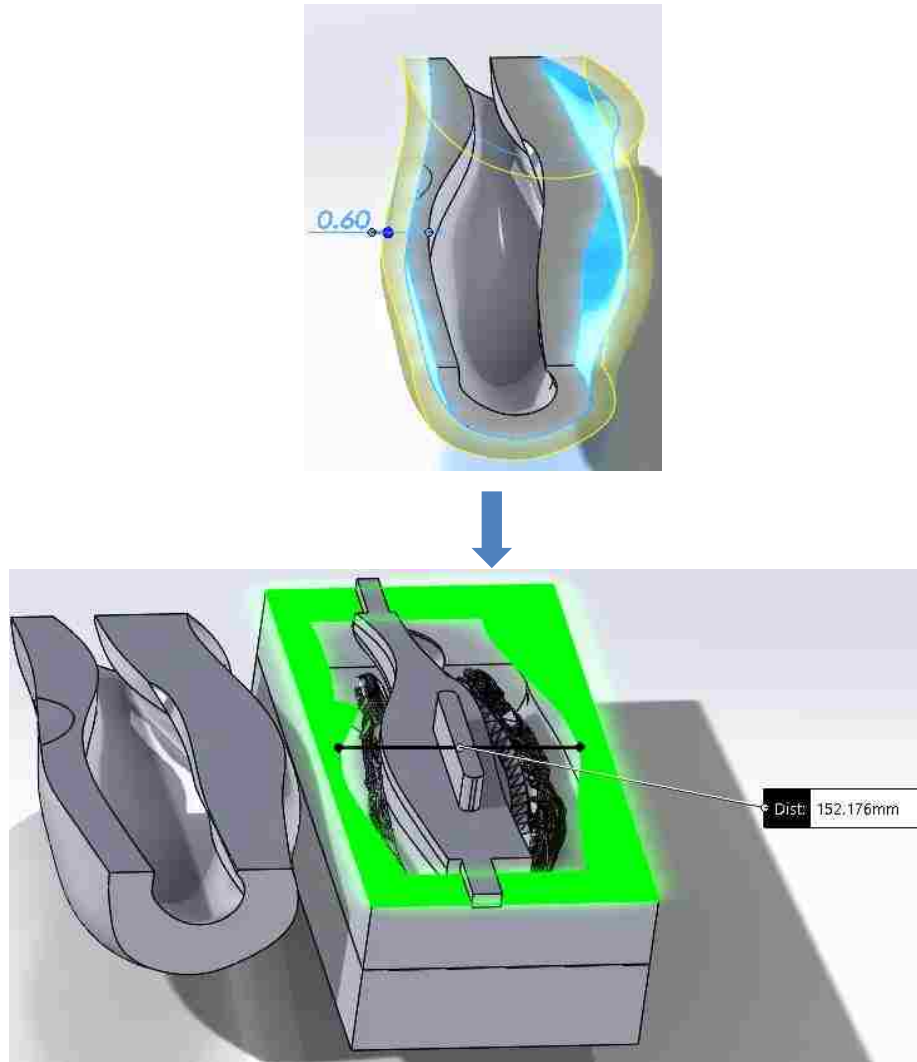
**Figure 4.4-4: Parametric obesity adaptation of overmould elements**

A scaling factor of 0.923 was used to scale mould and tissue models to represent the cadaver patient. The mould configuration to represent the cadaver patient is depicted in Figure 4.4-5 with a thoracic wall thickness of 25mm, and mould dimensions of 244.11mm x 417.08mm x 170.38mm.
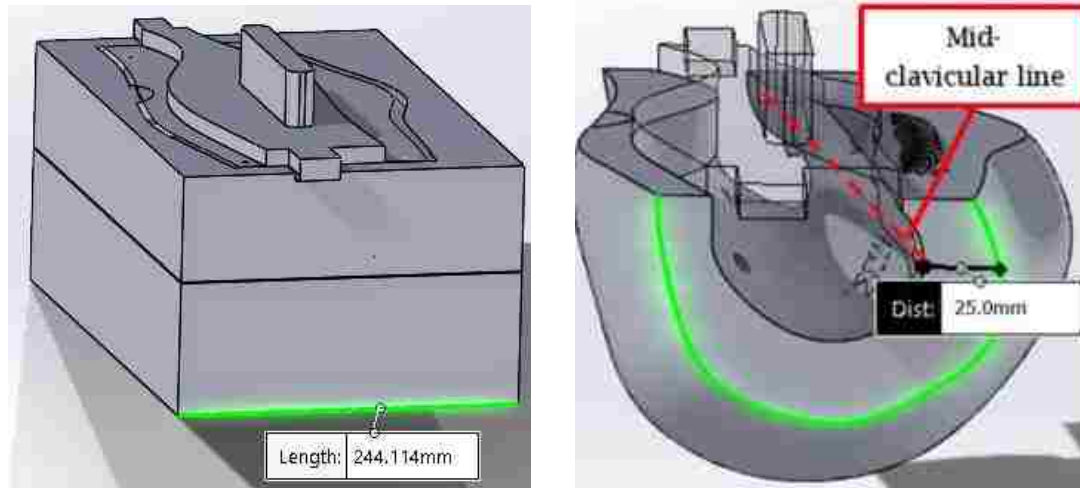
**Figure 4.4-5: Mould and tissue configuration to represent cadaver subject**

Based on the cross-sectional analysis of elements developed with the above mould sets, it was determined that strength was not a primary factor in the fabrication of moulds (indicated by proper silicone curing; no bubbles). As such, mould modifications were performed to accommodate smaller additive manufacturing machines and reduce material and time for fabrication. Figure 4.4-6 depicts the completed mould set described in Chapter 3.3.2. The next section describes the material and time savings associated with the optimized moulds, compared to the conventional moulds.
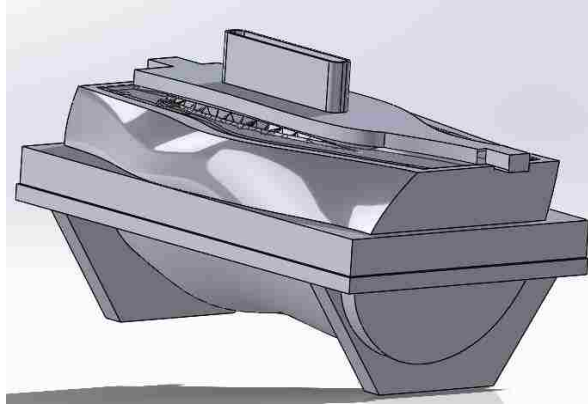
**Figure 4.4-6: Completed, assembled optimized mould set**

## 4.5. Additive Manufacturing

Completed CAD models were fabricated using fused deposition modelling. The use of a Fortus 400mc enabled the rapid production of moulding and skeletal elements shown in Figure 4.5-1 and Figure 4.5-2. Highlighted in Figure 4.5-1, are the model (ABS-M30) and support material (SR-30).
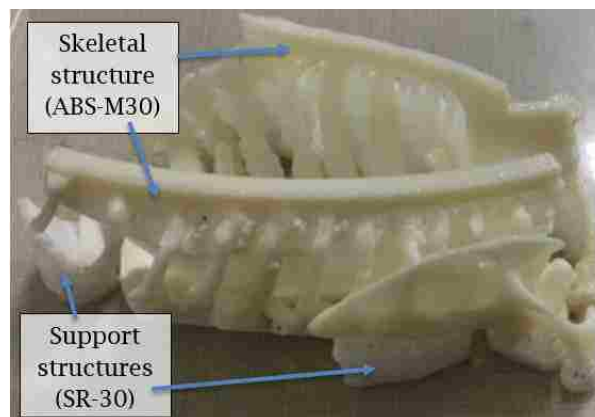


**Figure 4.5-1: Skeletal component assembly (ABS-M30) and support material structures (SR-30)**

**Figure 4.5-2 (a): Fabricated overmould elements (ABS-M30), (b): Tissue spacer insert (ABS-M30)**

Measurement values for the clavicle and 9$^{th}$ intercostal space of the 2-year old male and 18-year old female patient representations are reconfirmed in the fabricated models depicted in Figure 4.5-3 and Figure 4.5-4.



**Figure 4.5-3: Clavicle measurement for 2-year old male patient representation**
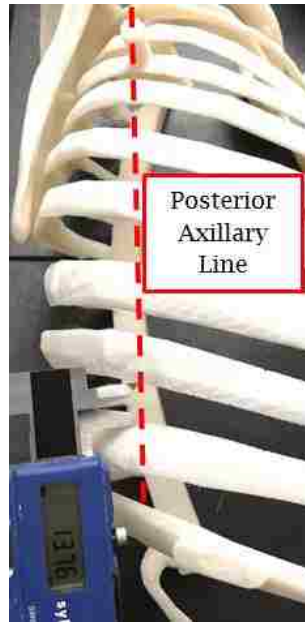
**Figure 4.5-4 (a): Clavicle measurement for 18-100-year-old female, (b): 9th intercostal space measurement for 18-100-year-old female (posterior axillary line)**

Elements developed for tissue interchangeability (quick-change design) are depicted in Figure 4.5-5. Key elements detailed in Chapters 3.3 and 4.4 (Table 3.3.1-1) are highlighted in Figure 4.5-6. Grooves for alignment are numbered 1-3 and alignment "pegs" are numbered 4.



**Figure 4.5-5: Quick-change mould elements**
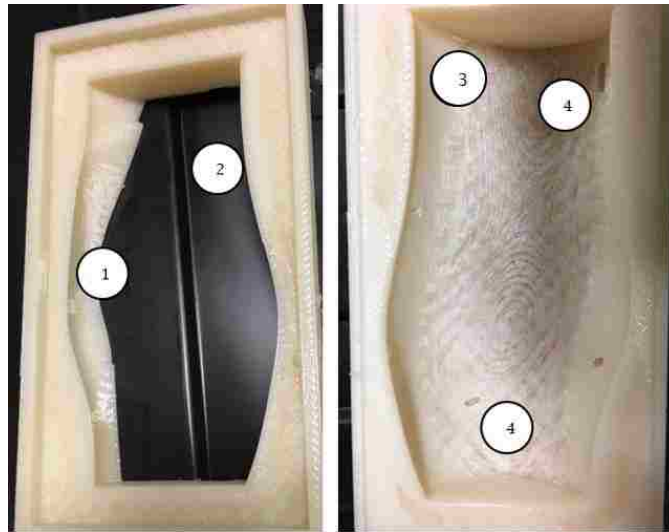
**Figure 4.5-6: Key quick-change mould element features**

Optimized moulds for the 2-year old male patient representation are depicted in Figure 4.5-7 (a) and the adhered mould set for the 18-year-old female patient representation is presented in Figure 4.5-7 (b). A comparison of the fabrication time and material usage between the conventional mould sets and the optimized set is provided in Table 4.7-1.


**Figure 4.5-7 (a): Split optimized mould set for 2-year old male patient representation, (b): Adhered mould set for 18-year old female patient representation**

**Table 4.5-1: Fabrication time and material consumption for target patient representation models**

| Model | Fabrication Time (hrs) | ABS-M30 Material Consumption (cm³) | SR-30 Material Consumption (cm³) |
|---|---|---|---|
| 2-Year-Old Male | | | |
| Conventional mould set (solid infill) | 23:29 | 1061.06 | 132.24 |
| Optimized mould Set (2-year old male) (sparse infill) | 21:30 | 680.06 | 167.64 |
| 18-Year-Old Female) | | | |
| Conventional mould set (solid infill) | 214:41 | 16183.54 | 1277.86 |
| Optimized Mould Set (18-year old female) (sparse infill) | 100:29 | 2914.60 | 1542.68 |

Implementing the mould optimizations for the female set yields a 53.19% reduction in time, an 81.99% reduction in model material and a 20.72% increase in support material (support material increase due to hollow geometries needing additional support). The 2-year-old male patient representation moulds show an 8.45% in time, a 35.9% reduction in model material, and a 26.77% increase in support material. Additional benefit is observed in the larger mould sets, as the hollowing of models removes more material. Furthermore, the splitting of models enables for fabrication in AM machines with smaller build envelopes.

## 4.6. Fabrication and Evaluation of Thoracic Wall Tissue Representation

This section presents results from individual patient representation fabrications and evaluations. All SPSS data readouts are presented in Appendix D.

### 4.6.1. Fabrication of 2-Year-Old Male Patient Model

Utilizing the conventional mould set, the 2-year-old male patient representation was fabricated and used for cross-sectional analysis. The first

tissue layer was fabricated by using the tissue spacer insert (Figure 4.5-2 (b)) to obtain an outer layer, representative of the position 2 elements (skin, adipose tissues) using a silicone mixture matching the composition of sample 0 (Table 4.3.1-1, Figure 4.6.1-1).



**Figure 4.6.1-1: Position 2 tissue for 2-year-old male patient representation**

Upon completion of the second pour, a finalized model was obtained. Key structural elements highlighted in this research include the need for a clavicle, scapula and ribs, as well as a dual layer composition with variable tissue thickness and density. These elements are highlighted in the initial prototype in Figure 4.6.1-2 and Figure 4.6.1-3 (a) and (b).
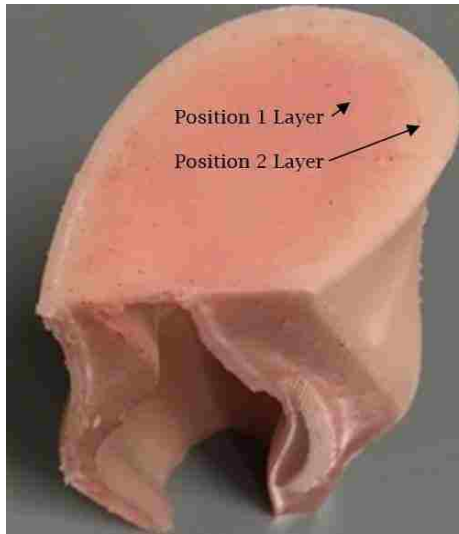
**Figure 4.6.1-2: Dual layer composition of alpha prototype**
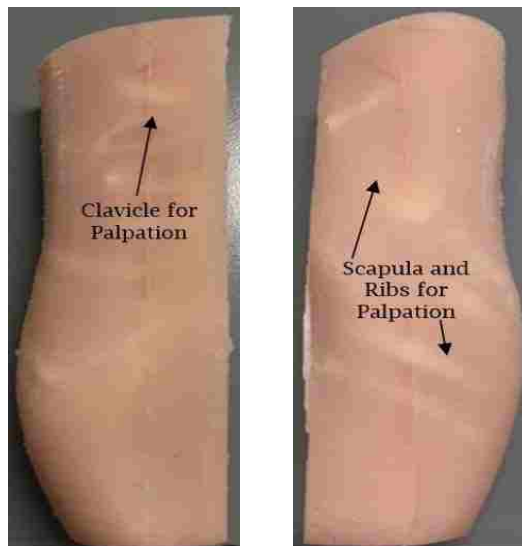


**Figure 4.6.1-3 (a): Clavicle for palpation, (b): Scapula and ribs for palpation**

Employing the quick-change mould sets and silicone pouring strategies outlined in Chapters 3.3, 3.4 and 4.5, silicone elements depicted in Figure 4.6.1-4 and Figure 4.6.1-5 complete with key features from Table 3.3.1-1 highlighted, were obtained.
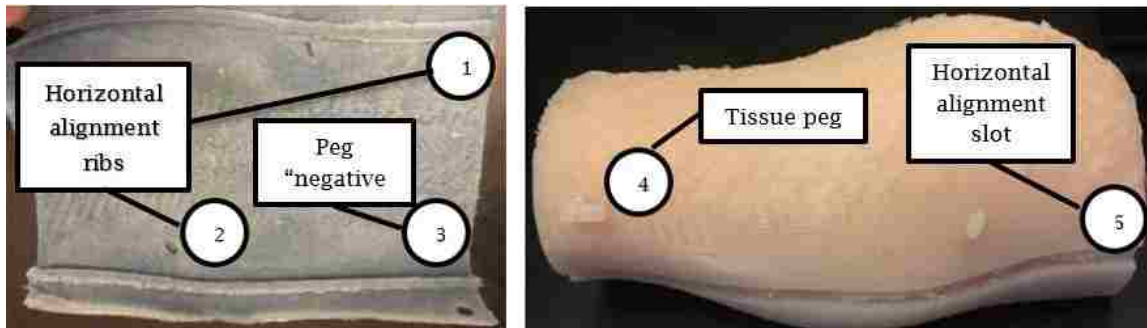
**Figure 4.6.1-4: Silicone quick-change modifications**



**Figure 4.6.1-5: Quick-change tissue assembly**

### 4.6.2. Cross-Sectional Analysis

Upon completion of the 2-year-old male patient thoracic wall representation, a cross-sectional analysis of the silicone was performed to determine if any inconsistencies were present, due to the silicone curing process. Results from this cross-sectional analysis showed no inconsistencies within the tissues, thereby confirming the lack of the need for vacuum curing of the silicone (Figure 4.6.2-1).

**Figure 4.6.2-1: Cross sectional analysis of silicone prototype**

Based on the consistent silicone tissues obtained without vacuum curing, the optimized mould set was employed to fabricate the final 18-year-old female patient representation.

### 4.6.3. Fabrication of 18-Year-Old Female Patient Representation

Utilizing the optimized moulds, an outer tissue representation of appropriate thickness and consistency (to represent position 2, with a composition matching that of silicone sample 0) was obtained (Figure 4.6.3-1).
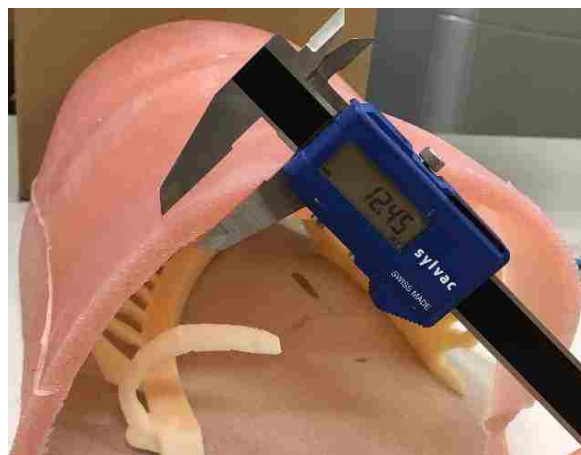


**Figure 4.6.3-1: Position 2 tissue measurement**

Fabrication of the second layer (position 1 tissue, corresponding to sample 1) followed (Figure 4.6.3-2) and yielded the final, accurately sized patient representation for an 18-year-old female. Once removed, a completed prototype of a two-layer model was obtained (Figure 4.6.1-1).



**Figure 4.6.3-2: Position 1 silicone pouring set-up (weights included in image are for holding down the hollow—and therefore buoyant mould inserts)**
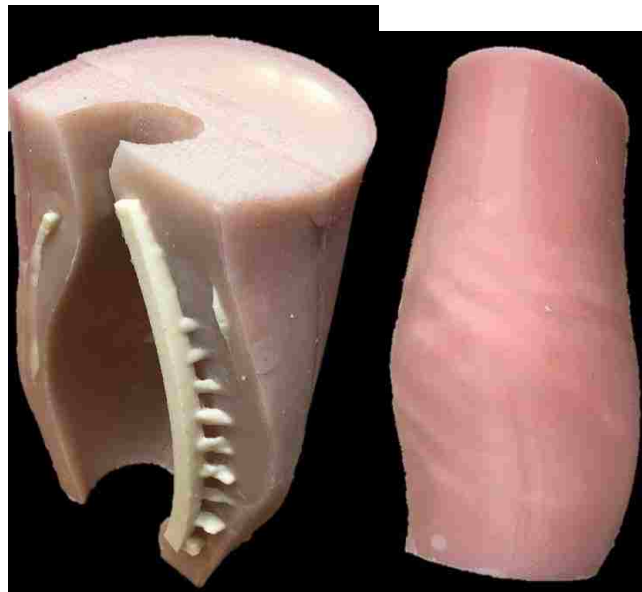


**Figure 4.6.3-3: Finalized 18-year-old female patient thoracic wall representation**

Measurements for total thoracic wall depth (Figure 4.6.3-4) showed a thickness of 25.60mm, along the mid-clavicular line, in the 9th intercostal space.
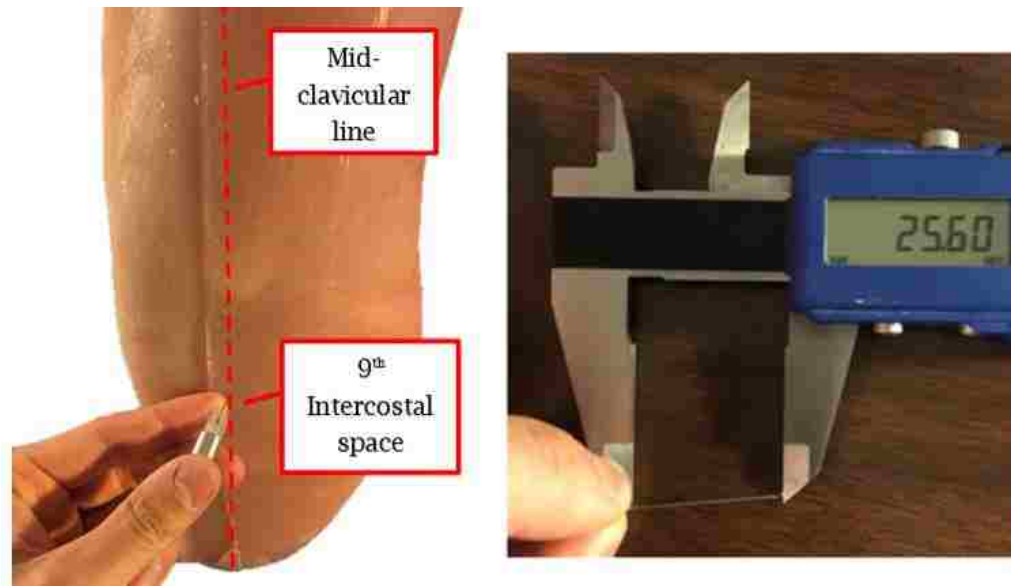
**Figure 4.6.3-4: Thoracic wall thickness measurement for 18-year-old female patient representation**

Results from the ANOVA comparing the combined position 1 and 2 tissues, the cadaver position 3 needle insertion result, and the THM-30 needle insertions are presented in the following section.

### 4.6.4. Experimental Needle Insertion Results

5X3 Repeated Measures ANOVAs revealed a main effect of tissue in all three criteria for the cadaver needle insertions. For the peak force analysis, Mauchly's Test of Sphericity was violated ($p$=.001<0.05). The Greenhouse-Geisser correction was used to produce a more accurate reporting of data ($F_{(1.107,11.072)}$=10.651, $p$=0.007<.05). For impulse, Mauchly's Test of Sphericity was violated ($p$=.006>.05), so the Greenhouse-Geisser correction was used to report data ($F_{(1.190, 11.90)}$=2.585, $p$=.131<.05). Data from pulse width violated Mauchly's Test of Sphericity ($p$=.019>.05) and the Greenhouse-Geisser correction was used to report data ($F_{(1.262, 12.624)}$=21.208, $p$=.000299<.050). Results from Tukey's pairwise

comparisons for the cadaveric needle insertions showed a correlation between the position 1 and 2 silicone tissues and the cadaver position 3 needle insertions, in terms of peak force ($p=.996>.05$) and impulse ($p=.990>.05$), as well as a nearly statistically similar pulse width comparison ($p=.031<.05$). Contrastingly, the THM-30 shared only one statistical similarity to the cadaver tissues, with impulse ($p=.115>.05$). For peak force and pulse width comparisons of the THM-30 and cadaver, however, no similarities were observed (($p=.004<.05$), ($p=0.000225<.05$), respectively).

A graphical comparison of the three needle insertions is provided in Figure 4.6.4-1. This figure shows that the tissues developed in this thesis more accurately simulate the needle insertion properties of the human thoracic cross section than the THM-30 in terms of all criteria (28.54%, 20.17% and 36.31%, for peak force (N), impulse (N.s), and pulse width (s), respectively). Furthermore, variances in peak force and impulse values are 76.7% and 84.3% closer to cadaver values in the silicone tissues developed in this thesis, compared to the THM-30 (peak force variances of 3.47 N, 2.94 N and .23 N, and impulses of .81 N·s, .84 N·s and .092 N·s, for the cadaver, silicone tissues, and THM-30, respectively). Pulse width variance values however, are more accurately represented in the THM-30, with an error 66% less than that observed in the silicone tissues developed in this thesis (.19 s, .41 s and .09 s for the cadaver, silicone tissues and THM-30, respectively). The similarities are speculated to be due to the nature of the varying tissue layer constitutions in the silicone and the cadaver tissues. Trends in literature describing the dominance of the harder skin tissue on overall needle insertion resistive characteristics are observed in the simulated silicone skin tissue in the dual-layer model developed in this thesis, which is indicative of a

qualitative similarity between the cadaver and simulated tissues. No such trend is observed in the THM-30 simulated tissue however.
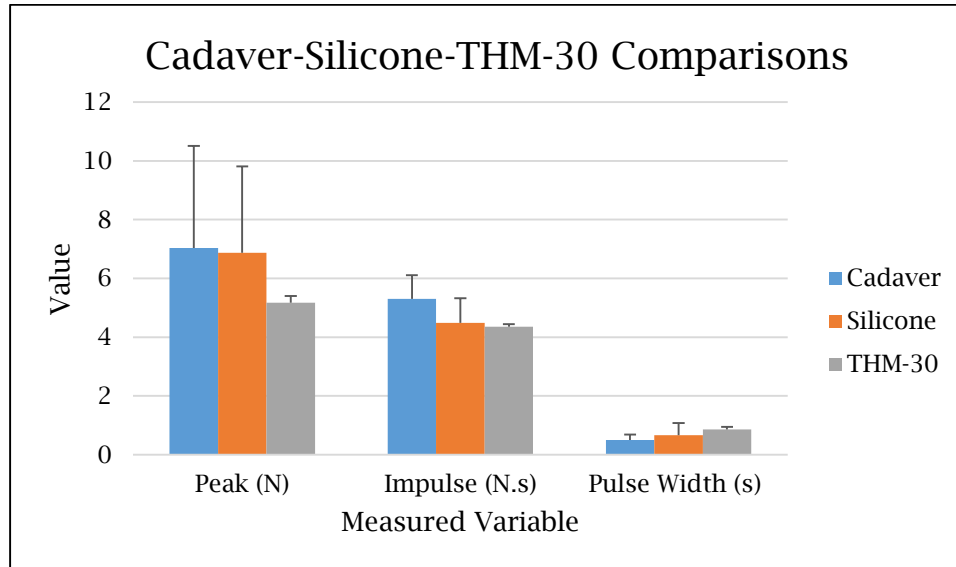


**Figure 4.6.4-1: Graphical comparison of THM-30, silicone tissue representation, and cadaver needle insertion results**

## 4.7. Time and Cost Comparisons

The implementation of additive manufacturing techniques enabled the economical and rapid fabrication of initial and subsequent iterations of prototype models. Table 4.7-1 presents a rough comparison between the time and cost (according to the University of Windsor AM fabrication fee template (Template 1 and Template 2 in Appendix F)) required the approach in this study, and an estimate from a local engineering company [79]. The time and cost saving are further amplified with consecutive iterations on elements developed, as the iterations and fabrication time are where the most significant savings lie.

121

Table 4.7-1: Comparison of time for procedures between conventional and alternative methodologies [79]

| | Step | Time (Conventional) | Time (Proposed) | Cost ($ CAD) (Conventional) | Cost ($ CAD) (Proposed) |
|---|---|---|---|---|---|
| 18-Year Old Female | Manufacturing and shipping of moulds | 38-25 wks. | 100.5 hrs. | 360000-229000 | 2600.05 |
| | Mould set up | 20 hrs. | 2 min. | 1310 | N/A |
| | Process time (silicone injection / pouring and curing) | 10.5 min. | 24 hrs. | 100 | N/A |
| Total | | ≈6404.185 hrs. | 124.538 hrs | ≈295000 | 2700.05 |
| 2-Year Old Male | Manufacturing and shipping of moulds | 38-25 wks. | 21.5 hrs. | ≈220000-110000 | 546.70 |
| | Mould set up | 20 hrs. | 2 min. | 1310 | N/A |
| | Process time (silicone injection / pouring and curing) | 10.5 min. | 24 hrs. | 10 | N/A |
| Total | | ≈4220.18 hrs. | 45.53 hrs. | ≈165000 | 556.70 |

While the value added with time and cost are significant, it must be considered alongside other aspects coupled with this alternative methodology. Modifications are possible where they were not previously, and a higher degree of user customizability is available. Furthermore, replicating results does not require in depth technical skill; the proposed methodology is intuitive and includes simple, discrete steps. The proposed process offers an efficient methodology to develop and fabricate functional models as compared to conventional means.

It must be noted however, that the conventional methodology yields moulds of superior quality (i.e. surface finish, production life). While potentially superior for the mass production, the estimated production volumes for this application are low (i.e. hundreds vs. thousands), meaning that an AM-based approach would

be superior for this application. The low production volume of each mould is further lessened by the fact that multiple moulds may be used to produce different patient representations, meaning that obtaining sufficient models for a classroom could be performed by splitting the number of models into different patient categories (thereby reducing the number of uses per mould).

## 4.8. Hypotheses Revisited

To evaluate the models developed, hypotheses are revisited;

$H_1$: Tissue re-configurability (ability to be modified to represent different characteristics) will be achieved in terms of tissue thickness, and needle insertion resistive properties of the cadaver subject will be replicated by obtaining experimental needle insertion data from a cadaver patient, and implementing a variable-hardness silicone.

$H_1$: Tissue re-configurability was achieved, in terms of both thickness, as well as needle insertion properties for the particular cadaver subject used in this thesis. With the default mould settings, a thoracic wall thickness ranging from 0mm (no tissue) to 113.5mm, encompassing the range of reported thoracic wall thicknesses (26.6mm to 80.2mm [55]), with the option to increase beyond the upper range to account for obesity trends [57] by modifying the original mould block. Thoracic wall tissue resistive properties have been shown to be controllable with the addition of oil and have been correlated to individual cadaveric tissue layers. Comparing individual tissue layers from the cadaver with selected silicone representations showed statistical similarities in terms of peak force (p=.929>.05), impulse (p=.058>.05) and pulse width (p=.948>.05) for position 1

123

elements (muscle, pleura), and peak force (p=.519>.05) and impulse (p=.245>.05) for position 2 elements (skin, adipose tissue). Thoracic cross section comparisons with the joined position 1 and 2 elements showed statistical similarities in terms of peak force (p=.996>.05) and impulse (p=.990>.05), and was nearly statistically similar in terms of pulse width (p=.031<.05). With the simulated thoracic cross-section, an improvement on the THM-30 needle insertion properties, compared to the cadaver insertions was observed in terms of peak force (28.54%), impulse (20.17%) and pulse width (36.31%). Based on the improvements to needle insertion resistive properties, as well as the ability to represent all of the thoracic wall thicknesses described in the literature, $H_2$ is accepted.

$H_{1.1}$: Simulated thoracic wall representations require more than one artificial tissue layer to represent the cadaver subject.

$H_{1.1}$: Statistical analysis of position 1 (muscle, pleura), position 2 (skin, adipose tissue) and position 3 (entire thoracic cross section) showed statistical similarities between the position 2 and 3 elements (peak force, impulse). This, along with the statistical difference between position 1 and 2 elements, led to the conclusion that 2 simulated tissue layers were needed to represent the thoracic cross-section. Based on the statistical evidence from the Repeated Measures ANOVAs, $H_{2.1}$ is accepted.

$H_{1.2}$: Furthermore, it is hypothesized that the needle insertion property representation of the THM-30 simulated tissue will be statistically different than the cadaver subject in terms of peak force (N), impulse (N·s) and pulse width (s). $H_{1.2}$: Statistical comparisons between the THM-30 and the cadaveric needle insertions showed statistical similarity in terms of impulse

(p=.115>.05) for the position 3 insertions, however, for peak force and pulse width, statistical comparisons showed highly significant variations in mean values (p=.004<.05, p=0.000225<.05), respectively. Furthermore, a comparison between the two tissues showed a 28.6% difference in peak force (N), 20.4% in terms of impulse (N.s) and 66% in terms of pulse width (s). Based on the statistical evidence showing a difference between the tissues evaluated in terms of the majority of the needle insertion characteristics, $H_{2.2}$ is accepted.

Furthermore, anatomical landmark palpation capabilities are speculated to have been improved in the thoracic wall representations for all of the patients represented. The appropriate sizing (.4% error for 2-year-old male, 1.3% error for 18-year-old female and 1.1% error for 30-year-old male) of the clavicle (where there was previously none) is of particular benefit to the palpation procedures, which commence with the identification of the mid clavicular line. The skeletal structures of the thoracic wall are more accurately represented in the proposed model (i.e. curved vs. flat, appropriate intercostal spacing for various patient representations; 2.8% error for 18-year-old female and 0.7% error for 30-year-old male). However, in order to determine if experiential learning is improved through the use of this model, compared to the THM-30, further investigation is needed. A study must be performed to compare the two models objectively, in terms of palpation training before a confident conclusion can be drawn.

CHAPTER 5

Conclusions, Limitations and Future Work

Conventional teaching and training methodologies are inadequate for thoracentesis training. Over 40% of experienced emergency physicians were unable to identify key landmarks for the procedure using these methodologies [41]. The implementation of training simulators has been successful, with written and clinical performance scores of students trained with such methods increasing by up to 71% when performed on the same simulator [49], though training with different simulators has not been adequately investigated at this time, and may yield different results. Thoracentesis patient demographic physical characteristics vary, with elevated obesity rates and age ranges with spikes in the 0-9 and 50-59 years' groups. Furthermore, existing simulators, particularly the THM-30 Thoracentesis Training Simulator, do not accurately simulate the tissues associated with thoracentesis needle insertions. The lack of fidelity in these aspects is problematic, as Crofts et al. [23] showed that for simulators with force-perception elements (i.e. needle insertion, palpation), high fidelity is necessary for optimal effectiveness. In order to provide this fidelity, representation of the entire demographic, complete with anatomical landmarks and tissues of the human body, is necessary.

The methodologies presented in this thesis outline the development of an anatomically accurate (i.e. tissue thickness, skeletal structure inclusion and sizing), high fidelity (in terms of tissue layers present, and composition of tissues) representation of the thoracic wall for male and female patients ranging from 0-100 years of age, assuming negligible skeletal growth after 18-years of age. The

126

final product of this thesis is a reconfigurable CAD model, capable of representing the entire thoracentesis demographic and being rapidly fabricated through the use of AM (FDM). Static skeletal structures can be scaled according to growth rates identified in the literature and reconfigurable mould sets enable the modification of tissue thicknesses. Furthermore, these tissues may be interchanged physically upon fabrication, using the quick-change tissue approach detailed in Chapter 4.6. Where gaps in the literature existed, educated decisions were made (i.e. generalization of skeletal growth rates, thoracic wall tissue characteristics), to produce an adaptable, high fidelity model.

## 5.1. Contributions to Field

While a need for high fidelity is described in the literature [22], [23], no research was found that sought to evaluate and improve on existing training simulator solutions. Gaps in the literature also included the lack of thorough, detailed skeletal growth rates for the rib cage and scapula. No literature was found regarding needle insertion forces into the thoracic wall, nor was there any research discovered which sought to accurately recreate these specific tissues in terms of thickness, and needle insertion resistive properties. The thoracic wall representations developed in this thesis provide a foundation off of which to progress towards a fully functional thoracentesis training simulator.

Of additional note is that the general methodology outlined in Figure 1.4-1 can be tailored to specific applications, as demonstrated in the development of custom finger braces by Kalami et al. [75]. The multidisciplinary techniques, centered on the integration of key constraints gained through the reverse engineering of human attributes into dynamic CAD models, as well as the

integration of medical knowledge and Human Kinetics data collection techniques, coupled with AM, allow for the rapid prototyping of innovative tools for learning. Parametric modelling allows for manipulation of models (with a default tissue range of 0mm (no tissue) to 113.5mm), without the time and cost associated with the development of subsequent iterations using conventional methods (i.e. 6404 hrs. vs. 124 hrs. and $295000 vs. $2700, for the 18-year old female patient model). The ability to develop silicone tissues with tactile (needle insertion resistive properties) and physiological (tissue thickness) accuracy, regardless of the biological constitution they represent, is a powerful tool that has applications extending to surgical training, prototype development and educational training in the classroom, including the development of lumbar puncture training simulators [117]. There is potential for expansion into the design of custom orthotics, braces and other medical devices, given the adaptability and universality of the tools and techniques descried in this thesis. The ability to modify mould sets to represent different patient characteristics is powerful, particularly so when coupled with parametric design. With dynamic moulds, complex surface geometry can be obtained, where not previously feasible. In a similar manner to the framework outlined by Kalami et al., this thesis provides a framework for the development of subsequent medical training tools.

## 5.2.  Limitations

In the development of the thoracic wall representation presented in this thesis, several limitations were observed. First and foremost is the lack of *in-vivo* needle insertion information for the thoracic wall. Given that no data were available pertaining to the peak force, impulse and pulse width observed

throughout the insertion of a thoracentesis needle into the thoracic wall of a living patient, a cadaveric alternative to acquiring these data was used. While accepted in the literature, which highlights the benefits of the exact replication of tissue thicknesses, there are chemical and physical changes which occur *post-mortem* [59]. To account for the potential variations in tissue characteristics between living and dead tissues, the methodology was laid out in such a way that, upon availability of *in-vivo* needle insertion experimentation, tissues could be modified to represent the values observed in various insertions. Relatedly, there was also no literature describing the distribution of various tissues along the vertical plane of the thoracic cage (i.e. excess adipose tissue in certain regions). To account for this, modifiable splines were used in the CAD modelling of the thoracic tissue insert in Chapter 3.3. in so doing, upon obtaining of additional information from new research, modifications could be made using the same procedures to more accurately represent patient characteristics.

In order to obtain skeletal models representative of various patients, scaling factors based on the clavicle growth rates were implemented to the entire skeletal assembly (clavicle, rib cage, scapula). Growth rates for the rib cage and scapula were however, not clearly described in the literature; with only specific measurements throughout patients' lives being available. The implementation of the scaling factors yielded clavicle lengths within 1.3% of literature values and intercostal space measurements within 2.8% of reported values, but does not account for morphometric changes of the rib cage with age. Throughout the aging process, the rib cage exhibits changes in shape, with the thoracic index (measure of rib cage depth to width) varying, and rib orientation shifting. The incorporation of these elements into this thesis was not deemed necessary at this time, as the

scapula-7$^{th}$ intercostal space reference was found to be constant throughout life, regardless of thoracic index. As this reference, along with the mid-clavicular line, are not affected by the orientation changes, they were deemed to be negligible.

The participant pool in this experiment consisted of 5 participants performing each test, which may have led to potential errors in the reporting of mean values. Furthermore, different participants performed needle insertions in the experiments, which may have led to inconsistencies in results. Despite literature suggesting similar technique regardless of age or sex, this is not ideal. In the future, a consistent and larger participant pool should be used. Given that the needle insertions were performed by humans, rather than robots, there is much variation in the results, exemplified by the variation in peak force values from the position 3 (entire thoracic cross section) needle insertions ($\sigma$=3.474N, while the peak force was 7.04N). The procedure followed, however, is universal, meaning that with a different cadaver (or living patient) and additional participants, identical steps could be taken to achieve the final goal of obtaining accurate needle insertion data.

It was found that in the younger patient representations (2-year old male), that the skeletal structures became too brittle to sustain mechanical stresses associated with manual palpation. The scaling of the ribs (specifically, thickness) is not currently represented adequately in this thesis, and must be addressed in future research.

## 5.3. Future Work

To advance this research, further investigation into material choices should be conducted. To complete the thoracentesis training simulator, additional elements are needed which do not necessarily contribute to the high-fidelity aspect of the simulator, but are still necessary for proper function. Internal organs should be incorporated, along with a user-friendly fluid feedback mechanism, which should contain two colored fluids; one for proper site drainage, and the other to represent air in the lungs. Ease of use for the filling and draining of these reservoirs of fluid is imperative. The entire structure must be packaged in a convenient frame. Based on knowledge gained from the literature review [19]-[23] and other determined design constraints, a low-fidelity box frame would be appropriate for this simulator. The only elements deemed influential on fidelity are the needle insertion resistive forces, the anatomical land-marking completeness and the overall size. Given that all of these elements are incorporated directly into the tissue elements developed in this research, the frame in which they are housed, and its respective shape, are of little importance to the final product's functional fidelity.

A circuit-completion-based notification system to indicate procedural error should be implemented. This system could consist of a metallic coating covering the internal organs, creating an open-circuit. Upon contact with the metallic needle, circuit completion would trigger a notification to the user, indicating procedural error; specifically, organ laceration or puncture. Additionally, a sensor to identify improper insertion of the needle with respect to the nerve bundles located on the underside of the ribs would be beneficial. There are slight

131

orientation changes of the ribs with growth and age. Currently, rib cage scaling incorporations do not account for this. With future development of this research, the angular changes should be accounted for. Furthermore, to address frailty of skeletal structures in the younger patient representations, additional supports should be modelled, to provide additional strength to the rib cage without interfering with proper needle insertion or palpation.

   CT scan file "cleanup" was laborious in this research. With the modification of meshes came several tedious meshing errors that need to be manually repaired. An automated file cleanup would be beneficial in the development of future functional models.

   This thesis is the result of ongoing research. Tissues are being further investigated and improved by a capstone group at the University of Windsor. This investigation aims to further improve tissue fidelity, as well as developing a custom proprietary blend, with a clearly described composition. Future needle insertion experiments should be performed with additional participants, and a consistent participant pool, along with additional cadaver subjects. The implementation of a mechanical automatic needle insertion apparatus would reduce errors attributed to manual needle insertion behaviour. Furthermore, additional phenomenon occurring during needle insertions, including shearing and frictional forces must be analyzed to more accurately recreate synthetic tissues. Variances in measured variables should also be incorporated into the future experiments, as similarities between the cadaver and simulated tissues were observed, while no such similarity was noted in the cadaver—THM-30 comparisons. While speculated to be due to the skin tissues and multiple tissue layer constitution of the thoracic wall, additional research is needed to ascertain

this. Obtaining *in-vivo* data would be of benefit to the accurate representation of patient tissues, and should be performed in the future.

Relatedly, patient posture should be incorporated into future research, as the needle insertion characteristics may differ depending on patient orientation (i.e. hunched over—with tissues stretched vs lying flat—with tissues relaxed). Scar tissue also possesses different physical properties than otherwise unharmed tissue and could also be incorporated into future models.

To provide additional realism to the training experience, virtual reality may be incorporate into the training regiment. By coupling a virtual reality headset with an accurate representation of patient thoracic anatomy, the clinician may obtain superior training quality, with a complete training experience. By also incorporating a vibration mechanism, a trembling patient may be represented. In this way, flinching and other nervous behaviours of various patients can be included into the clinical scenario. Adding an element of warmth to the tissue may also increase the realism of the simulation "package", as haptic qualities of the virtual patient would coincide with the clinician expectation.

Upon completion, a follow-up study comparing learning curves of this model and the THM-30 training simulator should be performed, to determine the effect of the improvements in selected fields deemed influential on fidelity.

### 5.4. Conclusions

This thesis provides a foundation for the future development of a fully functional thoracentesis training simulator, capable of representing varying patient statures and physical constitutions. By implementing open-ended design strategies (i.e. modifiable splines, individually scalable skeletal structures,

133

reconfigurable mould sets), a thoracic wall representation of higher fidelity (in terms of anthropometric land-marking, tissue needle insertion resistance properties and overall patient stature representation) compared to the THM-30 Thoracentesis Training Simulator was obtained. Errors attributed to improper or insufficient training may be reduced through the implementation of high fidelity training simulators. Elements lacking in the THM-30 (flat rib cage, tissue representation, skeletal completeness) are thoroughly addressed and improved in this model. This research warrants further investigation, as with a higher fidelity training simulator, better preparation and performance for medical residents is possible, potentially reducing procedural error, and improving overall patient safety.

# REFERENCES/BIBLIOGRAPHY

[1]     "Study Suggests Medical Errors Now Third Leading Cause of Death in the U.S.," John Hopkins Medicine, May 3 2016. [Online]. Available: https://www.hopkinsmedicine.org/news/media/releases/study_suggests_medical_errors_now_third_leading_cause_of_death_in_the_us

[2]     A. Makary and M. Daniel, "Medical error—the third leading cause of death in the US," *BMJ 2016*, vol. 353, May 2016. [Online]. Available: https://www.bmj.com/content/353/bmj.i2139

[3]     T.A. Brennan, L.L. Leape, N.M. Laird, L. Hebert, A.G. Lawthers, J.P. Newhouse, P.C. Weiler and H.H. Hiatt, "Incidence of adverse events and negligence in hospitalized patients. Results of the Harvard Medical Practice Study I.," *New England Journal of Medicine,* vol. 324, pp. 370-376, Feb. 1991. [Online]. Available: https://www.ncbi.nlm.nih.gov/pubmed/1987460

[4]     R.M. Wilson, W.B. Runciman, R.W. Gibberd, B.T. Harrison, L. Newby and J.D. Hamilton, "The quality of Australian health care study.," *Medical Journal 1995*, vol. 163, pp. 458-471, Nov. 1995. [Online]. Available: https://www.ncbi.nlm.nih.gov/pubmed/7476634

[5]     F. Jones, C.E. Passos-Neto, O.F.M. Braghiroli, "Simulation in medical education: Brief history and methodology," *Principles and Practice of Clinical Research*, vol. 1, pp. 56-63, Aug. 2015. [Online]. Available: http://ppcr.org/journal/index.php/ppcrjournal/article/view/12/13

[6]     A. Bari, R.A. Khan, and A.W. Rathore, "Medical errors; causes, consequences, emotional response and resulting behavioral change," *Pakistan Journal of Medical Sciences*, vol. 32, pp. 523–528, [Online]. http://doi.org/10.12669/pjms.323.9701

[7]     A.N. Hopper, M.H. Jamison and W.G. Lewis, "Learning curves in surgical practice," *Post Graduate Medical Journal*, vol. 83, pp. 777-779, 2007. [Online]. http://doi.org/10.1136/pgmj.2007.057190

[8]     G. Wulf, C. Shea and R. Lewthwaite, "Motor skill learning and performance: a review of influential factors," *Medical Education*, vol. 44 pp. 75-84, Dec. 2009. [Online]. https://doi.org/10.1111/j.1365-2923.2009.03421.x

[9]     J.C. Manuel-Palazuelos, M. Riano-Molleda, J.L. Ruiz-Gomez, J.I. Martin-Parra, C. Redondo-Figuero and J.M. Maestro, "Learning curve patterns generated by a training method for

laparoscopic small bowel anastomosis," *Advances in Simulation,* vol. 1, pp. 16, May 2016. [Online]. https://doi.org/10.1186/s41077-016-0017-y.

[10]    M. Maruthappu, A. Duclos, S.R. Lipsitz, D. Orgill and M.J. Carty, "Surgical learning curves and operative efficiency: a cross-specialty observational study," *BMJ Open 2015*, vol. 5, Mar. 2015. [Online]. Available: http://bmjopen.bmj.com/content/5/3/e006679

[11]    L.P. Morvan and B. Stock, "Medical learning curves and the Kantian ideal," *Journal of Medical Ethics*, vol. 319, pp. 513–518, Aug. 2005. [Online]. http://doi.org/10.1136/jme.2004.009316

[12]    B. Zevin, R. Aggarwal and T.T. Grantcharov, "Simulation-based training and learning curves in laparoscopic Roux-en-Y gastric bypass.," *The British journal of surgery*, vol. 99, pp. 887-895, Apr. 2012. [Online]. https://doi.org/10.1002/bjs.8748

[13]    K. Subramonian and G. Muir, "The 'learning curve' in surgery: what is it, how do we measure it and can we influence it?," *BJU International*, vol. 93, pp. 1173-1174, May 2004. [Online]. https://doi.org/10.1111/j.1464-410X.2004.04891.x

[14]    R. Aggarwal, O.T. Mytton, M. Derbrew, D. Hananel, M. Heydenburg, B. Issenberg, C. MacAulay, M.E. Mancini, T. Morimoto, N. Soper, A. Ziv and R. Reznick, "Training and simulation for patient safety," *BMJ Quality and Safety 2010*, vol. 19, pp. 34-43, Aug. 2010. [Online]. Available: http://qualitysafety.bmj.com/content/19/Suppl_2/i34

[15]     "What is the difference between modeling and simulation?," ResearchGate. Accessed May 20, 2018. [Online]. Available:

https://www.researchgate.net/post/What_is_the_difference_between_modeling_and_simulation

[16]    "Medical Simulators," GT Simulators. Accessed May 15, 2018. [Online]. Available:

https://www.gtsimulators.com/Medical-Training-Models-and-Nursing-Skills-Manikins-s/50.html

[17]    T. Reynolds and L.M.L. Kong, "Shifting the learning curve," *BMJ 2010*, vol. 341, Dec. 2010. [Online]. https://doi.org/10.1136/bmj.c6260

[18]    I. Motola, L.A. Devine, H.S. Chung, J.E. Sullivan, B. Issenberg, "Simulation in healthcare education: A best evidence practical guide," *AMEE Guide No. 82 Medical Teacher*, vol. 35, pp. 1511-1530, Aug. 2013. [Online]. https://doi.org/10.3109/0142159X.2013.818632

[19]    F. Munshi, H. Lababidi and S. Alyoussef, "Low-versus high-fidelity simulations in teaching and assessing clinical skills," *Journal of Taibah University Medical Sciences*, vol. 10, pp. 12-15, Mar. 2015. [Online]. https://doi.org/10.1016/j.jtumed.2015.01.008

[20]    N.J. Maran and R.J. Glavin, "Low- to high-fidelity simulation – a continuum of medical education?," *Medical Education*, vol. 37, pp. 22-28, Oct. 2003. [Online]. https://doi.org/10.1046/j.1365-2923.37.s1.9.x

[21]    J.L. Grady, R.G. Kehrer, C.E. Trusty, E.B. Entin, E.E. Entin, and T.T. Brunye, "Learning nursing procedures: The influence of simulator fidelity and student gender on teaching effectiveness," *Journal of Nursing Education*, vol. 47, pp. 403-408, Sept. 2008. [Online]. https://doi.org/10.3928/01484834-20080901-09

[22]    D.L. Rodgers, S. Securro and R.D. Pauley, "The effect of high-fidelity simulation on educational outcomes in an advanced cardiovascular life support course," *Simulation in Healthcare*, vol. 4, pp. 200-206, Dec. 2009. [Online]. https://doi.org/10.1097/SIH.0b013e3181b1b877

[23]    J.F., Crofts, C. Bartleett, D. Ellis, L.P. Hunt, R. Fox and T.J. Draycott, "Training for shoulder dystocia: a trial of simulation using low-fidelity and high-fidelity mannequins," *Obstet Gynecol*, vol. 107, pp. 1477-1485, Dec. 2006. [Online]. https://doi.org/10.1097/01.AOG.0000246801.45977.c8

[24]    "Thoracentesis and Thoracostomy Ultrasound Model," Blue Phantom. Accessed May 15 2018. [Online]. Available: http://www.bluephantom.com/product/Thoracentesis-and-Thoracostomy-Ultrasound-Model.aspx?cid=528

[25]    "Ultrasound Thoracentesis Model THM-30," Abacus, Accessed May 15 2018. [Online]. Available: http://www.abacus-als.com/product/ultrasound-thoracentesis-model-thm-20-2/

[26]    "Adult Thoracentesis Simulator," Mediquip. Accessed May 15 2018. [Online]. Available: http://www.mediquip.com.au/adult-thoracentesis-simulator.html

[27]    "Ultrasound Guided Thoracentesis Simulator Strap On Set," Erler Zimmer. Accessed May 15 2018. [Online]. Available: https://www.erler-zimmer.de/shop/en/medical-simulators/ultrasound/10075/ultrasound-guided-thoracentesis-simulator-strap-on-set

[28]    "Ultrasound Guided Thoracentesis Simulator," KK America. Accessed May 15 2018. [Online]. Available: https://www.kkamericainc.com/mw4_ultrasound_guided_thoracentesis_simulator/

[29]    "Thoracentesis" John Hopkins Health Library. Accessed April 18, 2018. [Online]. Available: https://www.hopkinsmedicine.org/healthlibrary/test_procedures/pulmonary/thoracentesis_92,P07761

[30]   "Thoracentesis," Canadian Cancer Society. Accessed Aug. 24, 2018. [Online]. Available:

http://www.cancer.ca/en/cancer-information/diagnosis-and-treatment/tests-and-

procedures/thoracentesis/?region=on

[31]   "Schematic diagram of pleural anatomy," Geoface. Accessed May 2, 2018. [Online].

Available: http://geoface.info/ef8714/anatomy-and-physiology-of-pleural-effusion

[32]   "Thoracentesis," Marine Corps Training and Education Command. Accessed May 5, 2018.

[Online]. Available: https://search.usa.gov/search?affiliate=tecom&query=thoracentis, accessed

May 2018.

[33]   D. Berg, K. Berg, L.A. Riesenberg, D. Weber, D. King, K. Mealey, E.M. Justice, K. Geffe and G.

Tinkoff, "The development of a validated checklist for thoracentesis: Preliminary results,"

*American Journal of Medical Quality*, vol. 28, pp. 220-226, Sept. 2012. [Online]. Available:

https://doi.org/10.1177%2F1062860612459881

[34]   A. Prestridge, "Thoracentesis," in *Current Procedures: Pediatrics.* New York: McGraw-Hill

Education, 2007. [Online]. Available:

https://accesspediatrics.mhmedical.com/content.aspx?bookid=444&sectionid=40089969

[35]   D.C. Sobush, G.G, Simoneau, K.E. Dietz, J.A. Levene, R.E. Grossman and W.B. Smith, "The

Lennie Test for measuring scapular position in healthy young adult females: A reliability and

validity study," *Journal of Orthopaedics & Sports Physical Therapy*, vol. 1, pp. 39-50, Jan 1996.

[Online]. Available: https://www.ncbi.nlm.nih.gov/pubmed/8749749

[36]   A.J. Chandrasekhar, "Pulmonary advanced physical diagnosis," *Anatomy,* Accessed Sept 15,

2018. [Online]. Available:

http://www.meddean.luc.edu/lumen/meded/medicine/pulmonar/apd/apds.htm

[37]   J. Lewandoski, "Assessment of nonorthopedic sports injuries: A sideline reference manual,"

1st Ed., Georgia: SLACK Inc., 2001, pp. 97-98. [Online]. Available:

https://books.google.ca/books?id=li9aPYuIcoYC&pg=PA97&lpg=PA97&dq=child+inferior+angle+sc

apula+7th+rib&source=bl&ots=BFUWDW_zeD&sig=-

FcA6fvkBTroBjqHVti4CjEv7mM&hl=en&sa=X&ved=2ahUKEwj90PaOm5DdAhUDzVMKHRpGDHA4C

hDoATACegQICBAB#v=onepage&q=child%20inferior%20angle%20scapula%207th%20rib&f=false

[38]   N. Lechtzin, "How to do thoracentesis," Merck Manual. Accessed May 22, 2018. [Online].

Available: https://www.merckmanuals.com/en-ca/professional/pulmonary-disorders/diagnostic-

and-therapeutic-pulmonary-procedures/how-to-do-thoracentesis

[39]    D.L. Simel, "The rational clinical examination: Evidence-based clinical diagnosis," in *The Rational Clinical Examination.* New York: McGraw-Hill education, 2008. [Online]. Available: http://jamaevidence.mhmedical.com/content.aspx?bookid=845&sectionid=75186098

[40]    M.E. Brauner, "Thoracentesis," Medscape. Accessed May 15, 2018. [Online]. Available: https://emedicine.medscape.com/article/80640-overview#a9

[41]    E.P. Ferrie, N. Collum and S. McGovern, "The right place in the right space? Awareness of site for needle thoracocentesis," *Emergency Medicine Journal*, vol. 22, pp. 788-789, Oct. 2005. [Online]. https://doi.org/10.1136/emj.2004.015107

[42]    G.C. Huang, C.C. Smith, C.E. Gordon, D.J. Feller-Kopman, R.B. Davis, R.S. Phillips and S.N. Weinhart, "Beyond the comfort zone: Residents assess their comfort performing inpatient medical procedures," *The American Journal of Medicine*, vol. 119, pp. 17-24, Jan. 2006. [Online]. https://doi.org/10.1016/j.amjmed.2005.08.007

[43]    A. Ziv, P.R. Wolpe, S.D. Small and S. Glick, "Simulation-based medical education: an ethical imperative," *Academic Medicine*, vol. 78, pgs. 783-788, Aug. 2003. [Online]. Available: https://www.ncbi.nlm.nih.gov/pubmed/12915366

[44]    T. Golczewski, A.M. Stecks, M. Michnikowski, E.M. Grabczak, P. Korczynski and R. Krenke, "The use of a virtual patient to follow pleural pressure changes associated with therapeutic thoracentesis," *The International Journal of Artificial Organs*, vol. 40, pp. 690-695, July 2017. [Online]. https://doi.org/10.5301/ijao.5000636

[45]    C. Ngo, R. Schlözer, T. Vollmer, S. Winter, B. Misgeld and S. Leonhardt, "A simulative model approach of cardiopulmonary interaction," *IFMBE Proceedings*, vol. 51, pp. 1679-1682, June 2015. [Online]. https://doi.org/10.1007/978-3-319-19387-8_408

[46]    N.B. Berman, S.J. Durning, M.R. Fischer, S. Huwendiek and M.M. Triola, "The role of virtual patients in the future of medical education," *The Journal of Academic Medicine*, vol. 91, pp. 1217-1222, Sept. 2016. [Online]. https://doi.org/10.1097/ACM.0000000000001146

[47]    D. Shanks, R.Y. Wong, J.M. Roberts, P. Nair and I.W.Y. Ma, "Use of simulator-based medical procedural curriculum: the learner's perspectives," *BMC Medical Education*, vol. 10, pp. 77, Nov. 2010. [Online]. https://doi.org/10.1186/1472-6920-10-77

[48]    G. Jiang, H. Chen, S. Wang, Q. Zhou, X. Li, K. Chen and X. Sui, "Learning curves and long-term outcome of simulation-based thoracentesis training for medical students," *BMC Medical Education*, vol. 11, pp. 39, June 2011. [Online]. https://doi.org/10.1186/1472-6920-11-39

[49]    D.B. Wayne, J.H. Barsuk, K.J. O'Leary, M.J. Fudala, W.C. McGaghie, "Mastery learning of thoracentesis skills by internal medicine residents using simulation technology and deliberate practice," *Journal of Hospital Medicine*, vol. 3, pp. 48-54, Jan. 2008. [Online]. https://doi.org/10.1002/jhm.268

[50]    S. McDermott, D.A. Levis, & R.S. Arellano, "Chest Drainage," in *Seminars in Interventional Radiology*, vol. 29. New York: Thieme Medical Publishers, 2012, pp. 247–255. [Online]. Available: https://www.ncbi.nlm.nih.gov/pmc/articles/PMC3577621/

[51]    G. Mynarek, K. Brabrand, J.A. Jakobsen, and A. Kolbenstvedt, "Complications following ultrasound-guided thoracentesis," *Acta Radiologica*, vol. 45, pp. 519-533, Aug, 2004. [Online]. Available: https://www.ncbi.nlm.nih.gov/pubmed/15515513

[52]    O. Efrati and A. Barak, "Pleural effusions in the pediatric population," *American Academy of Pediactrics*, vol. 23, pp. 417-426, Dec. 2002. [Online]. Available: https://www.ncbi.nlm.nih.gov/pubmed/12456894

[53]    A.J. Chandrasekhar and E. Garrity, "Thoracentesis and fluid analysis," Loyola University Medical Education Network, Jan. 10, 2006. [Online]. Available: http://www.lumen.luc.edu/lumen/MedEd/MEDICINE/PULMONAR/PROCEDUR/thorac_f.htm

[54]    R. Dancel, D. Schnobrich, N. Puri, R. Franco-Sadud, J. Cho, L. Grikis, B.P. Lucas, M. El-Barbary, "Recommendations on the use of ultrasound guidance for adult thoracentesis: A position statement of the society of hospital medicine," *Journal of Hospital Medicine*, vol. 13, pp. 126-135, Feb. 2018. [Online]. https://doi.org/10.12788/jhm.2940

[55]    H.T. Harcke, L.A. Pearse, A.D. Levy, J.M. Getz and S.R. Robinson, "Chest wall thickness in military personnel: implications for needle thoracentesis in tension pneumothorax," *Journal of Military Medicine*, vol. 172, pp. 1260-1263, Dec. 2007. [Online]. Available: https://www.ncbi.nlm.nih.gov/m/pubmed/18274025/

[56]    C. Jones and A. Adejuwon, "Ultrasound measurement of chest wall thickness in elite rugby players; a comparison between the needle thoracocentesis sites," *Birtish Journal of Sports Medicine*, vol. 50, pp. 1350. [Online]. Available: https://bjsm.bmj.com/content/50/21/1350.2

[57]    "Statistics," Childhood Obesity Foundation, April 2015. [Online]. Available: https://childhoodobesityfoundation.ca/what-is-childhood-obesity/statistics/

[58]  "Overweight & Obesity Statistics," National Institute of Diabetes and Digestive and Kidney Diseases, August 2007. [Online]. Available: https://www.niddk.nih.gov/health-information/health-statistics/overweight-obesity

[59]  P.N. Brett, T.J. Parker, A.J. Harrison, T.A. Thomas and A. Carr, "Simulation of resistance forces acting on surgical needles," *Journal of engineering in medicine,* vol. 211, pp. 335-347. [Online]. Available: http://journals.sagepub.com/doi/pdf/10.1243/0954411971534467

[60]  L.L. Holton, "Force models for needle insertion created from measured puncture data," *Studies in health technology and informatics,* vol. 81, pp. 180-186. [Online]. Available: https://www.ncbi.nlm.nih.gov/pubmed/11317736#

[61]  E.M. DeBiasi, M.A. Pisani, T.E. Murphy, K. Araujo, A. Kookoolis, A.C. Argento and J. Puchalski, "Mortality among patients with pleural effusion undergoing thoracentesis," *The European Respiratory Journal*, vol. 46, pp. 495–502, Feb. 2015. [Online]. http://doi.org/10.1183/09031936.00217114

[62]  S.B. Issenberg, W.C. McGaghie, E.R. Petrusa, D. Lee-Gordon and R.J. Scalede, "Features and uses of high-fidelity medical simulations that lead to effective learning: a BEME systematic review," *Medical Teaching*, vol. 27, pp. 10-28, Jan. 2005. [Online]. Available: https://www.ncbi.nlm.nih.gov/pubmed/16147767

[63]  "Industry Challenges," Moldex3D. Accessed May 25, 2018. [Online]. Available: http://www.moldex3d.com/en/solutions/solutions-by-industry/medical/

[64]  "5 Questions: Injection molding for medical devices," Medical Product Outsourcing. Accessed May 15, 2018. [Online]. Available: https://www.mpo-mag.com/contents/view_online-exclusives/2017-08-23/5-questions-injection-molding-for-medical-devices

[65]  "Advantages and disadvantages of injection molding," Design-Tek Tools & Plastics Inc.,. Accessed May 25, 2018. [Online]. Available: http://designtekplastics.com/tips/disadvantages-and-advantages-of-injection-molding/

[66]  "Injection molding basics (advantages and disadvantages," ACO Mold. Accessed May 20, 2018. [Online]. Available: http://www.acomold.com/injection-molding-basics.html

[67]    "Advantages and disadvantages of injection moulding," AV Plastics. Accessed May 15, 2018.
[Online]. Available: http://www.avplastics.co.uk/advantages-and-disadvantages-of-injection-
moulding

[68]    "How long does it take to build an injection mold?," PlastiCert Inc.. Accessed May 21, 2018.
[Online]. Available: https://www.plasticert.com/2015/02/how-long-does-it-take-to-build-an-
injection-mold/

[69]    "How much does an injection mold cost?," ICO Mold. Accessed May 25, 2018. [Online].
Available: https://icomold.com/much-injection-molding-cost/

[70]    "Advantages and disadvantages of injection moulding," Martin's Rubber Company. Accessed
May 25, 2018. [Online]. Available: http://www.martins-rubber.co.uk/blog/advantages-and-
disadvantages-of-injection-moulding/

[71]    "Everything you need to now about injection molding," Creative Mechanisms. Accessed May
22, 2018. [Online]. Available: https://www.creativemechanisms.com/blog/everything-you-need-to-
know-about-injection-molding

[72]    Additive anufacturing: Medical Indiustry," GE Additive. Accessed May 15, 2018. [Online].
Available: https://www.ge.com/additive/additive-manufacturing/industries/medical

[73]    J.P. Lichtenberger, P.S. Tatum, S. Gada, M. Wyn, V.B. Ho and P. Liacouras, "Using 3-D printing
(additive manufacturing) to produce low-cost simulation models for medical training," *Military
Medicine,* vol. 183, pp. 73-77. [Online]. Available:
https://academic.oup.com/milmed/article/183/suppl_1/73/4959929#114966891

[74]    S.B. Issenberg, R.J. Scalese, "Simulation in health care education," *Perspectives in Biology and
Medicine*, vol. 51, pp. 31-46, Dec. 2008. [Online]. https://doi.org/10.1353/pbm.2008.0004

[75]    H. Kalami, A. Khayat and R.J. Urbanic, "Investigating 'Exo-skeleton' design and fabrication
challenges for the hand region using material extrusion processes," *IFAC-PapersOnLine*, vol. 49,
pp. 30-35, Feb. 2017. [Online]. https://doi.org/10.1016/j.ifacol.2016.12.157

[76]    P.Y.F. Lee, T.G. Winfield, S.R.S. Harris, E. Storey and A. Chandratreya, "Unloading knee brace
is a cost-effective method to bridge and delay surgery in unicompartmental knee arthritis," *BMJ
Open Sport & Exercise Medicine*, vol. 2, Feb. 2017. [Online].  https://doi.org/10.1136/bmjsem-2016-
000195

[77]    K.S. Malyala, A. Manmadhachary, Y.R. Kumar and A. Alwala, "Manufacturing of patient specific AM medical models for complex surgeries," *Materials Today Proceedings*, vol. 4, pp. 1134-1139, Jan. 2017. [Online].  https://doi.org/10.1016/j.matpr.2017.01.129

[78]    C.L. Ventola, "Medical applications for 3D printing: Current and projected uses," *Pharmacy and Therapeutics*, vol.39, pp. 704–711, Oct. 2014. [Online]. Available: https://www.ncbi.nlm.nih.gov/pmc/articles/PMC4189697/

[79]    "Mould Set Estimate," Mahle Filter Systems. [Online]. Available: http://www.us.mahle.com/

[80]     "Top five benefits of additive manufacturing (You never considered)," ManufacturingNet. Accessed Apr. 15, 2018. [Online]. Available: https://www.manufacturing.net/article/2013/02/top-five-benefits-additive-manufacturing-you-never-considered

[81]    "Welcome," Schulich School of Medicine & Dentistry- Windsor Campus. Accessed May 18, 2018. [Online]. Available: http://www.uwindsor.ca/medicine/

[82]    "What is the procedure for a thoracentesis?," Healthline. Accessed May 19, 2018. [Online]. Available: https://www.healthline.com/health/thoracentesis#procedure

[83]    "How safe is thoracentesis? Giant case series sheds light," PulmCCM. Accessed May 19, 2018. [Online]. Available: https://pulmccm.org/review-articles/how-safe-is-thoracentesis-giant-case-series-sheds-light/

[84]    T. Havelock, R. Teoh, D. Laws and F. Gleeson, "Pleural procedures and thoracic ultrasound: British Thoracic Society pleural disease guideline 2010," *BMJ Journals,* vol. 65, pp. 61-76. [Online]. Available: https://thorax.bmj.com/content/65/Suppl_2/i61

[85]    M. Vera, "Thoracentesis," *Fundamentals of Nursing*, Jan 2012. Accessed: Sept. 15, 2018. [Online]. Available: https://nurseslabs.com/thoracentesis-procedure-nursing-management/

[86]    R. Dancel, D. Scjnobrich, N. Puri, R. Franco-Sadud, J. Cho, L. Grikis, B.P. Lucas, M. El-Barbary and N.J. Soni, "Recommendations on the use of ultrasound guidance for adult thoracentesis: A position statement of the society of hospital medicine," *Journal of Hospital Medicine*, vol. 13, pp. 126-135. [Online]. Available: https://www.ncbi.nlm.nih.gov/pubmed/29377972

[87]    P. Mayo, "Thoracic ultrasound: Indications, advantages, and technique," *UpToDate*, Nov. 2016. Accessed: Sept. 15, 2018. [Online]. Available: https://www.uptodate.com/contents/thoracic-ultrasound-indications-advantages-and-technique

[88]    A.A. Weaver, S.L. Schoell and J.D. Stitzel, "Morphometric analysis of variation in the ribs with age and sex," *Journal of Anatomy*, vol. 225, pp. 246-261, June 2014. [Online]. Available: https://www.ncbi.nlm.nih.gov/pmc/articles/PMC4111931/pdf/joa0225-0246.pdf

[89]    D. Subit, B. Sandoz, J. Choisne, C. Amabile, C. Vergari, W. Skalli and S. Laporte, "Rib length variation with age and sex - Measurements from high-resolution low-radiation X-ray images of volunteer subjects," presented at *4th International Technical Conference on the Enhanced Safety of Vehicles (ESV): Traffic Safety Through Integrated Technologies*, Gothenburg, Sweden, 2015. [Online]. Available:                                https://www-esv.nhtsa.dot.gov/Proceedings/24/files/24ESV-000313.PDF

[90]    Y.S. Kim, M.J. Park, H. Rhim, M.W. Lee and H.K. Lim, "Sonographic analysis of the intercostal spaces for the application of high-intensity focused ultrasound therapy to the liver," *American Journal of Roentgeneology*, vol. 203, pp. 201-208, July 2014.  [Online]. Available: https://www.ajronline.org/doi/full/10.2214/AJR.13.11744

[91]    M.A. Mcgraw, C.T. Mehlman, C.J. Lindsell and C.C. Kirby, "Postnatal growth of the clavicle: Birth to eighteen years of age," Journal of Pediatric Orthopaedics, vol. 29, pp. 937-943, Dec. 2009. [Online]. Available: https://www.ncbi.nlm.nih.gov/pmc/articles/PMC2806601/

[92]    C. Cunningham, L. Scheuer and S. Black, *Developmental Juvenile Osteology.* 2nd Ed. United States of America: Academic Press, 2016, pp. 280-284. [Online]. Available: https://books.google.ca/books?id=MR-cAAAAQBAJ&pg=PA281&lpg=PA281&dq=cunningham+et+al+scapula+23+years+inferior+angle&source=bl&ots=RLqztPRLqm&sig=NsfB21x9NB8IfzHRcslRIZrtLrQ&hl=en&sa=X&ved=2ahUKEwiLjbuV65DdAhXxUt8KHTR7BVQQ6AEwDHoECAUQAQ#v=onepage&q=cunningham%20et%20al%20scapula%2023%20years%20inferior%20angle&f=false

[93]    F. Canavese and A. Dimeglio, "Normal and abnormal spice and thoracic cage development," *World Journal of Orthopaedics,* vol. 4, pp. 167-174. [Online]. Available: https://www.ncbi.nlm.nih.gov/pmc/articles/PMC3801235/

[94]    E.M. Debiasi and J. Puchalski, "Thoracentesis," *Sage Journals,* vol. 3, May 2016. [Online]. https://doi.org/10.1177%2F2373997516646554

[95]    M.G. Seneff, R.W. Corwin, L.H. Gold and R.S. Irwin, "Complications associated with thoracentesis," *Chest*, vol. 90, pp. 97-100, July 1986. [Online]. Available: https://www.ncbi.nlm.nih.gov/pubmed/3522123

[96]   A.A. Keefe, H. Angel and B. Mangan, "2012 Canadian forces anthropometric survey (CFAS)," *Scientific Report, September 2015, Accessed: Sept 15 2018. [Online]. Available:* cradpdf.drdc-rddc.gc.ca/PDFS/unc224/p803174_A1b.pdf

[97]   A. Camily, P.P.F.D. Albuquerque, P.V.D. Albuquerque, B. Duarte, Y.M.L.D. Albuquerque and V. Caiaffo, "Morphometric analysis of the scapula and their differences between females and males," *Journal of Morphology*, vol. 34, pp. 1164-1168, October 2016. [Online]. Available: https://www.researchgate.net/publication/309672211_Morphometric_Analysis_of_the_Scapula_and_Their_Differences_between_Females_and_Males

[98]   OpenStax, *The Thoracic Cage,* Anatomy & Physiology, Texas, United States of Americs, Feb. 2016, pp. 46. Accessed: Sept 17 2018. [Online]. Available: https://opentextbc.ca/anatomyandphysiology/chapter/7-4-the-thoracic-cage/

[99]   F. Canavese and A. Dimeglio, "Normal and abnormal spine and thoracic cage development," *World Journal of Orthopaedics,* vol. 4, pp. 167-174, Oct. 2013. [Online]. Available: https://www.ncbi.nlm.nih.gov/pmc/articles/PMC3801235/

[100]  Texas Tech University Health Sciences Center, "Clinical Cases-Thoracic wall, Pleura, & Pericardium," Accessed: Sept 20, 2018. [Online]. Available: https://anatomy.elpaso.ttuhsc.edu/cardiovascular_system/thorax_wall_case.html

[101]  Advantage International Registrar, "Conventional manufacturing" Accessed: Sept. 12, 2018. [Online]. Available: https://oromfg.com/services/conventional-manufacturing/

[102]  J. Anderson, "Five reasons for flash on plastic and rubber parts," July 2017. Accessed: October 11, 2018. [Online]. Available: http://nitrofreeze.com/five-reasons-for-flash-on-plastic-and-rubber-parts/

[103]  M. Ahart, "Manufacturing workmanship standards: Amount of flash acceptable at parting lines," February 28, 2018. Accessed: Sept 25, 2018. [Online]. Available: https://www.protolabs.com/resources/blog/manufacturing-workmanship-standards-amount-of-flash-acceptable-at-parting-lines/

[104]  3D Systems, "Basics of injection molding design," Accessed: Oct. 9, 2018. [Online]. Available: https://www.3dsystems.com/quickparts/learning-center/injection-molding-basics#parting

[105]  K. Chwatko and S. Piszczatowski, "Modelling of the musculoskeletal system using commercial CAD software," 2010. Accessed Sept 2, 2018. [Online]. Available: https://pdfs.semanticscholar.org/61e0/492819023420425447c6c0ff6526078619ae.pdf

[106]  PTC, "About tesselated files," Accessed: Oct. 22, 2018. [Online]. Available:

http://support.ptc.com/help/creo/creo_pma/usascii/index.html#page/data_exchange/interface/About_Tessellated_Files.html

[107]  T.M. Bucking, E.R. Hill, J.L. Robertson, E. Maneas, A.A. Plumb and D.I. Nikitichev, "From medical imaging data to 3D printed anatomical models," *PLOS ONE*, vol. 12. May 2017. [Online]. Available: http://journals.plos.org/plosone/article?id=10.1371/journal.pone.0178540

[108]  "Autodesk Meshmixer," Meshmixer. Accessed Sept. 12, 2018. [Online]. Available: http://www.meshmixer.com/

[109]  "Windows 3D builder," Microsoft. Accessed Mar. 26, 2018. [Online]. Available: https://www.microsoft.com/en-ca/store/p/3d-builder/9wzdncrfj3t6

[110]  "FreeCAD," FreeCAD. Accessed May 3, 2018. [Online]. Available: https://www.freecadweb.org

[111]  "CATIA V5," Dassault Systemes. Accessed May 20, 2018. [Online]. Available: https://www.3ds.com/products-services/catia/products/v5/portfolio/

[112]  P.J. Antunes, G.R. Dias, A.T. Coelho, F. Rebelo and T. Pereira, "Non-linear finite element modelling of anatomically detailed 3D foot model," January 8, 2008. Accessed: August 2, 2018. [Online]. Available: http://vahabonline.com/wp-content/uploads/2014/07/0Non-Linear-Finite-Element-Modelling-of-Anatomically-Detailed-3D-Foot-Model.pdf

[113]  "SolidWorks," Dassault Systemes. Accessed Mar. 24, 2018. [Online]. Available: https://www.solidworks.com/

[114]  "Netfabb—Standard," Autodesk. Accessed May 2, 2018. [Online]. Available: https://www.autodesk.ca/en/products/netfabb/subscribe?AID=12797027&PID=8206971&SID=jkp_CImqzbm4ydoCFSGSxQIdkpsAYw&gclsrc=ds&mktvar002=afc_ca_nmpi_ppc&gclid=CImqzbm4ydoCFSGSxQIdkpsAYw&plc=NETFS&term=1-YEAR&support=ADVANCED&quantity=1

[115]  R. Olszewski, P. Szymor and M. Kozakiewicz, "Accuracy of three-dimensional, paper-based models generated using a low-cost, three-dimensional printer," *Journal of Cranio-maxillo-facial surgery,* vol. 42, pp. 1847-1852, Dec. 2014. [Online]. Available: https://www.ncbi.nlm.nih.gov/pubmed/25176496

[116]  DesignTech, "Parametric modelling," Accessed: Oct. 21, 2018. [Online]. Available: https://www.designtechsys.com/articles/parametric-modelling

146

[117]  J.J. Shah, "Designing with parametric CAD: Classification and comparison of construction techniques," *Geometric Modelling,* vol. 75, pp. 53-68, 1998. [Online]. Available: https://link.springer.com/chapter/10.1007/978-0-387-35490-3_4

[118] Y. Bodein, B. Rose and E. Caillaud, "A roadmap for parametric CAD efficiency in the automotive industry," *Computer-Aided Design*, vol. 45, pp. 1198-1214, Oct. 2013. [Online]. Available: https://www.sciencedirect.com/science/article/pii/S0010448513000833?via%3Dihub

[119] J.D. Camba, M. Contero and P. Company, "Parametric CAD modelling: An analysis of strategies for design reusability," *Computer-Aided Design*, vol. 74, pp. 18-31, May 2016. [Online]. Available: https://www.sciencedirect.com/science/article/pii/S0010448516000051

[120] M. Brunelli, "Parametric vs. direct modeling: Which side are you on?," ptc. [Accessed May 27, 2018. [Online]. Available: https://www.ptc.com/en/cad-software-blog/parametric-vs-direct-modeling-which-side-are-you-on

[121] M. Eragubi, "Slicing 3D CAD model in STL format and laser path generation," *International Journal of Innovation, Management and Technology,* vol. 4, August 2013. [Online]. Available: https://pdfs.semanticscholar.org/cf34/4528fe44e65b8b94676089ddca2e4da6a25c.pdf

[122]  "About additive manufacturing," Loughborough University. Accessed May 24, 2018. [Online]. Available: http://www.lboro.ac.uk/research/amrg/about/the7categoriesofadditivemanufacturing/

[123] M. Thielen, R. Joshi, F. Delbressine, S.B. Oetomo and L. Fejis, "An innovative design for cardiopulmonary resuscitation manikins based on a human-like thorax and embedded flow sensors," *Proceedings of the Institution of Mechanical Engineers*, vol. 231, pp. 243-249, Feb. 2017. [Online]. Available: http://www.geometrysummit.org/proceedings/fase2016/papers/5.pdf

[124] "Human rib cage 3D model" CadNav, Accessed Sept 11, 2018. [Online]. Available: http://www.cadnav.com/3d-models/model-23866.html

[125] "Thorax bone anatomy 3D Model" CadNav, Accessed Sept 11, 2018. [Online]. Available: http://www.cadnav.com/3d-models/model-19344.html

[126] "Left clavicle" Sketchfab, Accessed Sept. 11, 2018. [Online]. Available: https://sketchfab.com/models/b58db46ed8564fedade966310a3e95ae

[127] "Scapula," Sketchfab, Accessed Sept. 11, 2018. [Online]. Available: https://sketchfab.com/models/4eb3b5eee74a422e8b870f40e7c032ca

[128] A. Natanzon and I. Kronzon, "Pericardial and pleural effusions in congestive heart failure-anatomical, pathophysiologic, and clinical considerations," *The American Journal of the Medical* Sciences, vol. 338, pp. 211-216, Sept. 2009. [Online]. Available:

https://www.ncbi.nlm.nih.gov/pubmed/19574887

[129] C. Smith, "3D skeletal system: Bones of the thoracic cage," Visible Body, Oct. 24, 2012. [Online]. Available: https://www.visiblebody.com/blog/3d-skeletal-system-bones-of-the-thoracic-cage

[130] L.H. Poniatowski, S.S. Somani, D. Veneziano, S. McAdams and R.M. Sweet, "Characterizing and simulating needle insertion forces for percutaneous renal access," Journal of Endourology, vol. 30, pp. 1049-1055, Oct. 2016. [Online]. Available:

https://www.ncbi.nlm.nih.gov/pubmed/27519947

[131] S.P. DiMaio and S.E. Salcudean, "Interactive simulation of needle insertion models," *IEEE Transactions on Biomedical Engineering,* vol. 52, pp. 1167-1179, July 2005. [Online]. Available: https://ieeexplore.ieee.org/document/1440595/

[132] N. Abolhassani, R. Patel and M. Moallem, "Needle insertion into soft tissue: a survey," *Medical Engineering & Physics,* vol. 4, pp. 413-431, May 2007. [Online]. Available:

https://www.ncbi.nlm.nih.gov/pubmed/16938481

[133] M. Mahvash and P.E. Dupont, "Mechanics of dynamic needle insertion into a biological material," *IEEE Transactions on Biomedical Engineering,* vol. 57, pp. 934-943, Apr. 2010. [Online]. Available: https://www.ncbi.nlm.nih.gov/pmc/articles/PMC3021974/

[134] S. Jiang, P. Li, Y. Yu, J. Liu and Z. Yang, "Experimental study of needle-tissue interaction forces: effect of needle geometries, insertion methods, and tissue characteristics, *Department of Radiation Oncology Faculty Papers,* vol. 47, pp. 3344-3353, Oct. 2014. [Online]. Available: https://jdc.jefferson.edu/cgi/viewcontent.cgi?article=1051&context=radoncfp

[135] A.M. Okamura, C. Simone and M.D. O'Leary, "Force modeling for needle insertion into soft tissue," IEEE Transactions on Bio-Medical Engineering, vol. 51, pp. 1707-1716, Oct. 2004. [Online]. Available: https://www.ncbi.nlm.nih.gov/pubmed/15490818

[136] S. Perry, M. Drum, A. Reader, J. Nusstein and M. Beck, "Effect of operator and subject gender on injection pain: A randomized double-blind study," *Journal of Endodontics,* vol. 41, pp. 141-145, Feb. 2015. [Online]. Available: https://www.jendodon.com/article/S0099-2399(14)00933-9/fulltext

[137] C. Simone and A.M. Okamura, "Modeling of needle-insertion forces for robot-assisted percutaneous therapy," *Proceedings of the 2002 IEEE International Conference on Robotics & Automation*, Washington, DC. May 2002. [Online]. Available: http://citeseerx.ist.psu.edu/viewdoc/download?doi=10.1.1.90.9322&rep=rep1&type=pdf

[138] Y. Wang, B.L. Tai, H. Yu and A.J. Shih, "Silicone-based tissue-mimicking phantom for needle insertion simulation," *Journal of Medical Devices*, vol. 8, pp. 1-7, Mar. 2014. [Online]. Available: http://medicaldevices.asmedigitalcollection.asme.org/article.aspx?articleid=1876523

[139] A.E. Forte, S. Galvan, F. Manieri, F.R.Y. Baena and D. Dini, "A composite hydrogel for brain tissue phantoms," *Materials and Design,* vol. 112, pp. 227-238, Sept. 2016. [Online]. Available: https://www.sciencedirect.com/science/article/pii/S0264127516312370

[140] A. Gordon, I. Kim, A.C. Barnett and J.Z. Moore, "Needle insertion force model for haptic simulation," *Proceedings of the ASME 2015 International Manufacturing Science and Engineering Conference,* June 8-12, 2005, North Carolina. [Online]. Available: https://www.researchgate.net/publication/283526739_Needle_Insertion_Force_Model_for_Haptic_Simulation

[141] M. Abayazid and S. Misra, "Effect of skin thickness on target motion during needle insertion into soft-tissue phantoms," *IEEE Engineering in Medicine and Biology Society,* pp. 755-760, June 2012. [Online]. Available: https://research.utwente.nl/en/publications/effect-of-skin-thickness-on-target-motion-during-needle-insertion

[142] "Butterworth filter design," Electronic Tutorials. Accessed: Sept. 12, 2018. [Online]. Available: https://www.electronics-tutorials.ws/filter/filter_8.html

[143] FK.R. Ford, G.D. Myer and T.E. Hewett, "Valgus knee motion during landing in high school female and male basketball players," *Medicine and science in sports and exercise,* vol. 35, pp. 1745-1750, Oct. 2003. [Online]. Available: https://www.ncbi.nlm.nih.gov/pubmed/14523314

[144] "You Compare," Aniwaa. Accessed May 28, 2018. [Online]. Available: https://www.aniwaa.com/you-compare/

[145] "PLUTO 3D printer: Review the facts," ALL3DP. Accessed Sept 24, 2018. [Online]. Available: https://all3dp.com/1/pluto-3d-printer-review/

[146] "T3500," ANIWAA. Accessed Sept 24, 2018. [Online]. Available: https://www.aniwaa.com/product/3d-printers/tractus3d-t3500-rtp/

149

[147] S.H. Ahn, M. Montero, D. Odell, S. Roundy and P.K. Wright, "Anisotropic material properties of fused deposition modeling ABS," Rapid Prototyping Journal, vol. 8, pp. 248-257, 2002. [Online]. https://doi.org/10.1108/13552540210441166

[148] J. Kranz, "Design guidelines for laser additive manufacturing of lightweight structures in TiAl6V4," Journal of Laser Applications, vol. 27, Dec. 2014. [Online]. https://doi.org/10.2351/1.4885235

[149] "Fortus 400 mc," Stratasys. Accessed May 26, 2018. [Online]. Available: https://proto3000.com/fortus-400mc.php , Stratasys.

[150] "Replicator 2X Experimental 3D Printer," MakerBot. Accessed: Sept 24, 2018. [Online]. Available: https://store.makerbot.com/printers/replicator2x/

[151] "ABS-M30," Stratasys. Accessed May 26, 2018. [Online]. Available: http://www.stratasys.com/materials/search/abs-m30

[152] "Filaments," Filaments. Accessed May 24, 2018. [Online]. Available: https://filaments.ca

[153] "Clean Stations," Cimetrix. Accessed May 16, 2018. [Online]. Available: http://www.cimetrixsolutions.com/products/clean-stations/pm-technologies

[154] "Investor relations," Stratasys. Accessed May 16, 2018. [Online]. Available: http://investors.stratasys.com/news-releases/news-release-details/new-fortus-support-material-helps-make-fdm-prototypes-and

[155] "Ultem 9085 Support," RND-Tech. Accessed Sept 21, 2018. [Online]. Available: https://www.rnd-tech.com/shop/support-material/49

[156] "FDM for end-use parts," Stratasys. Accessed Sept 25, 2018. [Online]. Available: http://usglobalimages.stratasys.com/Main/Secure/Applications/End%20Use%20Parts/SSYS-TAG-End-UseParts-11-13.pdf

[157] C.X.F. Lam, X.M. Mo, S.H. Teoh and D.W. Hutmacher, "Scaffold development using 3D printing with a starch-based polymer," Materials Science and Engineering, vol. 20, pp. 49-56, May 2002. [Online]. Available: https://www.sciencedirect.com/science/article/pii/S0928493102000127

[158] J.W. Jung, J.S. Lee and D.W. Cho, "Computer-aided multiple-head 3D printing system for printing of heterogeneous organ/tissue constructs," Scientific Reports, vol. 6, Feb. 2016. [Online]. Available: https://www.nature.com/articles/srep21685

[159] A. Shapi'i, R. Sulaiman, M.K. Hasan, A.Y.M. Kassim and H.A. Hamid, "Applications of computer aided design (CAD) in medical image technology," *International Journal on Advanced*

*Science*, vol. 1, pp. 698-701, Jan. 2011. [Online]. Available:

http://ijaseit.insightsociety.org/index.php?option=com_content&view=article&id=9&Itemid=1&article_id=140

[160]  K. Torres, G. Staskiewicz, A. Drop and R. Maciejewski, "Application of rapid prototyping

techniques for modelling of anatomical structures in medical training and education," Folia

Morphologica, vol. 70, pp. 1-4. [Online]. Available:

https://www.ncbi.nlm.nih.gov/pubmed/21604245

[161]  Sun, B. Starly, J. Nam and A. Darling, "Bio-CAD modeling and its applications in computer-

aided tissue engineering," Computer-Aided Design, vol. 37, pp. 1097-1114, Sept 2005. [Online].

Available: https://www.researchgate.net/publication/220582565_Bio-

CAD_modeling_and_its_applications_in_computer-aided_tissue_engineering

[162]  T.D. Harpool, "Observing the effects of infill shapes on the tensile characteristics of 3D

printed plastic parts," M.S. thesis, Mech. Eng., Wichita State Univ., Wichita, KS. USA, 2014. [Online].

Available:

https://soar.wichita.edu/bitstream/handle/10057/13504/t16070_Harpool.pdf?sequence=1

[163]  "Cadnav Models," Cadnav 3D. Accessed May 26, 2018. [Online]. Available: www.Cadnav.com

[164]   "The thoracic cage," BC Campus. Accessed Mar. 2018. [Online]. Available:

https://opentextbc.ca/anatomyandphysiology/chapter/7-4-the-thoracic-cage/

[165]  "Argyle TURKEL Safety Thoracentesis System, 8 French, 3 1/2inch Catheter Length," Bound

Tree. Accessed Mar. 6, 2018. [Online]. Available: https://www.boundtree.com/argyle-turkel-safety-

thoracentesis-system-1640-03408-pharm-5032-296.aspx

[166]   "0-1000N Micro load cell 0~100kgf," Forsentek. Accessed Mar. 19, 2018. [Online]. Available:

http://www.forsentek.com/prodetail_7.html

[167]   "Dr. Joel Cort," University of Windsor. Accessed Mar. 27, 2018. [Online]. Available:

http://www.uwindsor.ca/kinesiology/482/dr-joel-cort

[168]   "Pocket Juice Power Bank Charger," Pocket Juice. Accessed Mar. 28, 2018. [Online].

Available: http://buypocketjuice.com

[169]   "HP EliteBook 800 Series," hp. Accessed Mar. 25, 2018. [Online]. Available:

http://www8.hp.com/ca/en/home.html

[170]  "Microsoft Excel," Microsoft. Accessed Mar. 25, 2018. [Online]. Available:

https://products.office.com/en-ca/excel

[171]  "Repeated Measures ANOVA," Laerd Statistics. Accessed Oct. 2, 2018. [Online]. Available:

https://statistics.laerd.com/statistical-guides/repeated-measures-anova-statistical-guide-3.php

[172]  "Sphericity," Laerd Statistics. Accessed Oct. 3, 2018. [Online]. Available:

https://statistics.laerd.com/statistical-guides/sphericity-statistical-guide-2.php

[173]  S. Alderson, "How to make silicone moulds without air bubbles," *Aldax Enterprises Pty. Ltd.,*

2010. [Accessed Sept 12, 2018. [Online]. Available:

https://www.aldax.com.au/Silicone_article_bubbles.htm

[174]  J. Cordes, "Bonding and gluing," Accessed Sept 29, 2018. [Online]. Available:

http://articles.stratasys.com/finishing-processes/bonding-and-gluing

[175]  B. Kalajdzic, R.J. Urbanic, A. Khayat and A. "Utilizing advanced manufacturing technologies

to develop a reconfigurable lumbar puncture training model," in Proc. of the ASME 2018 Intl.

Mech. Eng. Cong. and Expo., Forthcoming.

[176]  "ABS-M30," Stratasys. Accessed Oct. 4, 2018. [Online]. Available: http://www.stratasys.com/-

/media/files/material-spec-sheets/mss_fdm_absm30_1117a.pdf

[177]  "ULTEM 9085," Stratasys. Accessed Oct. 4, 2018. [Online]. Available:

http://www.stratasys.com/-/media/files/material-spec-sheets/mss_fdm_ultem9085_1117a.pdf

[178]  "Nylon 12CF," Stratasys. Accessed Oct. 4, 2018. [Online]. Available:

http://www.stratasys.com/-/media/files/nylon-12cf/mg_fdm_nylon12cf_0217a_web.pdf

[179]  "PC (Polocarbonate)," Stratasys. Accessed Oct. 4, 2018. [Online]. Available:

http://www.stratasys.com/-/media/files/material-spec-sheets/mss_fdm_pc_1117a.pdf

[180]  Dongguan Guochuang Silicone Co. LTD.: "Variable hardness silicone," Dongguan Guochuang

Silicone Co. Ltd.. Accessed May 26, 2018. [Online]. Available:

http://www.liquidsilicone.net/product/list-155-en.html

[181]  "Alumilite Silicone Oil," Alumilite. Accessed Sept 26, 2018. [Online[]. Available:

https://www.alumilite.com/store/p/961-Silicone-Oil-1lb.aspx

[182]  "Merit Medical," MeritMedical. Accessed May 22, 2018. [Online]. Available:

https://www.merit.com/

APPENDICES

## Appendix A: Literature Review Content

**List 1: Thoracentesis procedure checklist [33]**

- Obtains informed consent
- Performs a preprocedure time-out immediately before procedure
  - Confirms patient ID, procedire, and site by all members of ream doing procedure;
  - Confirms no allergy to local anesthetic
- Positions patient appropriately
  - Sits on edge of bed;
  - Arms resting on a table with a pillow
- Inspects posterior chest wall
  - Notes location of scars, cellulitis, or herpes zoster
- Notes upper level of fluid via ultrasound, or if ultrasound not available, percusses thorax
- Identifies or marks site that is
  - An intercostal space 1-2 ribs below the upper level of fluid;
  - Site 5-10 cm lateral to spine and never below $9^{th}$ rib
- Washes hands
- Opens kit
- Applies cap, mask, sterile gown
- Applies sterile gloves
- Arranges material approprately
- Preps over marked site and surrounding skin with chlorhexidine or approproate alternative
- Reconfirms that puncture site is on the superior aspect of lower rib of the selected intercostal space
  - Must make puncture on top, never bottom of rib
- Injects lidocaine at sitre of procedure
  - Subcutaneous injection, 25-22 G neegle, wheal formation, then deeper into skin; when pleural fluid obtained, note depth, inject 2-3 cc more to anesthetixe the parietal pleura
- Inserts 18 G over the needle catheter
  - Either from a kit of IV catheter, attached to 60-mL syringe;
- Pull back on plunger as one is reaching depth of effusion;
- Once resched, slide catheter over needle;
- Always over the top of lower rib
- Places finger/thumb top over exposed hub

- Attaches a 60-ml syringe with a 3-way stopcock to catheter   remove 30-50 cc of fluid in 60 cc syringe;
    - Have assistant immediately place in appropriate tubes or blood culture bottles
- If therapeutic thoracentesis is needed, applies flexible tube from manometer to needle hub
- Pulls out the catheter and gently aplies pressure to site
    - Instructs patient to exhale or hum as catheter is withdrawn
- Disposes of needle in sharps container
- Cleans up
- Wirtes procedure note in appropriate space
- Orders a chest radiograph

## Appendix B: SPSS Cadaver Data Readouts

### Readout 1: Cadaver peak force data readout
**General Linear Model (PEAK FORCE)**

#### Within-Subjects Factors

Measure: Force_N

| Peak_Force | Dependent Variable |
|---|---|
| 1 | Pos_1 |
| 2 | Pos_2 |
| 3 | Pos_3 |

#### Descriptive Statistics

| | Participant | Mean | Std. Deviation | N |
|---|---|---|---|---|
| Pos_1 | A | 2.62367 | .151688 | 3 |
| | B | 3.53067 | 1.568564 | 3 |
| | C | 4.30267 | .999582 | 3 |
| | D | 4.94533 | .644643 | 3 |
| | E | 5.44300 | .645000 | 3 |
| | Total | 4.16907 | 1.302355 | 15 |
| Pos_2 | A | 5.86433 | .437502 | 3 |
| | B | 6.19592 | 1.200351 | 3 |
| | C | 6.98667 | 1.391446 | 3 |
| | D | 5.97567 | .278814 | 3 |
| | E | 6.11067 | .741000 | 3 |

| | | | | |
|---|---|---|---|---|
| | Total | 6.22665 | .876244 | 15 |
| Pos_3 | A | 3.05667 | 2.576986 | 3 |
| | B | 5.13043 | 2.556158 | 3 |
| | C | 7.18183 | 2.186762 | 3 |
| | D | 10.47700 | 1.444855 | 3 |
| | E | 10.30133 | 1.845228 | 3 |
| | Total | 7.22945 | 3.508239 | 15 |

## Mauchly's Test of Sphericity[a]

Measure:   Force_N

| Within Subjects Effect | Mauchly's W | Approx. Chi-Square | df | Sig. | Epsilon[b] Greenhouse-Geisser |
|---|---|---|---|---|---|
| Peak_Force | .295 | 10.990 | 2 | .004 | .586 |

## Tests of Within-Subjects Effects

Measure:   Force_N

| Source | | Type III Sum of Squares | df | Mean Square | F |
|---|---|---|---|---|---|
| Peak_Force | Sphericity Assumed | 73.026 | 2 | 36.513 | 15.649 |
| | Greenhouse-Geisser | 73.026 | 1.173 | 62.258 | 15.649 |
| | Huynh-Feldt | 73.026 | 1.767 | 41.336 | 15.649 |
| | Lower-bound | 73.026 | 1.000 | 73.026 | 15.649 |
| Peak_Force * Participant | Sphericity Assumed | 65.410 | 8 | 8.176 | 3.504 |
| | Greenhouse-Geisser | 65.410 | 4.692 | 13.941 | 3.504 |
| | Huynh-Feldt | 65.410 | 7.067 | 9.256 | 3.504 |

| | | | | | |
|---|---|---|---|---|---|
| | Lower-bound | 65.410 | 4.000 | 16.352 | 3.504 |
| Error(Peak_Force) | Sphericity Assumed | 46.666 | 20 | 2.333 | |
| | Greenhouse-Geisser | 46.666 | 11.730 | 3.978 | |
| | Huynh-Feldt | 46.666 | 17.667 | 2.641 | |
| | Lower-bound | 46.666 | 10.000 | 4.667 | |

## Pairwise Comparisons

Measure: Force_N

| (I) Peak_Force | (J) Peak_Force | Mean Difference (I-J) | Std. Error | Sig.[b] | 95% Confidence Interval for Difference[b] Lower Bound |
|---|---|---|---|---|---|
| 1 | 2 | -2.058[*] | .235 | .000 | -2.582 |
| | 3 | -3.060[*] | .627 | .001 | -4.457 |
| 2 | 1 | 2.058[*] | .235 | .000 | 1.533 |
| | 3 | -1.003 | .697 | .181 | -2.555 |
| 3 | 1 | 3.060[*] | .627 | .001 | 1.664 |
| | 2 | 1.003 | .697 | .181 | -.549 |

157

**Readout 2: Cadaver impulse data readout**

**General Linear Model (IMPULSE)**

**Within-Subjects Factors**

Measure:  Impulse_N.s

| Impulse | Dependent Variable |
|---------|--------------------|
| 1 | Pos_1 |
| 2 | Pos_2 |
| 3 | Pos_3 |

## Descriptive Statistics

| | Participant | Mean | Std. Deviation | N |
|---|---|---|---|---|
| Pos_1 | A | 1.76467 | .480517 | 3 |
| | B | 4.31200 | 1.293123 | 3 |
| | C | 1.73360 | 1.428209 | 3 |
| | D | 4.15300 | 2.371815 | 3 |
| | E | 7.26300 | 2.344515 | 3 |
| | Total | 3.84525 | 2.570084 | 15 |
| Pos_2 | A | 6.17300 | 2.373800 | 3 |
| | B | 4.44804 | .788818 | 3 |
| | C | 3.38933 | .818038 | 3 |
| | D | 3.21467 | 1.679038 | 3 |
| | E | 5.29377 | .685035 | 3 |
| | Total | 4.50376 | 1.677189 | 15 |
| Pos_3 | A | 2.77267 | 2.728097 | 3 |

| | | | | |
|---|---|---|---|---|
| B | 4.69155 | 3.292125 | 3 | |
| C | 3.59713 | 2.270370 | 3 | |
| D | 7.30733 | 1.451334 | 3 | |
| E | 8.43767 | 1.859828 | 3 | |
| Total | 5.36127 | 3.030086 | 15 | |

## Mauchly's Test of Sphericity[a]

Measure: Impulse_N.s

| Within Subjects Effect | Mauchly's W | Approx. Chi-Square | df | Sig. | Epsilon[b] Greenhouse-Geisser |
|---|---|---|---|---|---|
| Impulse | .853 | 1.432 | 2 | .489 | .872 |

## Tests of Within-Subjects Effects

Measure: Impulse_N.s

| Source | | Type III Sum of Squares | df | Mean Square | F |
|---|---|---|---|---|---|
| Impulse | Sphericity Assumed | 17.336 | 2 | 8.668 | 3.687 |
| | Greenhouse-Geisser | 17.336 | 1.744 | 9.943 | 3.687 |
| | Huynh-Feldt | 17.336 | 2.000 | 8.668 | 3.687 |
| | Lower-bound | 17.336 | 1.000 | 17.336 | 3.687 |
| Impulse * Participant | Sphericity Assumed | 63.877 | 8 | 7.985 | 3.396 |
| | Greenhouse-Geisser | 63.877 | 6.974 | 9.159 | 3.396 |
| | Huynh-Feldt | 63.877 | 8.000 | 7.985 | 3.396 |
| | Lower-bound | 63.877 | 4.000 | 15.969 | 3.396 |
| Error(Impulse) | Sphericity Assumed | 47.025 | 20 | 2.351 | |

| | Greenhouse-Geisser | 47.025 | 17.436 | 2.697 | |
| | Huynh-Feldt | 47.025 | 20.000 | 2.351 | |
| | Lower-bound | 47.025 | 10.000 | 4.703 | |

# Impulse
## Estimates

Measure:  Impulse_N.s

| | | | 95% Confidence Interval | |
| Impulse | Mean | Std. Error | Lower Bound | Upper Bound |
|---|---|---|---|---|
| 1 | 3.845 | .448 | 2.847 | 4.844 |
| 2 | 4.504 | .369 | 3.681 | 5.326 |
| 3 | 5.361 | .622 | 3.976 | 6.747 |

## Pairwise Comparisons

Measure:  Impulse_N.s

| | | | | | 95% Confidence Interval for Difference[b] | |
| (I) Impulse | (J) Impulse | Mean Difference (I-J) | Std. Error | Sig.[b] | Lower Bound | Upper Bound |
|---|---|---|---|---|---|---|
| 1 | 2 | -.659 | .440 | .166 | -1.640 | .323 |
| | 3 | -1.516[*] | .620 | .035 | -2.897 | -.135 |
| 2 | 1 | .659 | .440 | .166 | -.323 | 1.640 |
| | 3 | -.858 | .602 | .185 | -2.199 | .484 |
| 3 | 1 | 1.516[*] | .620 | .035 | .135 | 2.897 |
| | 2 | .858 | .602 | .185 | -.484 | 2.199 |

**General Linear Model (PULSE WIDTH)**

**Within-Subjects Factors**

Measure:  Pulse_Width_s

| Pulse_Width | Dependent Variable |
|---|---|
| 1 | Pos_1 |
| 2 | Pos_2 |
| 3 | Pos_3 |

## Descriptive Statistics

|  | Participant | Mean | Std. Deviation | N |
|---|---|---|---|---|
| Pos_1 | A | .45633 | .248138 | 3 |
|  | B | 1.02767 | .435353 | 3 |
|  | C | .41367 | .157306 | 3 |
|  | D | .63667 | .465599 | 3 |
|  | E | .87200 | .066121 | 3 |
|  | Total | .68127 | .362108 | 15 |
| Pos_2 | A | .52867 | .206171 | 3 |
|  | B | .49200 | .271365 | 3 |
|  | C | .37033 | .099912 | 3 |
|  | D | .49533 | .323299 | 3 |
|  | E | .36967 | .157561 | 3 |
|  | Total | .45120 | .203426 | 15 |
| Pos_3 | A | .54967 | .181698 | 3 |

| | | | |
|---|---|---|---|
| B | .34133 | .153132 | 3 |
| C | .35800 | .240433 | 3 |
| D | .62800 | .294776 | 3 |
| E | .69200 | .132182 | 3 |
| Total | .51380 | .229530 | 15 |

## Mauchly's Test of Sphericity[a]

Measure:   Pulse_Width_s

| Within Subjects Effect | Mauchly's W | Approx. Chi-Square | df | Sig. | Epsilon[b] Greenhouse-Geisser |
|---|---|---|---|---|---|
| Pulse_Width | .936 | .595 | 2 | .742 | .940 |

## Tests of Within-Subjects Effects

| Source | | Type III Sum of Squares | df | Mean Square | F |
|---|---|---|---|---|---|
| Pulse_Width | Sphericity Assumed | .424 | 2 | .212 | 5.965 |
| | Greenhouse-Geisser | .424 | 1.880 | .226 | 5.965 |
| | Huynh-Feldt | .424 | 2.000 | .212 | 5.965 |
| | Lower-bound | .424 | 1.000 | .424 | 5.965 |
| Pulse_Width * Participant | Sphericity Assumed | .802 | 8 | .100 | 2.818 |
| | Greenhouse-Geisser | .802 | 7.519 | .107 | 2.818 |
| | Huynh-Feldt | .802 | 8.000 | .100 | 2.818 |
| | Lower-bound | .802 | 4.000 | .201 | 2.818 |

| Error(Pulse_Width) | Sphericity Assumed | .712 | 20 | .036 | |
|---|---|---|---|---|---|
| | Greenhouse-Geisser | .712 | 18.797 | .038 | |
| | Huynh-Feldt | .712 | 20.000 | .036 | |
| | Lower-bound | .712 | 10.000 | .071 | |

## Estimated Marginal Means
## Pulse_Width Estimates

Measure:   Pulse_Width_s

| Pulse_Width | Mean | Std. Error | 95% Confidence Interval | |
|---|---|---|---|---|
| | | | Lower Bound | Upper Bound |
| 1 | .681 | .081 | .500 | .863 |
| 2 | .451 | .058 | .321 | .581 |
| 3 | .514 | .054 | .393 | .634 |

## Pairwise Comparisons

Measure:   Pulse_Width_s

| (I) Pulse_Width | (J) Pulse_Width | Mean Difference (I-J) | Std. Error | Sig.[b] | 95% Confidence Interval for Difference[b] Lower Bound |
|---|---|---|---|---|---|
| 1 | 2 | .230* | .066 | .006 | .082 |
| | 3 | .167 | .077 | .054 | -.004 |
| 2 | 1 | -.230* | .066 | .006 | -.378 |
| | 3 | -.063 | .063 | .341 | -.202 |
| 3 | 1 | -.167 | .077 | .054 | -.339 |
| | 2 | .063 | .063 | .341 | -.077 |

# Appendix C: SPSS Silicone-Cadaver Data Readouts

**Readout 4: Silicone sample-cadaver position 1 and 2 peak force data readout**

## Within-Subjects Factors

Measure: Peak force

| PeakForce | Dependent Variable |
|-----------|--------------------|
| 1 | CADP1 |
| 2 | CADP2 |
| 3 | S0 |
| 4 | S1 |
| 5 | S2 |
| 6 | S3 |
| 7 | S4 |
| 8 | S5 |
| 9 | S6 |
| 10 | S7 |
| 11 | S8 |

## Descriptive Statistics

| | Participant | Mean | Std. Deviation | N |
|---|---|---|---|---|
| CADP1 | A | 2.62333 | .150444 | 3 |
| | B | 3.53000 | 1.570096 | 3 |
| | C | 4.30333 | .998465 | 3 |
| | D | 4.94667 | .646555 | 3 |
| | E | 5.44333 | .645006 | 3 |
| | Total | 4.16933 | 1.303021 | 15 |
| CADP2 | A | 5.86667 | .434665 | 3 |
| | B | 6.19667 | 1.200930 | 3 |
| | C | 6.99000 | 1.392695 | 3 |
| | D | 5.97667 | .280238 | 3 |
| | E | 6.11000 | .741148 | 3 |
| | Total | 6.22800 | .876887 | 15 |
| S0 | A | 6.77033 | .522201 | 3 |
| | B | 5.83300 | .456829 | 3 |

|  | | | | |
|---|---|---|---|---|
|  | C | 5.62067 | .264606 | 3 |
|  | D | 5.84100 | .799613 | 3 |
|  | E | 6.19200 | .540503 | 3 |
|  | Total | 6.05140 | .621533 | 15 |
| S1 | A | 4.08633 | .160628 | 3 |
|  | B | 4.37000 | .279193 | 3 |
|  | C | 4.04433 | .352242 | 3 |
|  | D | 4.01833 | .196841 | 3 |
|  | E | 4.22033 | .486721 | 3 |
|  | Total | 4.14787 | .300544 | 15 |
| S2 | A | 3.47700 | .363595 | 3 |
|  | B | 3.30500 | .099232 | 3 |
|  | C | 3.07433 | .081402 | 3 |
|  | D | 3.29333 | .356643 | 3 |
|  | E | 3.37567 | .059375 | 3 |
|  | Total | 3.30507 | .242391 | 15 |
| S3 | A | 2.76500 | .106381 | 3 |
|  | B | 2.86133 | .171165 | 3 |
|  | C | 2.90933 | .144005 | 3 |
|  | D | 2.86867 | .357385 | 3 |
|  | E | 3.17033 | .321710 | 3 |
|  | Total | 2.91493 | .248339 | 15 |
| S4 | A | 2.70367 | .218198 | 3 |
|  | B | 2.58300 | .335549 | 3 |
|  | C | 2.54767 | .111563 | 3 |
|  | D | 2.36833 | .130209 | 3 |
|  | E | 2.69167 | .081837 | 3 |
|  | Total | 2.57887 | .209326 | 15 |
| S5 | A | 2.04533 | .277929 | 3 |
|  | B | 1.83133 | .109391 | 3 |
|  | C | 1.96267 | .234148 | 3 |
|  | D | 1.78833 | .055627 | 3 |
|  | E | 1.82167 | .172946 | 3 |
|  | Total | 1.88987 | .188538 | 15 |
| S6 | A | 1.33767 | .222192 | 3 |
|  | B | 1.46067 | .108316 | 3 |
|  | C | 1.40500 | .115235 | 3 |
|  | D | 1.31333 | .158105 | 3 |

|    |       |         |          |    |
|----|-------|---------|----------|----|
|    | E     | 1.34133 | .200901  | 3  |
|    | Total | 1.37160 | .151896  | 15 |
| S7 | A     | 1.22567 | .128904  | 3  |
|    | B     | 1.27533 | .071459  | 3  |
|    | C     | 1.26133 | .053295  | 3  |
|    | D     | 1.16733 | .057839  | 3  |
|    | E     | 1.12200 | .066701  | 3  |
|    | Total | 1.21033 | .090575  | 15 |
| S8 | A     | 1.12733 | .068245  | 3  |
|    | B     | 1.06133 | .045081  | 3  |
|    | C     | 1.10767 | .057873  | 3  |
|    | D     | 1.08933 | .094537  | 3  |
|    | E     | 1.15333 | .087008  | 3  |
|    | Total | 1.10780 | .069672  | 15 |

## Mauchly's Test of Sphericity[a]

Measure:   Peak force

| Within Subjects Effect | Mauchly's W | Approx. Chi-Square | df | Sig. | Epsilon[b] | | |
|---|---|---|---|---|---|---|---|
| | | | | | Greenhouse-Geisser | Huynh-Feldt | Lower-bound |
| PeakForce | .000 | 111.823 | 54 | .000 | .265 | .514 | .100 |

Tests the null hypothesis that the error covariance matrix of the orthonormalized transformed dependent variables is proportional to an identity matrix.

a. Design: Intercept + Participant

 Within Subjects Design: PeakForce

b. May be used to adjust the degrees of freedom for the averaged tests of significance. Corrected tests are displayed in the Tests of Within-Subjects Effects table.

## Tests of Within-Subjects Effects

Measure:   Peak force

| Source | | Type III Sum of Squares | df | Mean Square | F | Sig. | Partial Eta Squared | Noncent. Parameter | Observed Power[a] |
|---|---|---|---|---|---|---|---|---|---|
| PeakForce | Sphericity Assumed | 495.096 | 10 | 49.510 | 239.090 | .000 | .960 | 2390.898 | 1.000 |
| | Greenhouse-Geisser | 495.096 | 2.651 | 186.744 | 239.090 | .000 | .960 | 633.876 | 1.000 |

| | | | | | | | | | |
|---|---|---|---|---|---|---|---|---|---|
| | Huynh-Feldt | 495.096 | 5.139 | 96.334 | 239.090 | .000 | .960 | 1228.766 | 1.000 |
| | Lower-bound | 495.096 | 1.000 | 495.096 | 239.090 | .000 | .960 | 239.090 | 1.000 |
| PeakForce * Participant | Sphericity Assumed | 20.049 | 40 | .501 | 2.421 | .000 | .492 | 96.822 | 1.000 |
| | Greenhouse-Geisser | 20.049 | 10.605 | 1.891 | 2.421 | .032 | .492 | 25.669 | .850 |
| | Huynh-Feldt | 20.049 | 20.557 | .975 | 2.421 | .005 | .492 | 49.760 | .983 |
| | Lower-bound | 20.049 | 4.000 | 5.012 | 2.421 | .117 | .492 | 9.682 | .484 |
| Error(PeakForce) | Sphericity Assumed | 20.708 | 100 | .207 | | | | | |
| | Greenhouse-Geisser | 20.708 | 26.512 | .781 | | | | | |
| | Huynh-Feldt | 20.708 | 51.394 | .403 | | | | | |
| | Lower-bound | 20.708 | 10.000 | 2.071 | | | | | |

a. Computed using alpha = .05

## Estimates

Measure: Peak force

| PeakForce | Mean | Std. Error | 95% Confidence Interval | |
|---|---|---|---|---|
| | | | Lower Bound | Upper Bound |
| 1 | 4.169 | .240 | 3.635 | 4.704 |
| 2 | 6.228 | .237 | 5.701 | 6.755 |
| 3 | 6.051 | .141 | 5.738 | 6.365 |
| 4 | 4.148 | .082 | 3.965 | 4.330 |
| 5 | 3.305 | .061 | 3.169 | 3.441 |
| 6 | 2.915 | .062 | 2.776 | 3.054 |
| 7 | 2.579 | .051 | 2.465 | 2.693 |
| 8 | 1.890 | .049 | 1.782 | 1.998 |
| 9 | 1.372 | .043 | 1.275 | 1.468 |
| 10 | 1.210 | .021 | 1.164 | 1.257 |
| 11 | 1.108 | .019 | 1.066 | 1.150 |

## Pairwise Comparisons

Measure:   Peak force

| (I) PeakForce | (J) PeakForce | Mean Difference (I-J) | Std. Error | Sig.[b] | 95% Confidence Interval for Difference[b] | |
|---|---|---|---|---|---|---|
| | | | | | Lower Bound | Upper Bound |
| 1 | 2 | -2.059[*] | .235 | .000 | -2.583 | -1.535 |
| | 3 | -1.882[*] | .328 | .000 | -2.613 | -1.151 |
| | 4 | .021 | .233 | .929 | -.499 | .542 |
| | 5 | .864[*] | .240 | .005 | .328 | 1.400 |
| | 6 | 1.254[*] | .238 | .000 | .723 | 1.786 |
| | 7 | 1.590[*] | .237 | .000 | 1.063 | 2.118 |
| | 8 | 2.279[*] | .237 | .000 | 1.751 | 2.808 |
| | 9 | 2.798[*] | .240 | .000 | 2.262 | 3.334 |
| | 10 | 2.959[*] | .241 | .000 | 2.421 | 3.497 |
| | 11 | 3.062[*] | .247 | .000 | 2.510 | 3.613 |
| 2 | 1 | 2.059[*] | .235 | .000 | 1.535 | 2.583 |
| | 3 | .177 | .264 | .519 | -.412 | .766 |
| | 4 | 2.080[*] | .265 | .000 | 1.490 | 2.670 |
| | 5 | 2.923[*] | .234 | .000 | 2.401 | 3.445 |
| | 6 | 3.313[*] | .251 | .000 | 2.755 | 3.871 |
| | 7 | 3.649[*] | .263 | .000 | 3.064 | 4.234 |
| | 8 | 4.338[*] | .243 | .000 | 3.796 | 4.880 |
| | 9 | 4.856[*] | .227 | .000 | 4.350 | 5.362 |
| | 10 | 5.018[*] | .237 | .000 | 4.489 | 5.547 |
| | 11 | 5.120[*] | .239 | .000 | 4.587 | 5.653 |
| 3 | 1 | 1.882[*] | .328 | .000 | 1.151 | 2.613 |
| | 2 | -.177 | .264 | .519 | -.766 | .412 |
| | 4 | 1.904[*] | .148 | .000 | 1.575 | 2.232 |
| | 5 | 2.746[*] | .128 | .000 | 2.462 | 3.031 |
| | 6 | 3.136[*] | .178 | .000 | 2.739 | 3.534 |
| | 7 | 3.473[*] | .165 | .000 | 3.104 | 3.841 |
| | 8 | 4.162[*] | .159 | .000 | 3.806 | 4.517 |
| | 9 | 4.680[*] | .158 | .000 | 4.327 | 5.032 |
| | 10 | 4.841[*] | .144 | .000 | 4.519 | 5.163 |
| | 11 | 4.944[*] | .127 | .000 | 4.660 | 5.227 |
| 4 | 1 | -.021 | .233 | .929 | -.542 | .499 |
| | 2 | -2.080[*] | .265 | .000 | -2.670 | -1.490 |

| | | | | | | |
|---|---|---|---|---|---|---|
| | 3 | -1.904* | .148 | .000 | -2.232 | -1.575 |
| | 5 | .843* | .102 | .000 | .615 | 1.071 |
| | 6 | 1.233* | .113 | .000 | .981 | 1.484 |
| | 7 | 1.569* | .079 | .000 | 1.393 | 1.745 |
| | 8 | 2.258* | .113 | .000 | 2.005 | 2.511 |
| | 9 | 2.776* | .100 | .000 | 2.554 | 2.998 |
| | 10 | 2.938* | .082 | .000 | 2.754 | 3.121 |
| | 11 | 3.040* | .081 | .000 | 2.861 | 3.219 |
| 5 | 1 | -.864* | .240 | .005 | -1.400 | -.328 |
| | 2 | -2.923* | .234 | .000 | -3.445 | -2.401 |
| | 3 | -2.746* | .128 | .000 | -3.031 | -2.462 |
| | 4 | -.843* | .102 | .000 | -1.071 | -.615 |
| | 6 | .390* | .102 | .003 | .163 | .617 |
| | 7 | .726* | .085 | .000 | .537 | .915 |
| | 8 | 1.415* | .076 | .000 | 1.246 | 1.585 |
| | 9 | 1.933* | .071 | .000 | 1.776 | 2.091 |
| | 10 | 2.095* | .068 | .000 | 1.943 | 2.247 |
| | 11 | 2.197* | .055 | .000 | 2.074 | 2.321 |
| 6 | 1 | -1.254* | .238 | .000 | -1.786 | -.723 |
| | 2 | -3.313* | .251 | .000 | -3.871 | -2.755 |
| | 3 | -3.136* | .178 | .000 | -3.534 | -2.739 |
| | 4 | -1.233* | .113 | .000 | -1.484 | -.981 |
| | 5 | -.390* | .102 | .003 | -.617 | -.163 |
| | 7 | .336* | .089 | .004 | .137 | .535 |
| | 8 | 1.025* | .064 | .000 | .882 | 1.168 |
| | 9 | 1.543* | .069 | .000 | 1.389 | 1.698 |
| | 10 | 1.705* | .071 | .000 | 1.547 | 1.862 |
| | 11 | 1.807* | .075 | .000 | 1.641 | 1.973 |
| 7 | 1 | -1.590* | .237 | .000 | -2.118 | -1.063 |
| | 2 | -3.649* | .263 | .000 | -4.234 | -3.064 |
| | 3 | -3.473* | .165 | .000 | -3.841 | -3.104 |
| | 4 | -1.569* | .079 | .000 | -1.745 | -1.393 |
| | 5 | -.726* | .085 | .000 | -.915 | -.537 |
| | 6 | -.336* | .089 | .004 | -.535 | -.137 |
| | 8 | .689* | .068 | .000 | .538 | .840 |
| | 9 | 1.207* | .067 | .000 | 1.058 | 1.356 |
| | 10 | 1.369* | .050 | .000 | 1.258 | 1.479 |
| | 11 | 1.471* | .058 | .000 | 1.343 | 1.599 |

| | | | | | | |
|---|---|---|---|---|---|---|
| 8 | 1 | -2.279* | .237 | .000 | -2.808 | -1.751 |
| | 2 | -4.338* | .243 | .000 | -4.880 | -3.796 |
| | 3 | -4.162* | .159 | .000 | -4.517 | -3.806 |
| | 4 | -2.258* | .113 | .000 | -2.511 | -2.005 |
| | 5 | -1.415* | .076 | .000 | -1.585 | -1.246 |
| | 6 | -1.025* | .064 | .000 | -1.168 | -.882 |
| | 7 | -.689* | .068 | .000 | -.840 | -.538 |
| | 9 | .518* | .064 | .000 | .376 | .660 |
| | 10 | .680* | .062 | .000 | .542 | .818 |
| | 11 | .782* | .057 | .000 | .655 | .909 |
| 9 | 1 | -2.798* | .240 | .000 | -3.334 | -2.262 |
| | 2 | -4.856* | .227 | .000 | -5.362 | -4.350 |
| | 3 | -4.680* | .158 | .000 | -5.032 | -4.327 |
| | 4 | -2.776* | .100 | .000 | -2.998 | -2.554 |
| | 5 | -1.933* | .071 | .000 | -2.091 | -1.776 |
| | 6 | -1.543* | .069 | .000 | -1.698 | -1.389 |
| | 7 | -1.207* | .067 | .000 | -1.356 | -1.058 |
| | 8 | -.518* | .064 | .000 | -.660 | -.376 |
| | 10 | .161* | .047 | .007 | .056 | .267 |
| | 11 | .264* | .053 | .001 | .145 | .383 |
| 10 | 1 | -2.959* | .241 | .000 | -3.497 | -2.421 |
| | 2 | -5.018* | .237 | .000 | -5.547 | -4.489 |
| | 3 | -4.841* | .144 | .000 | -5.163 | -4.519 |
| | 4 | -2.938* | .082 | .000 | -3.121 | -2.754 |
| | 5 | -2.095* | .068 | .000 | -2.247 | -1.943 |
| | 6 | -1.705* | .071 | .000 | -1.862 | -1.547 |
| | 7 | -1.369* | .050 | .000 | -1.479 | -1.258 |
| | 8 | -.680* | .062 | .000 | -.818 | -.542 |
| | 9 | -.161* | .047 | .007 | -.267 | -.056 |
| | 11 | .103* | .031 | .008 | .033 | .172 |
| 11 | 1 | -3.062* | .247 | .000 | -3.613 | -2.510 |
| | 2 | -5.120* | .239 | .000 | -5.653 | -4.587 |
| | 3 | -4.944* | .127 | .000 | -5.227 | -4.660 |
| | 4 | -3.040* | .081 | .000 | -3.219 | -2.861 |
| | 5 | -2.197* | .055 | .000 | -2.321 | -2.074 |
| | 6 | -1.807* | .075 | .000 | -1.973 | -1.641 |
| | 7 | -1.471* | .058 | .000 | -1.599 | -1.343 |

| | | | | | | |
|---|---|---|---|---|---|---|
| 8 | | -.782* | .057 | .000 | -.909 | -.655 |
| 9 | | -.264* | .053 | .001 | -.383 | -.145 |
| 10 | | -.103* | .031 | .008 | -.172 | -.033 |

Based on estimated marginal means

*. The mean difference is significant at the .05 level.

b. Adjustment for multiple comparisons: Least Significant Difference (equivalent to no adjustments).

## Readout 5:  Silicone sample-cadaver position 1 and 2 impulse data readout

### Within-Subjects Factors

Measure:  Impulse

| Impulse | Dependent Variable |
|---|---|
| 1 | CADP1 |
| 2 | CADP2 |
| 3 | S0 |
| 4 | S1 |
| 5 | S2 |
| 6 | S3 |
| 7 | S4 |
| 8 | S5 |
| 9 | S6 |
| 10 | S7 |
| 11 | S8 |

### Descriptive Statistics

| | Participant | Mean | Std. Deviation | N |
|---|---|---|---|---|
| CADP1 | A | 1.76467 | .480517 | 3 |
| | B | 4.31200 | 1.293123 | 3 |
| | C | 1.73360 | 1.428209 | 3 |
| | D | 4.15300 | 2.371815 | 3 |
| | E | 7.26300 | 2.344515 | 3 |
| | Total | 3.84525 | 2.570084 | 15 |
| CADP2 | A | 6.17300 | 2.373800 | 3 |
| | B | 4.44804 | .788818 | 3 |
| | C | 3.38933 | .818038 | 3 |
| | D | 3.21467 | 1.679038 | 3 |
| | E | 5.29377 | .685035 | 3 |
| | Total | 4.50376 | 1.677189 | 15 |

| | | | | |
|---|---|---|---|---|
| S0 | A | 3.84533 | 1.184037 | 3 |
| | B | 3.97100 | .625002 | 3 |
| | C | 3.10800 | .648174 | 3 |
| | D | 4.25900 | .726050 | 3 |
| | E | 4.48367 | .389757 | 3 |
| | Total | 3.93340 | .805397 | 15 |
| S1 | A | 3.41133 | .425245 | 3 |
| | B | 3.57800 | .851103 | 3 |
| | C | 2.73067 | .526690 | 3 |
| | D | 1.93133 | .213226 | 3 |
| | E | 1.94500 | .387248 | 3 |
| | Total | 2.71927 | .847963 | 15 |
| S2 | A | 2.19533 | .371130 | 3 |
| | B | 2.22267 | .675348 | 3 |
| | C | 1.54867 | .115902 | 3 |
| | D | 1.47000 | .391092 | 3 |
| | E | 1.47367 | .102295 | 3 |
| | Total | 1.78207 | .491138 | 15 |
| S3 | A | 2.10300 | .565922 | 3 |
| | B | 2.12400 | .400734 | 3 |
| | C | 1.26433 | .558536 | 3 |
| | D | 1.15267 | .737470 | 3 |
| | E | 1.40100 | .191384 | 3 |
| | Total | 1.60900 | .620213 | 15 |
| S4 | A | 2.03367 | .096028 | 3 |
| | B | 2.09033 | .213809 | 3 |
| | C | 1.11567 | .172402 | 3 |
| | D | 1.06333 | .246403 | 3 |
| | E | 1.37533 | .474156 | 3 |
| | Total | 1.53567 | .512904 | 15 |
| S5 | A | 1.41733 | .204745 | 3 |
| | B | 1.32167 | .285009 | 3 |
| | C | .73563 | .322935 | 3 |
| | D | .80130 | .121681 | 3 |
| | E | .83630 | .084561 | 3 |
| | Total | 1.02245 | .351796 | 15 |
| S6 | A | .55873 | .209955 | 3 |
| | B | .71213 | .128755 | 3 |

| | | | | |
|---|---|---|---|---|
| | C | .52833 | .195596 | 3 |
| | D | .45883 | .166583 | 3 |
| | E | .54607 | .179652 | 3 |
| | Total | .56082 | .173536 | 15 |
| S7 | A | .51697 | .092367 | 3 |
| | B | .58487 | .160019 | 3 |
| | C | .56820 | .134150 | 3 |
| | D | .62460 | .117137 | 3 |
| | E | .51440 | .087244 | 3 |
| | Total | .56181 | .111244 | 15 |
| S8 | A | .38457 | .067768 | 3 |
| | B | .19557 | .082780 | 3 |
| | C | .23940 | .049821 | 3 |
| | D | .62220 | .125181 | 3 |
| | E | .34923 | .113704 | 3 |
| | Total | .35819 | .172824 | 15 |

## Mauchly's Test of Sphericity[a]

Measure: Impulse

| Within Subjects Effect | Mauchly's W | Approx. Chi-Square | df | Sig. | Epsilon[b] | | |
|---|---|---|---|---|---|---|---|
| | | | | | Greenhouse-Geisser | Huynh-Feldt | Lower-bound |
| Impulse | .000 | 166.331 | 54 | .000 | .248 | .469 | .100 |

Tests the null hypothesis that the error covariance matrix of the orthonormalized transformed dependent variables is proportional to an identity matrix.

a. Design: Intercept + Participant

 Within Subjects Design: Impulse

b. May be used to adjust the degrees of freedom for the averaged tests of significance. Corrected tests are displayed in the Tests of Within-Subjects Effects table.

## Tests of Within-Subjects Effects

Measure: Impulse

| Source | | Type III Sum of Squares | df | Mean Square | F | Sig. | Partial Eta Squared | Noncent. Parameter | Observed Power[a] |
|---|---|---|---|---|---|---|---|---|---|
| Impulse | Sphericity Assumed | 331.785 | 10 | 33.178 | 55.902 | .000 | .848 | 559.023 | 1.000 |

| | | | | | | | | | |
|---|---|---|---|---|---|---|---|---|---|
| | Greenhouse-Geisser | 331.785 | 2.483 | 133.637 | 55.902 | .000 | .848 | 138.790 | 1.000 |
| | Huynh-Feldt | 331.785 | 4.688 | 70.773 | 55.902 | .000 | .848 | 262.069 | 1.000 |
| | Lower-bound | 331.785 | 1.000 | 331.785 | 55.902 | .000 | .848 | 55.902 | 1.000 |
| Impulse * Participant | Sphericity Assumed | 84.632 | 40 | 2.116 | 3.565 | .000 | .588 | 142.596 | 1.000 |
| | Greenhouse-Geisser | 84.632 | 9.931 | 8.522 | 3.565 | .005 | .588 | 35.403 | .957 |
| | Huynh-Feldt | 84.632 | 18.752 | 4.513 | 3.565 | .000 | .588 | 66.849 | .999 |
| | Lower-bound | 84.632 | 4.000 | 21.158 | 3.565 | .047 | .588 | 14.260 | .665 |
| Error(Impulse) | Sphericity Assumed | 59.351 | 100 | .594 | | | | | |
| | Greenhouse-Geisser | 59.351 | 24.827 | 2.391 | | | | | |
| | Huynh-Feldt | 59.351 | 46.880 | 1.266 | | | | | |
| | Lower-bound | 59.351 | 10.000 | 5.935 | | | | | |

a. Computed using alpha = .05

## Estimates

Measure: Impulse

| Impulse | Mean | Std. Error | 95% Confidence Interval | |
|---|---|---|---|---|
| | | | Lower Bound | Upper Bound |
| 1 | 3.845 | .448 | 2.847 | 4.844 |
| 2 | 4.504 | .369 | 3.681 | 5.326 |
| 3 | 3.933 | .196 | 3.496 | 4.371 |
| 4 | 2.719 | .136 | 2.417 | 3.021 |
| 5 | 1.782 | .101 | 1.556 | 2.008 |
| 6 | 1.609 | .135 | 1.307 | 1.911 |
| 7 | 1.536 | .070 | 1.379 | 1.692 |
| 8 | 1.022 | .058 | .894 | 1.151 |
| 9 | .561 | .046 | .458 | .663 |
| 10 | .562 | .031 | .492 | .632 |
| 11 | .358 | .024 | .305 | .411 |

**Pairwise Comparisons**

Measure: Impulse

| (I) Impulse | (J) Impulse | Mean Difference (I-J) | Std. Error | Sig.[b] | 95% Confidence Interval for Difference[b] Lower Bound | Upper Bound |
|---|---|---|---|---|---|---|
| 1 | 2 | -.659 | .440 | .166 | -1.640 | .323 |
| | 3 | -.088 | .489 | .860 | -1.177 | 1.000 |
| | 4 | 1.126 | .526 | .058 | -.046 | 2.298 |
| | 5 | 2.063* | .485 | .002 | .982 | 3.145 |
| | 6 | 2.236* | .449 | .001 | 1.237 | 3.236 |
| | 7 | 2.310* | .480 | .001 | 1.241 | 3.379 |
| | 8 | 2.823* | .447 | .000 | 1.826 | 3.819 |
| | 9 | 3.284* | .464 | .000 | 2.251 | 4.318 |
| | 10 | 3.283* | .438 | .000 | 2.308 | 4.259 |
| | 11 | 3.487* | .434 | .000 | 2.520 | 4.454 |
| 2 | 1 | .659 | .440 | .166 | -.323 | 1.640 |
| | 3 | .570 | .462 | .245 | -.459 | 1.600 |
| | 4 | 1.784* | .433 | .002 | .820 | 2.749 |
| | 5 | 2.722* | .422 | .000 | 1.781 | 3.662 |
| | 6 | 2.895* | .412 | .000 | 1.976 | 3.813 |
| | 7 | 2.968* | .349 | .000 | 2.191 | 3.745 |
| | 8 | 3.481* | .370 | .000 | 2.656 | 4.306 |
| | 9 | 3.943* | .372 | .000 | 3.113 | 4.773 |
| | 10 | 3.942* | .373 | .000 | 3.110 | 4.773 |
| | 11 | 4.146* | .354 | .000 | 3.358 | 4.933 |
| 3 | 1 | .088 | .489 | .860 | -1.000 | 1.177 |
| | 2 | -.570 | .462 | .245 | -1.600 | .459 |
| | 4 | 1.214* | .236 | .000 | .689 | 1.740 |
| | 5 | 2.151* | .234 | .000 | 1.631 | 2.672 |
| | 6 | 2.324* | .255 | .000 | 1.756 | 2.892 |
| | 7 | 2.398* | .211 | .000 | 1.927 | 2.868 |
| | 8 | 2.911* | .246 | .000 | 2.364 | 3.458 |
| | 9 | 3.373* | .168 | .000 | 2.997 | 3.748 |
| | 10 | 3.372* | .190 | .000 | 2.948 | 3.795 |
| | 11 | 3.575* | .197 | .000 | 3.137 | 4.014 |
| 4 | 1 | -1.126 | .526 | .058 | -2.298 | .046 |
| | 2 | -1.784* | .433 | .002 | -2.749 | -.820 |

175

| | | | | | | |
|---|---|---|---|---|---|---|
| | 3 | -1.214* | .236 | .000 | -1.740 | -.689 |
| | 5 | .937* | .105 | .000 | .704 | 1.171 |
| | 6 | 1.110* | .201 | .000 | .661 | 1.559 |
| | 7 | 1.184* | .145 | .000 | .862 | 1.506 |
| | 8 | 1.697* | .163 | .000 | 1.333 | 2.061 |
| | 9 | 2.158* | .130 | .000 | 1.869 | 2.448 |
| | 10 | 2.157* | .140 | .000 | 1.845 | 2.470 |
| | 11 | 2.361* | .148 | .000 | 2.032 | 2.690 |
| 5 | 1 | -2.063* | .485 | .002 | -3.145 | -.982 |
| | 2 | -2.722* | .422 | .000 | -3.662 | -1.781 |
| | 3 | -2.151* | .234 | .000 | -2.672 | -1.631 |
| | 4 | -.937* | .105 | .000 | -1.171 | -.704 |
| | 6 | .173 | .145 | .260 | -.150 | .496 |
| | 7 | .246* | .104 | .039 | .014 | .478 |
| | 8 | .760* | .117 | .000 | .500 | 1.019 |
| | 9 | 1.221* | .105 | .000 | .988 | 1.454 |
| | 10 | 1.220* | .103 | .000 | .991 | 1.450 |
| | 11 | 1.424* | .112 | .000 | 1.174 | 1.674 |
| 6 | 1 | -2.236* | .449 | .001 | -3.236 | -1.237 |
| | 2 | -2.895* | .412 | .000 | -3.813 | -1.976 |
| | 3 | -2.324* | .255 | .000 | -2.892 | -1.756 |
| | 4 | -1.110* | .201 | .000 | -1.559 | -.661 |
| | 5 | -.173 | .145 | .260 | -.496 | .150 |
| | 7 | .073 | .160 | .657 | -.284 | .430 |
| | 8 | .587* | .135 | .001 | .285 | .888 |
| | 9 | 1.048* | .152 | .000 | .709 | 1.387 |
| | 10 | 1.047* | .117 | .000 | .786 | 1.309 |
| | 11 | 1.251* | .134 | .000 | .951 | 1.550 |
| 7 | 1 | -2.310* | .480 | .001 | -3.379 | -1.241 |
| | 2 | -2.968* | .349 | .000 | -3.745 | -2.191 |
| | 3 | -2.398* | .211 | .000 | -2.868 | -1.927 |
| | 4 | -1.184* | .145 | .000 | -1.506 | -.862 |
| | 5 | -.246* | .104 | .039 | -.478 | -.014 |
| | 6 | -.073 | .160 | .657 | -.430 | .284 |
| | 8 | .513* | .095 | .000 | .301 | .726 |
| | 9 | .975* | .063 | .000 | .835 | 1.114 |
| | 10 | .974* | .084 | .000 | .787 | 1.160 |
| | 11 | 1.177* | .072 | .000 | 1.017 | 1.338 |

| | | | | | | |
|---|---|---|---|---|---|---|
| 8 | 1 | -2.823* | .447 | .000 | -3.819 | -1.826 |
| | 2 | -3.481* | .370 | .000 | -4.306 | -2.656 |
| | 3 | -2.911* | .246 | .000 | -3.458 | -2.364 |
| | 4 | -1.697* | .163 | .000 | -2.061 | -1.333 |
| | 5 | -.760* | .117 | .000 | -1.019 | -.500 |
| | 6 | -.587* | .135 | .001 | -.888 | -.285 |
| | 7 | -.513* | .095 | .000 | -.726 | -.301 |
| | 9 | .462* | .094 | .001 | .253 | .670 |
| | 10 | .461* | .072 | .000 | .301 | .621 |
| | 11 | .664* | .066 | .000 | .516 | .812 |
| 9 | 1 | -3.284* | .464 | .000 | -4.318 | -2.251 |
| | 2 | -3.943* | .372 | .000 | -4.773 | -3.113 |
| | 3 | -3.373* | .168 | .000 | -3.748 | -2.997 |
| | 4 | -2.158* | .130 | .000 | -2.448 | -1.869 |
| | 5 | -1.221* | .105 | .000 | -1.454 | -.988 |
| | 6 | -1.048* | .152 | .000 | -1.387 | -.709 |
| | 7 | -.975* | .063 | .000 | -1.114 | -.835 |
| | 8 | -.462* | .094 | .001 | -.670 | -.253 |
| | 10 | -.001 | .056 | .986 | -.126 | .124 |
| | 11 | .203* | .053 | .004 | .083 | .322 |
| 10 | 1 | -3.283* | .438 | .000 | -4.259 | -2.308 |
| | 2 | -3.942* | .373 | .000 | -4.773 | -3.110 |
| | 3 | -3.372* | .190 | .000 | -3.795 | -2.948 |
| | 4 | -2.157* | .140 | .000 | -2.470 | -1.845 |
| | 5 | -1.220* | .103 | .000 | -1.450 | -.991 |
| | 6 | -1.047* | .117 | .000 | -1.309 | -.786 |
| | 7 | -.974* | .084 | .000 | -1.160 | -.787 |
| | 8 | -.461* | .072 | .000 | -.621 | -.301 |
| | 9 | .001 | .056 | .986 | -.124 | .126 |
| | 11 | .204* | .036 | .000 | .123 | .284 |
| 11 | 1 | -3.487* | .434 | .000 | -4.454 | -2.520 |
| | 2 | -4.146* | .354 | .000 | -4.933 | -3.358 |
| | 3 | -3.575* | .197 | .000 | -4.014 | -3.137 |
| | 4 | -2.361* | .148 | .000 | -2.690 | -2.032 |
| | 5 | -1.424* | .112 | .000 | -1.674 | -1.174 |
| | 6 | -1.251* | .134 | .000 | -1.550 | -.951 |
| | 7 | -1.177* | .072 | .000 | -1.338 | -1.017 |

| | | | | | |
|---|---|---|---|---|---|
| 8 | -.664[*] | .066 | .000 | -.812 | -.516 |
| 9 | -.203[*] | .053 | .004 | -.322 | -.083 |
| 10 | -.204[*] | .036 | .000 | -.284 | -.123 |

Based on estimated marginal means*. The mean difference is significant at the .05 level.

## Readout 6: Silicone sample-cadaver position 1 and 2 ulse width data readout

### Within-Subjects Factors

Measure: Pulse width

| PulseWidth | Dependent Variable |
|---|---|
| 1 | CADP1 |
| 2 | CADP2 |
| 3 | S0 |
| 4 | S1 |
| 5 | S2 |
| 6 | S3 |
| 7 | S4 |
| 8 | S5 |
| 9 | S6 |
| 10 | S7 |
| 11 | S8 |

### Descriptive Statistics

| | Participant | Mean | Std. Deviation | N |
|---|---|---|---|---|
| CADP1 | A | .45667 | .247857 | 3 |
| | B | 1.02667 | .433167 | 3 |
| | C | .41333 | .155027 | 3 |
| | D | .63667 | .463069 | 3 |
| | E | .87000 | .065574 | 3 |
| | Total | .68067 | .360663 | 15 |
| CADP2 | A | .52667 | .205994 | 3 |
| | B | .49333 | .270986 | 3 |
| | C | .37000 | .104403 | 3 |
| | D | .49667 | .321921 | 3 |
| | E | .37000 | .157162 | 3 |

|    |       |         |          |    |
|----|-------|---------|----------|----|
|    | Total | .45133  | .203254  | 15 |
| S0 | A     | .47867  | .046608  | 3  |
|    | B     | .64167  | .065987  | 3  |
|    | C     | .56100  | .108365  | 3  |
|    | D     | .71267  | .048758  | 3  |
|    | E     | .72767  | .135596  | 3  |
|    | Total | .62433  | .122503  | 15 |
| S1 | A     | .84233  | .099551  | 3  |
|    | B     | .85667  | .190663  | 3  |
|    | C     | .72433  | .189505  | 3  |
|    | D     | .51367  | .096443  | 3  |
|    | E     | .49633  | .113298  | 3  |
|    | Total | .68667  | .201910  | 15 |
| S2 | A     | .89367  | .126982  | 3  |
|    | B     | .78533  | .126429  | 3  |
|    | C     | .48567  | .105860  | 3  |
|    | D     | .42533  | .083393  | 3  |
|    | E     | .47833  | .078590  | 3  |
|    | Total | .61367  | .214976  | 15 |
| S3 | A     | .75500  | .146072  | 3  |
|    | B     | .72600  | .082274  | 3  |
|    | C     | .40500  | .069549  | 3  |
|    | D     | .50800  | .154049  | 3  |
|    | E     | .46767  | .042218  | 3  |
|    | Total | .57233  | .172614  | 15 |
| S4 | A     | .69333  | .038527  | 3  |
|    | B     | .78500  | .141163  | 3  |
|    | C     | .48400  | .036510  | 3  |
|    | D     | .46900  | .043000  | 3  |
|    | E     | .61833  | .278110  | 3  |
|    | Total | .60993  | .174041  | 15 |
| S5 | A     | .67433  | .015535  | 3  |
|    | B     | .66600  | .093787  | 3  |
|    | C     | .44533  | .088370  | 3  |
|    | D     | .48400  | .074303  | 3  |
|    | E     | .48300  | .102781  | 3  |
|    | Total | .55053  | .123057  | 15 |
| S6 | A     | .29867  | .049116  | 3  |

|  | B | .48367 | .100311 | 3 |
|  | C | .37533 | .073874 | 3 |
|  | D | .36333 | .024007 | 3 |
|  | E | .44700 | .044034 | 3 |
|  | Total | .39360 | .086426 | 15 |
| S7 | A | .36667 | .158954 | 3 |
|  | B | .49200 | .100464 | 3 |
|  | C | .43800 | .081357 | 3 |
|  | D | .53900 | .101356 | 3 |
|  | E | .51133 | .069816 | 3 |
|  | Total | .46940 | .110263 | 15 |
| S8 | A | .37500 | .018735 | 3 |
|  | B | .27333 | .016258 | 3 |
|  | C | .36633 | .022189 | 3 |
|  | D | .60633 | .171343 | 3 |
|  | E | .27200 | .127295 | 3 |
|  | Total | .37860 | .150416 | 15 |

## Mauchly's Test of Sphericity[a]

Measure: Pulse width

| Within Subjects Effect | Mauchly's W | Approx. Chi-Square | df | Sig. | Greenhouse-Geisser | Epsilon[b] Huynh-Feldt | Lower-bound |
|---|---|---|---|---|---|---|---|
| PulseWidth | .000 | 120.735 | 54 | .000 | .342 | .748 | .100 |

Tests the null hypothesis that the error covariance matrix of the orthonormalized transformed dependent variables is proportional to an identity matrix.

a. Design: Intercept + Participant

 Within Subjects Design: PulseWidth

b. May be used to adjust the degrees of freedom for the averaged tests of significance. Corrected tests are displayed in the Tests of Within-Subjects Effects table.

## Tests of Within-Subjects Effects

Measure: Pulse width

| Source | | Type III Sum of Squares | df | Mean Square | F | Sig. | Partial Eta Squared | Noncent. Parameter | Observed Power[a] |
|---|---|---|---|---|---|---|---|---|---|
| PulseWidth | Sphericity Assumed | 1.792 | 10 | .179 | 8.527 | .000 | .460 | 85.269 | 1.000 |
| | Greenhouse-Geisser | 1.792 | 3.417 | .524 | 8.527 | .000 | .460 | 29.136 | .993 |
| | Huynh-Feldt | 1.792 | 7.482 | .239 | 8.527 | .000 | .460 | 63.797 | 1.000 |
| | Lower-bound | 1.792 | 1.000 | 1.792 | 8.527 | .015 | .460 | 8.527 | .749 |
| PulseWidth * Participant | Sphericity Assumed | 2.226 | 40 | .056 | 2.648 | .000 | .514 | 105.903 | 1.000 |
| | Greenhouse-Geisser | 2.226 | 13.668 | .163 | 2.648 | .011 | .514 | 36.186 | .946 |
| | Huynh-Feldt | 2.226 | 29.927 | .074 | 2.648 | .000 | .514 | 79.235 | .999 |
| | Lower-bound | 2.226 | 4.000 | .556 | 2.648 | .097 | .514 | 10.590 | .523 |
| Error(PulseWidth) | Sphericity Assumed | 2.101 | 100 | .021 | | | | | |
| | Greenhouse-Geisser | 2.101 | 34.169 | .062 | | | | | |
| | Huynh-Feldt | 2.101 | 74.819 | .028 | | | | | |
| | Lower-bound | 2.101 | 10.000 | .210 | | | | | |

a. Computed using alpha = .05

## Estimates

Measure: Pulse width

| PulseWidth | Mean | Std. Error | 95% Confidence Interval | |
|---|---|---|---|---|
| | | | Lower Bound | Upper Bound |
| 1 | .681 | .081 | .500 | .861 |
| 2 | .451 | .058 | .321 | .581 |
| 3 | .624 | .023 | .574 | .675 |
| 4 | .687 | .037 | .604 | .770 |
| 5 | .614 | .027 | .553 | .675 |
| 6 | .572 | .028 | .510 | .635 |
| 7 | .610 | .037 | .528 | .692 |
| 8 | .551 | .021 | .504 | .597 |

| | | | | |
|---|---|---|---|---|
| 9 | .394 | .017 | .357 | .430 |
| 10 | .469 | .028 | .408 | .531 |
| 11 | .379 | .025 | .323 | .434 |

## Pairwise Comparisons

Measure: Pulse width

| (I) PulseWidth | (J) PulseWidth | Mean Difference (I-J) | Std. Error | Sig.[b] | 95% Confidence Interval for Difference[b] Lower Bound | Upper Bound |
|---|---|---|---|---|---|---|
| 1 | 2 | .229* | .066 | .006 | .082 | .376 |
|   | 3 | .056 | .086 | .529 | -.136 | .249 |
|   | 4 | -.006 | .090 | .948 | -.206 | .194 |
|   | 5 | .067 | .093 | .490 | -.141 | .275 |
|   | 6 | .108 | .083 | .221 | -.077 | .293 |
|   | 7 | .071 | .076 | .373 | -.098 | .240 |
|   | 8 | .130 | .080 | .136 | -.049 | .309 |
|   | 9 | .287* | .091 | .010 | .084 | .490 |
|   | 10 | .211* | .078 | .022 | .037 | .385 |
|   | 11 | .302* | .072 | .002 | .141 | .463 |
| 2 | 1 | -.229* | .066 | .006 | -.376 | -.082 |
|   | 3 | -.173* | .063 | .020 | -.313 | -.033 |
|   | 4 | -.235* | .063 | .004 | -.375 | -.096 |
|   | 5 | -.162* | .069 | .041 | -.317 | -.008 |
|   | 6 | -.121 | .058 | .062 | -.250 | .008 |
|   | 7 | -.159* | .049 | .009 | -.269 | -.048 |
|   | 8 | -.099 | .058 | .117 | -.228 | .030 |
|   | 9 | .058 | .059 | .353 | -.074 | .190 |
|   | 10 | -.018 | .055 | .749 | -.140 | .104 |
|   | 11 | .073 | .056 | .227 | -.053 | .199 |
| 3 | 1 | -.056 | .086 | .529 | -.249 | .136 |
|   | 2 | .173* | .063 | .020 | .033 | .313 |
|   | 4 | -.062 | .039 | .138 | -.148 | .024 |
|   | 5 | .011 | .043 | .807 | -.084 | .105 |
|   | 6 | .052 | .039 | .212 | -.035 | .139 |
|   | 7 | .014 | .047 | .766 | -.090 | .119 |
|   | 8 | .074 | .039 | .087 | -.013 | .161 |
|   | 9 | .231* | .028 | .000 | .169 | .293 |

| | | | | | | |
|---|---|---|---|---|---|---|
| | 10 | .155* | .034 | .001 | .080 | .230 |
| | 11 | .246* | .037 | .000 | .164 | .327 |
| 4 | 1 | .006 | .090 | .948 | -.194 | .206 |
| | 2 | .235* | .063 | .004 | .096 | .375 |
| | 3 | .062 | .039 | .138 | -.024 | .148 |
| | 5 | .073 | .041 | .102 | -.017 | .163 |
| | 6 | .114* | .049 | .040 | .006 | .223 |
| | 7 | .077 | .053 | .180 | -.042 | .195 |
| | 8 | .136* | .042 | .009 | .042 | .230 |
| | 9 | .293* | .044 | .000 | .196 | .391 |
| | 10 | .217* | .046 | .001 | .114 | .321 |
| | 11 | .308* | .046 | .000 | .206 | .410 |
| 5 | 1 | -.067 | .093 | .490 | -.275 | .141 |
| | 2 | .162* | .069 | .041 | .008 | .317 |
| | 3 | -.011 | .043 | .807 | -.105 | .084 |
| | 4 | -.073 | .041 | .102 | -.163 | .017 |
| | 6 | .041 | .043 | .357 | -.054 | .137 |
| | 7 | .004 | .045 | .936 | -.097 | .104 |
| | 8 | .063 | .031 | .066 | -.005 | .131 |
| | 9 | .220* | .031 | .000 | .152 | .289 |
| | 10 | .144* | .046 | .011 | .041 | .248 |
| | 11 | .235* | .036 | .000 | .156 | .315 |
| 6 | 1 | -.108 | .083 | .221 | -.293 | .077 |
| | 2 | .121 | .058 | .062 | -.008 | .250 |
| | 3 | -.052 | .039 | .212 | -.139 | .035 |
| | 4 | -.114* | .049 | .040 | -.223 | -.006 |
| | 5 | -.041 | .043 | .357 | -.137 | .054 |
| | 7 | -.038 | .047 | .440 | -.142 | .067 |
| | 8 | .022 | .031 | .491 | -.046 | .090 |
| | 9 | .179* | .035 | .000 | .101 | .256 |
| | 10 | .103* | .016 | .000 | .067 | .138 |
| | 11 | .194* | .029 | .000 | .129 | .259 |
| 7 | 1 | -.071 | .076 | .373 | -.240 | .098 |
| | 2 | .159* | .049 | .009 | .048 | .269 |
| | 3 | -.014 | .047 | .766 | -.119 | .090 |
| | 4 | -.077 | .053 | .180 | -.195 | .042 |
| | 5 | -.004 | .045 | .936 | -.104 | .097 |
| | 6 | .038 | .047 | .440 | -.067 | .142 |

| | | | | | | |
|---|---|---|---|---|---|---|
| | 8 | .059 | .029 | .064 | -.004 | .123 |
| | 9 | .216* | .041 | .000 | .125 | .308 |
| | 10 | .141* | .050 | .018 | .029 | .252 |
| | 11 | .231* | .051 | .001 | .118 | .345 |
| 8 | 1 | -.130 | .080 | .136 | -.309 | .049 |
| | 2 | .099 | .058 | .117 | -.030 | .228 |
| | 3 | -.074 | .039 | .087 | -.161 | .013 |
| | 4 | -.136* | .042 | .009 | -.230 | -.042 |
| | 5 | -.063 | .031 | .066 | -.131 | .005 |
| | 6 | -.022 | .031 | .491 | -.090 | .046 |
| | 7 | -.059 | .029 | .064 | -.123 | .004 |
| | 9 | .157* | .030 | .000 | .089 | .225 |
| | 10 | .081* | .036 | .046 | .002 | .161 |
| | 11 | .172* | .037 | .001 | .090 | .254 |
| 9 | 1 | -.287* | .091 | .010 | -.490 | -.084 |
| | 2 | -.058 | .059 | .353 | -.190 | .074 |
| | 3 | -.231* | .028 | .000 | -.293 | -.169 |
| | 4 | -.293* | .044 | .000 | -.391 | -.196 |
| | 5 | -.220* | .031 | .000 | -.289 | -.152 |
| | 6 | -.179* | .035 | .000 | -.256 | -.101 |
| | 7 | -.216* | .041 | .000 | -.308 | -.125 |
| | 8 | -.157* | .030 | .000 | -.225 | -.089 |
| | 10 | -.076 | .036 | .061 | -.156 | .004 |
| | 11 | .015 | .032 | .649 | -.056 | .086 |
| 10 | 1 | -.211* | .078 | .022 | -.385 | -.037 |
| | 2 | .018 | .055 | .749 | -.104 | .140 |
| | 3 | -.155* | .034 | .001 | -.230 | -.080 |
| | 4 | -.217* | .046 | .001 | -.321 | -.114 |
| | 5 | -.144* | .046 | .011 | -.248 | -.041 |
| | 6 | -.103* | .016 | .000 | -.138 | -.067 |
| | 7 | -.141* | .050 | .018 | -.252 | -.029 |
| | 8 | -.081* | .036 | .046 | -.161 | -.002 |
| | 9 | .076 | .036 | .061 | -.004 | .156 |
| | 11 | .091* | .028 | .009 | .028 | .154 |
| 11 | 1 | -.302* | .072 | .002 | -.463 | -.141 |
| | 2 | -.073 | .056 | .227 | -.199 | .053 |
| | 3 | -.246* | .037 | .000 | -.327 | -.164 |

| | | | | | | |
|---|---|---|---|---|---|---|
| 4 | -.308* | .046 | .000 | -.410 | -.206 |
| 5 | -.235* | .036 | .000 | -.315 | -.156 |
| 6 | -.194* | .029 | .000 | -.259 | -.129 |
| 7 | -.231* | .051 | .001 | -.345 | -.118 |
| 8 | -.172* | .037 | .001 | -.254 | -.090 |
| 9 | -.015 | .032 | .649 | -.086 | .056 |
| 10 | -.091* | .028 | .009 | -.154 | -.028 |

Based on estimated marginal means

*. The mean difference is significant at the .05 level.

b. Adjustment for multiple comparisons: Least Significant Difference (equivalent to no adjustments).

# Appendix D: SPSS Silicone Tissue-THM-30-Cadaver Data Readouts

## Readout 7: SPSS silicone-cadaver peak force data readout

### Within-Subjects Factors

Measure: Peak force

| PeakForce | Dependent Variable |
|-----------|--------------------|
| 1 | Silicone |
| 2 | Cadaver |
| 3 | THM30 |

### Descriptive Statistics

| | Participant | Mean | Std. Deviation | N |
|---|---|---|---|---|
| Silicone | 1.00 | 7.8753 | .26603 | 3 |
| | 2.00 | 6.9040 | 1.05607 | 3 |
| | 3.00 | 6.6693 | .30986 | 3 |
| | 4.00 | 7.3403 | 1.05816 | 3 |
| | 5.00 | 6.3923 | .66139 | 3 |
| | Total | 7.0363 | .83530 | 15 |
| Cadaver | 1.00 | 3.0567 | 2.57617 | 3 |
| | 2.00 | 4.1800 | 1.95000 | 3 |
| | 3.00 | 7.1833 | 2.18873 | 3 |
| | 4.00 | 10.4767 | 1.44535 | 3 |
| | 5.00 | 10.3000 | 1.84746 | 3 |
| | Total | 7.0393 | 3.59543 | 15 |
| THM30 | 1.00 | 5.0430 | .16379 | 3 |
| | 2.00 | 5.1933 | .11120 | 3 |
| | 3.00 | 4.9770 | .20824 | 3 |
| | 4.00 | 4.9483 | .28869 | 3 |
| | 5.00 | 4.9747 | .20900 | 3 |
| | Total | 5.0273 | .19589 | 15 |

## Mauchly's Test of Sphericity[a]

Measure: Peak force

| Within Subjects Effect | Mauchly's W | Approx. Chi-Square | df | Sig. | Epsilon[b] | | |
|---|---|---|---|---|---|---|---|
| | | | | | Greenhouse-Geisser | Huynh-Feldt | Lower-bound |
| PeakForce | .194 | 14.774 | 2 | .001 | .554 | .821 | .500 |

Tests the null hypothesis that the error covariance matrix of the orthonormalized transformed dependent variables is proportional to an identity matrix.

a. Design: Intercept + Participant

 Within Subjects Design: PeakForce

b. May be used to adjust the degrees of freedom for the averaged tests of significance. Corrected tests are displayed in the Tests of Within-Subjects Effects table.

## Tests of Within-Subjects Effects

Measure: Peak force

| Source | | Type III Sum of Squares | df | Mean Square | F | Sig. | Partial Eta Squared | Noncent. Parameter | Observed Power[a] |
|---|---|---|---|---|---|---|---|---|---|
| PeakForce | Sphericity Assumed | 40.423 | 2 | 20.211 | 10.651 | .001 | .516 | 21.301 | .976 |
| | Greenhouse-Geisser | 40.423 | 1.107 | 36.508 | 10.651 | .007 | .516 | 11.792 | .865 |
| | Huynh-Feldt | 40.423 | 1.643 | 24.607 | 10.651 | .002 | .516 | 17.496 | .951 |
| | Lower-bound | 40.423 | 1.000 | 40.423 | 10.651 | .009 | .516 | 10.651 | .836 |
| PeakForce * Participant | Sphericity Assumed | 105.894 | 8 | 13.237 | 6.975 | .000 | .736 | 55.802 | .998 |
| | Greenhouse-Geisser | 105.894 | 4.429 | 23.910 | 6.975 | .004 | .736 | 30.892 | .954 |
| | Huynh-Feldt | 105.894 | 6.571 | 16.116 | 6.975 | .001 | .736 | 45.833 | .994 |
| | Lower-bound | 105.894 | 4.000 | 26.473 | 6.975 | .006 | .736 | 27.901 | .933 |
| Error(PeakForce) | Sphericity Assumed | 37.954 | 20 | 1.898 | | | | | |

| | | 37.954 | 11.072 | 3.428 | | | | |
|---|---|---|---|---|---|---|---|---|
| | Greenhouse-Geisser | 37.954 | 11.072 | 3.428 | | | | |
| | Huynh-Feldt | 37.954 | 16.427 | 2.310 | | | | |
| | Lower-bound | 37.954 | 10.000 | 3.795 | | | | |

a. Computed using alpha = .05

## Estimates

Measure: Peak force

| | | | 95% Confidence Interval | |
|---|---|---|---|---|
| PeakForce | Mean | Std. Error | Lower Bound | Upper Bound |
| 1 | 7.036 | .195 | 6.603 | 7.470 |
| 2 | 7.039 | .526 | 5.868 | 8.211 |
| 3 | 5.027 | .053 | 4.909 | 5.145 |

## Pairwise Comparisons

Measure: Peak force

| (I) PeakForce | (J) PeakForce | Mean Difference (I-J) | Std. Error | Sig.[b] | 95% Confidence Interval for Difference[b] | |
|---|---|---|---|---|---|---|
| | | | | | Lower Bound | Upper Bound |
| 1 | 2 | -.003 | .658 | .996 | -1.470 | 1.464 |
| | 3 | 2.009* | .208 | .000 | 1.546 | 2.472 |
| 2 | 1 | .003 | .658 | .996 | -1.464 | 1.470 |
| | 3 | 2.012* | .532 | .004 | .828 | 3.197 |
| 3 | 1 | -2.009* | .208 | .000 | -2.472 | -1.546 |
| | 2 | -2.012* | .532 | .004 | -3.197 | -.828 |

Based on estimated marginal means

*. The mean difference is significant at the .05 level.

b. Adjustment for multiple comparisons: Least Significant Difference (equivalent to no adjustments).

### Readout 8: Silicone tissue-THM-30-cadaver impulse data readout

## Within-Subjects Factors

Measure: Impulse

| Impulse | Dependent Variable |
|---|---|
| 1 | Silicone |
| 2 | Cadaver |
| 3 | THM30 |

## Descriptive Statistics

| | Participant | Mean | Std. Deviation | N |
|---|---|---|---|---|
| Silicone | 1.00 | 6.2270 | .34700 | 3 |
| | 2.00 | 5.6637 | .59600 | 3 |
| | 3.00 | 5.2963 | .39464 | 3 |
| | 4.00 | 4.7983 | 1.15109 | 3 |
| | 5.00 | 4.4810 | .70189 | 3 |
| | Total | 5.2933 | .87176 | 15 |
| Cadaver | 1.00 | 2.7767 | 2.72720 | 3 |
| | 2.00 | 4.3900 | 3.25000 | 3 |
| | 3.00 | 3.5967 | 2.26780 | 3 |
| | 4.00 | 7.3067 | 1.44863 | 3 |
| | 5.00 | 8.4400 | 1.85857 | 3 |
| | Total | 5.3020 | 3.03951 | 15 |
| THM30 | 1.00 | 4.4340 | .06528 | 3 |
| | 2.00 | 4.5030 | .43898 | 3 |
| | 3.00 | 3.6103 | .28431 | 3 |
| | 4.00 | 4.2463 | .37931 | 3 |
| | 5.00 | 4.3263 | .29471 | 3 |
| | Total | 4.2240 | .42641 | 15 |

## Mauchly's Test of Sphericity[a]

Measure:   Impulse

| Within Subjects Effect | Mauchly's W | Approx. Chi-Square | df | Sig. | Greenhouse-Geisser | Huynh-Feldt | Lower-bound |
|---|---|---|---|---|---|---|---|
| | | | | | | Epsilon[b] | |
| Impulse | .319 | 10.273 | 2 | .006 | .595 | .900 | .500 |

Tests the null hypothesis that the error covariance matrix of the orthonormalized transformed dependent variables is proportional to an identity matrix.

a. Design: Intercept + Participant
 Within Subjects Design: Impulse

b. May be used to adjust the degrees of freedom for the averaged tests of significance. Corrected tests are displayed in the Tests of Within-Subjects Effects table.

## Tests of Within-Subjects Effects

Measure: Impulse

| Source | | Type III Sum of Squares | df | Mean Square | F | Sig. | Partial Eta Squared | Noncent. Parameter | Observed Power[a] |
|---|---|---|---|---|---|---|---|---|---|
| Impulse | Sphericity Assumed | 11.527 | 2 | 5.764 | 2.586 | .100 | .205 | 5.171 | .456 |
| | Greenhouse-Geisser | 11.527 | 1.190 | 9.687 | 2.586 | .131 | .205 | 3.077 | .338 |
| | Huynh-Feldt | 11.527 | 1.799 | 6.407 | 2.586 | .107 | .205 | 4.652 | .428 |
| | Lower-bound | 11.527 | 1.000 | 11.527 | 2.586 | .139 | .205 | 2.586 | .307 |
| Impulse * Participant | Sphericity Assumed | 63.635 | 8 | 7.954 | 3.568 | .010 | .588 | 28.547 | .913 |
| | Greenhouse-Geisser | 63.635 | 4.760 | 13.368 | 3.568 | .034 | .588 | 16.986 | .737 |
| | Huynh-Feldt | 63.635 | 7.197 | 8.842 | 3.568 | .013 | .588 | 25.680 | .884 |
| | Lower-bound | 63.635 | 4.000 | 15.909 | 3.568 | .047 | .588 | 14.274 | .665 |
| Error(Impulse) | Sphericity Assumed | 44.582 | 20 | 2.229 | | | | | |
| | Greenhouse-Geisser | 44.582 | 11.900 | 3.746 | | | | | |
| | Huynh-Feldt | 44.582 | 17.991 | 2.478 | | | | | |
| | Lower-bound | 44.582 | 10.000 | 4.458 | | | | | |

a. Computed using alpha = .05

## Estimates

Measure: Impulse

| Impulse | Mean | Std. Error | 95% Confidence Interval | |
|---|---|---|---|---|
| | | | Lower Bound | Upper Bound |
| 1 | 5.293 | .181 | 4.891 | 5.696 |
| 2 | 5.302 | .619 | 3.924 | 6.680 |
| 3 | 4.224 | .082 | 4.041 | 4.407 |

## Pairwise Comparisons

Measure: Impulse

| (I) Impulse | (J) Impulse | Mean Difference (I-J) | Std. Error | Sig.b | 95% Confidence Interval for Differenceb Lower Bound | Upper Bound |
|---|---|---|---|---|---|---|
| 1 | 2 | -.009 | .669 | .990 | -1.500 | 1.483 |
|   | 3 | 1.069* | .233 | .001 | .550 | 1.589 |
| 2 | 1 | .009 | .669 | .990 | -1.483 | 1.500 |
|   | 3 | 1.078 | .624 | .115 | -.312 | 2.468 |
| 3 | 1 | -1.069* | .233 | .001 | -1.589 | -.550 |
|   | 2 | -1.078 | .624 | .115 | -2.468 | .312 |

Based on estimated marginal means

*. The mean difference is significant at the .05 level.

b. Adjustment for multiple comparisons: Least Significant Difference (equivalent to no adjustments).

## Readout 9: Silicone tissue-THM-30-cadaver pulse width data readout

## Within-Subjects Factors

Measure: Pulse width

| PulseWidth | Dependent Variable |
|---|---|
| 1 | Silicone |
| 2 | Cadaver |
| 3 | THM30 |

## Descriptive Statistics

|  | Participant | Mean | Std. Deviation | N |
|---|---|---|---|---|
| Silicone | 1.00 | .6553 | .02344 | 3 |
|  | 2.00 | .6227 | .15451 | 3 |
|  | 3.00 | .7277 | .08833 | 3 |
|  | 4.00 | .5667 | .06783 | 3 |
|  | 5.00 | .6850 | .06351 | 3 |
|  | Total | .6515 | .09510 | 15 |
| Cadaver | 1.00 | .5500 | .18028 | 3 |
|  | 2.00 | .2600 | .07000 | 3 |
|  | 3.00 | .3567 | .23861 | 3 |
|  | 4.00 | .6300 | .29597 | 3 |
|  | 5.00 | .6900 | .13077 | 3 |
|  | Total | .4973 | .23888 | 15 |
| THM30 | 1.00 | .8657 | .01150 | 3 |

191

| | 2.00 | .8988 | .10264 | 3 |
|---|---|---|---|---|
| | 3.00 | .6983 | .02967 | 3 |
| | 4.00 | .8420 | .04335 | 3 |
| | 5.00 | .8570 | .11605 | 3 |
| | Total | .8324 | .09500 | 15 |

## Mauchly's Test of Sphericity[a]

Measure:  Pulse width

| Within Subjects Effect | Mauchly's W | Approx. Chi-Square | df | Sig. | Greenhouse-Geisser | Huynh-Feldt | Lower-bound |
|---|---|---|---|---|---|---|---|
| | | | | | | Epsilon[b] | |
| PulseWidth | .416 | 7.899 | 2 | .019 | .631 | .969 | .500 |

Tests the null hypothesis that the error covariance matrix of the orthonormalized transformed dependent variables is proportional to an identity matrix.

a. Design: Intercept + Participant

 Within Subjects Design: PulseWidth

b. May be used to adjust the degrees of freedom for the averaged tests of significance. Corrected tests are displayed in the Tests of Within-Subjects Effects table.

## Tests of Within-Subjects Effects

Measure:  Pulse width

| Source | | Type III Sum of Squares | df | Mean Square | F | Sig. | Partial Eta Squared | Noncent. Parameter | Observed Power[a] |
|---|---|---|---|---|---|---|---|---|---|
| PulseWidth | Sphericity Assumed | .844 | 2 | .422 | 21.208 | .000 | .680 | 42.417 | 1.000 |
| | Greenhouse-Geisser | .844 | 1.262 | .668 | 21.208 | .000 | .680 | 26.774 | .996 |
| | Huynh-Feldt | .844 | 1.938 | .435 | 21.208 | .000 | .680 | 41.109 | 1.000 |
| | Lower-bound | .844 | 1.000 | .844 | 21.208 | .001 | .680 | 21.208 | .985 |
| PulseWidth * Participant | Sphericity Assumed | .365 | 8 | .046 | 2.292 | .063 | .478 | 18.337 | .721 |
| | Greenhouse-Geisser | .365 | 5.050 | .072 | 2.292 | .107 | .478 | 11.575 | .542 |

| | | | | | | | | | |
|---|---|---|---|---|---|---|---|---|---|
| | Huynh-Feldt | .365 | 7.753 | .047 | 2.292 | .066 | .478 | 17.772 | .709 |
| | Lower-bound | .365 | 4.000 | .091 | 2.292 | .131 | .478 | 9.169 | .461 |
| Error(PulseWidth) | Sphericity Assumed | .398 | 20 | .020 | | | | | |
| | Greenhouse-Geisser | .398 | 12.624 | .032 | | | | | |
| | Huynh-Feldt | .398 | 19.383 | .021 | | | | | |
| | Lower-bound | .398 | 10.000 | .040 | | | | | |

a. Computed using alpha = .05

**Estimates**

Measure:   ulse width

| PulseWidth | Mean | Std. Error | 95% Confidence Interval | |
|---|---|---|---|---|
| | | | Lower Bound | Upper Bound |
| 1 | .651 | .023 | .599 | .703 |
| 2 | .497 | .052 | .383 | .612 |
| 3 | .832 | .019 | .790 | .875 |

**Pairwise Comparisons**

Measure:   Pulse width

| (I) PulseWidth | (J) PulseWidth | Mean Difference (I-J) | Std. Error | Sig.[b] | 95% Confidence Interval for Difference[b] | |
|---|---|---|---|---|---|---|
| | | | | | Lower Bound | Upper Bound |
| 1 | 2 | .154[*] | .061 | .031 | .018 | .291 |
| | 3 | -.181[*] | .025 | .000 | -.237 | -.125 |
| 2 | 1 | -.154[*] | .061 | .031 | -.291 | -.018 |
| | 3 | -.335[*] | .060 | .000 | -.468 | -.202 |
| 3 | 1 | .181[*] | .025 | .000 | .125 | .237 |
| | 2 | .335[*] | .060 | .000 | .202 | .468 |

Based on estimated marginal means

*. The mean difference is significant at the .05 level.

## Appendix E: Permissions

**Rights to use previously published content**

## Copyright conditions

# Research Ethics Board (REB) Approval

University of Windsor

September 18, 2017
**To:**      **Research Services**
**From:**  **Research Ethics Board (**ethics@uwindsor.ca**)**
**Re:**       **Human Ethics Certificate Issued**
To whom it may concern,
Please accept this email as confirmation that **Dr. Jill Urbanic** has been issued a **Human Ethics** certificate. This certificate is valid until September 15, 2018.
Therefore, please release all funds, if held, related to the following award(s):

| Awards File No | Title | Status | |
|---|---|---|---|
| 33948 | The Spinal Cord Mannequin Design and Build Project (Lakshmi Kamala,Sarah Zhang) | Active | Office of Research Services |

If you have any questions, please feel free to contact me directly.
Sincerely,

Sarah Braganza, B.A (H), B.Ed., Coordinator
Suzanne McMurphy, Ph.D., Chair

The Office of the Research Ethics Board
2146 Chrysler Hall North
University of Windsor
Telephone: 253-3000 ext. 3948
Email: ethics@uwindsor.ca

*Please note the office has moved to the 2nd Floor of Chrysler Hall North. If you require assistance please come to 2146 CHN or email* ethics@uwindsor.ca.
cc:      eRSO Certification Project File

# Appendix F: University of Windsor Student AM Pricing Template

**Template 1: Cost breakdown for 18-year old female model**

| QTY (cm³) | ITEM # | DESCRIPTION | UNIT PRICE ($ CAD) | DISCOUNT | LINE TOTAL ($) |
|---|---|---|---|---|---|
| 2914.6 | ABM-30 | Model Material | 0.35 | | 1,020.11 |
| 1542.68 | SR-30 | Support Material | 0.35 | | 539.94 |
| 100.5 | | Machine Time (hrs) | 10.00 | | 1005.00 |
| 1.00 | | Plating Fee | 10.00 | | 10.00 |
| 1.00 | | Sheet Fee | 25.00 | | 25.00 |
| | | **TOTAL DISCOUNT** | | | 0.00 |
| | | | **SUBTOTAL** | | $2,600.05 |
| | | | **SALES TAX** | | 0.00 |
| | | | **TOTAL** | | **$2,600.05** |

**Template 2: Cost breakdown for 2-year old male model**

| QTY (cm³) | ITEM # | DESCRIPTION | UNIT PRICE ($ CAD) | DISCOUNT | LINE TOTAL ($) |
|---|---|---|---|---|---|
| 680.06 | ABM-30 | Model Material | 0.35 | | 238.02 |
| 167.64 | SR-30 | Support Material | 0.35 | | 58.67 |
| 21.50 | | Machine Time (hrs) | 10.00 | | 215.00 |
| 1.00 | | Plating Fee | 10.00 | | 10.00 |
| 1.00 | | Sheet Fee | 25.00 | | 25.00 |
| | | **TOTAL DISCOUNT** | | | 0.00 |
| | | | **SUBTOTAL** | | $546.70 |
| | | | **SALES TAX** | | 0.00 |
| | | | **TOTAL** | | **$546.70** |

## VITA AUCTORIS

| | |
|---|---|
| NAME: | Andre Khayat |
| PLACE OF BIRTH: | Leamington, Ontario |
| YEAR OF BIRTH: | 1994 |
| EDUCATION | Cardinal Carter Secondary School, Leamington 2008-2012 |
| | University of Windsor Ontario, Windsor, Ontario 2012-2016 B.Sc. |
| | University of Windsor, Windsor, Ontario 2016-2018 MASc. |